HISTORY RESEARCH JOURNAL
इतिहास संशोधन पत्रिका

CERTIFICATE OF PUBLICATION

This is to certified that the article entitled

SOCIAL MEDIA CONSUMPTION AND PURCHASING PATTERN: A STUDY OF SOME SELECTED DISTRICTS OF HARYANA

Authored By

Rajesh Kumar
Research Scholar, School of Commerce & Management, Om Sterling Global University, Hisar

Issue.- XXX (January) 2023
History Research Journal with ISSN : 0976-5425
UGC-CARE List Group I
Publisher: Marathwada Itihas Parishad

Impact Factor: 5.23

UGC

HISTORY RESEARCH JOURNAL ISSN: 0976-5425

Editor-in-chief

ISSN No : 2581-6306 Impact Factor : 6.154

Shodhshauryam, International Scientific Refereed Research Journal

Certificate of Publication

Ref : SHISRRJ/Certificate/Volume 6/Issue 3/880 30-Jun-2023

This is to certify that the research paper entitled

महिला उद्यमिता - समस्याएं और संभावनाएं

Rajesh Kumar

Assistant Professor, Govt. College Bhattu Kalan, Fatehabad

After review is found suitable and has been published in the Shodhshauryam, International Scientific Refereed Research Journal(SHISRRJ), Volume 6, Issue 3, May-June 2023, [Page No : 25-37]

This Paper can be downloaded from the following SHISRRJ website link

https://shisrrj.com/SHISRRJ23636

SHISRRJ Team wishes all the best for bright future

Editor In Chief SHISRRJ

Associate Editor SHISRRJ

INTERNATIONAL JOURNAL OF NOVEL
RESEARCH AND DEVELOPMENT
International Peer Reviewed & Refereed Journals, Open Access Journal
ISSN Approved Journal No: 2456-4184 | Impact factor: 8.76 | ESTD Year: 2016
Scholarly open access journals, Peer-reviewed, and Refereed Journals, Impact factor 8.76 (Calculated by google scholar and Semantic Scholar | AI-Powered Research Tool), Multidisciplinary, Monthly, Multilanguage, all major database & Metadata, Citation Generator, Digital Object Identifier (DOI)

Published Paper Details

Paper Title:	ई -क्रांति की ओर बढ़ते कदम - डिजिटल इंडिया
Authors Name:	RAJESH KUMAR , VIKRANT MOHAN
Download E-Certificate:	Download
Author Reg. ID:	IJNRD_200492
Published Paper Id:	IJNRD2306582
Published In:	Volume 8 Issue 6, June-2023
DOI:	

Abstract:

भारत में प्रौद्योगिकी के उपयोग को बढ़ाने के लिए भारत सरकार द्वारा डिजिटल इंडिया अभियान शुरू किया गया था। इसका उद्देश्य पूरे देश में अपने ऑनलाइन बुनियादी ढांचे में सुधार करके नागरिकों को इलेक्ट्रॉनिक रूप से सरकारी सेवाएं आसानी से उपलब्ध कराना था। इंटरनेट कनेक्टिविटी में वृद्धि के द्वारा देश को डिजिटल रूप से सशक्त बनाने के लिए इस प्रक्रिया को अपनाया गया है। यह आम जनता तक पहुंचने का आसान तरीका है और उन्हें अपने दैनिक जीवन में प्रौद्योगिकी का उपयोग करने के लिए प्रोत्साहित करता है। प्रधान मंत्री श्री नरेंद्र मोदी द्वारा 1 जुलाई, 2015 को इस अभियान को शुरू किया गया। इस अभियान की सहायता से ग्रामीण भारत को हाई-स्पीड इंटरनेट कनेक्टिविटी से जोड़ना है।

Keywords: डिजिटल इंडिया

Cite Article: "ई -क्रांति की ओर बढ़ते कदम - डिजिटल इंडिया", International Journal of Novel Research and Development (www.ijnrd.org), ISSN:2456-4184, Vol.8, Issue 6, page no.f778-f782, June-2023, Available

Downloads: 000117950

2456-4184 | IMPACT FACTOR: 8.76 Calculated By Google Scholar | ESTD YEAR: 2016
An International Scholarly Open Access Journal, Peer-Reviewed, Refereed Journal Impact Factor 8.76 Calculate by Google Scholar and Semantic Scholar | AI-Powered Research Tool, Multidisciplinary, Monthly, Multilanguage Journal Indexing in All Major Database & Metadata, Citation Generator

ISSN:

Publication Details:
Published Paper ID: IJNRD2306582
Registration ID: 200492
Published In: Volume 8 Issue 6, June-2023
DOI (Digital Object Identifier)
Page No: f778-f782
Country: Hissar, Haryana, India
Research Area: Commerce
Publisher
Published Paper URL
Published Paper PDF

Share Article:

Understanding the Sector-Specific Antecedents of Customer Switching via Literature Review

The IUP Journal of Management Research, Vol. XIX, No. 4, October 2020, pp. 46-71

Posted: 31 Mar 2021

Ubba Savita
Guru Jambheshwar University of Science and Technology

Jyoti Jhajhra
Government College

Date Written: March 26, 2020

Abstract

The aim of this paper is to review the existing literature in the field of customer switching behavior and to identify the antecedents of customer switching that work in specific sectors and to suggest avenues for future research. Various online academic databases have been searched to collect research papers published in different journals from the year 1990 to the early part of 2020. The literature on antecedents of customer switching specifically on the basis of sector is almost nonexistent in the available literature. This is an attempt to study the

p-ISSN : 2335-1357 e-ISSN : 2437-1122

Mediterranean Journal of Modeling and Simulation

Med. J. Model. Simul. 09 (2018) 025-042

Transient analysis of nonlocal microstretch thermoelastic thick circular plate with phase lags

Rajneesh KUMAR [a,*] Aseem MIGLANI [b,†], Rekha RANI [b,‡]

[a] Department of Mathematics, Kurukshetra University, Kurukshetra, Haryana, India
[b] Department of Mathematics, Chaudhary Devilal University, Sirsa, Haryana, India

ARTICLE INFO

Article history :
Received December 2017
Accepted March 2018

Keywords :
Nonlocal microstretch;
Thermoelasticity;
Eigenvalue approach;
Laplace and Hankel transforms;
Circular plate;
Three phase lag model

ABSTRACT

The present investigation is concerned with the eigenvalue approach in a homogeneous, isotropic nonlocal microstretch thermoelastic circular plate with three phase lag model subjected to thermomechanical sources. The components of displacements, microrotation, microstretch, temperature distribution, normal stress, shear stress and couple shear stress are obtained in the transformed domain by using the Laplace and Hankel transforms. The resulting quantities are obtained in the physical domain by applying numerical inversion technique. Effects of nonlocal, phase lag, relaxation time, with and without energy dissipation are analyzed on the resulting quantities numerically and illustrated graphically.

1. Introduction

The nonlocal elasticity theory of continuum mechanics has received more attention recently. The basic idea behind the nonlocal theories is that the interacting forces between material points are far-reaching in character. The nonlocal theories are differing from the local theories by taking into account the master balance laws which is valid only on the whole body. In many cases, such as in phonon dispersion in solid, in fracture mechanics, in surface physics, in electromagnetic solids, the nonlocal effects are dominant and only the nonlocal theories might provide the right answer, while local theories would fail. The nonlocal elasticity theory can be employed to determine the dispersion relations of elastic crystals, [illegible] in the entire Brillouin zone. The physical phenomena involving microscopic internal characteristic length should be predictable by means of the nonlocal elasticity.

The nonlocal theory takes into account nonlocal effects hitherto almost entirely neglec-

*Email : rajneesh_kuk@rediffmail.com
†Email : miglani_aseem@rediffmail.com
‡Email : rekharani024@gmail.com

Article Navigation

Generalized Two Temperatures Thermoelasticity of Micropolar Porous Circular Plate with Three Phase Lag Model

R. Kumar, A. Miglani, R. Rani Author Notes

Journal of Mechanics, Volume 34, Issue 6, December 2018, Pages 779–789,
https://doi.org/10.1017/jmech.2017.69
Published: 24 August 2017 **Article history**

The present study is to focus on the two dimensional problem of micropolar porous circular plate with three phase lag model within the context of two temperatures generalized thermoelasticity theory. The problem is solved by applying Laplace and Hankel transforms after using potential functions. The expressions of displacements, microrotation, volume fraction field, temperature distribution and stresses are obtained in the transformed domain. To show the utility of the approach, normal

Mechanics and Mechanical Engineering
Vol. 22, No. 1 (2018) 189–196

A Two Dimensional Axisymmetric Thermoelastic Diffusion Problem of Micropolar Porous Circular Plate with Dual Phase Lag Model

Rajneesh KUMAR
Department of Mathematics
Kurukshetra University Kurukshetra
Haryana, India
rajneesh_kuk@rediffmail.com

Aseem MIGLANI
Rekha RANI
Department of Mathematics
Chaudhary Devilal University
Sirsa, Haryana, India
miglani_aseem@rediffmail.com
rekharani024@gmail.com

Received (12 June 2018)
Revised (20 July 2018)
Accepted (13 August 2018)

In the present investigation we consider a two dimensional axisymmetric problem of micropolar porous circular plate with thermal and chemical potential sources in the context of the theory of dual-phase-lag generalized thermoelastic diffusion. The potential functions are used to solve the problem. The Laplace and Hankel transforms techniques are used to find the expressions of displacements, microrotation, volume fraction field, temperature distribution, concentration and stresses in the transformed domain. The inversion of transforms based on Fourier expansion techniques is applied to obtain the results in the physical domain. The numerical results for resulting quantities are obtained and depicted graphically. Effect of porosity, LS theory and phase lag are presented on the resulting quantities. Some particular cases are also deduced.

Keywords: micropolar porous, thermoelastic diffusion, circular plate, thermal and chemical potential sources, Laplace and Hankel transforms.

1. Introduction

Nowacki [1] and Kröner [2] developed the theory of micropolar thermoelasticity. The linear theory of micropolar coupled thermoelasticity was examined by Tauchert, Claus and Ariman [3]. Boschi and Iesan [4] derived the governing equations of the linear theory of thermoelasticity investigated with two relaxation times. Many researchers [Eringen [5], Nowacki and Olszak [6], Dost and Tabarrok [7],

Mechanics and Mechanical Engineering
Vol. 22, No. 4 (2018) 999–1014
© Technical University of Lodz

https://doi.org/10.2478/mme-2018-0080

Response of Thermoelastic Interactions in Micropolar Porous Circular Plate with Three Phase Lag Model

Rajneesh KUMAR
Department of Mathematics, Kurukshetra University, Kurukshetra, Haryana, India
e-mail: rajneesh_kuk@rediffmail.com

Aseem MIGLANI
Department of Mathematics, Choudhary Devilal University, Sirsa, Haryana, India
e-mail: miglani_aseem@rediffmail.com

Rekha RANI
Department of Mathematics, Choudhary Devilal University, Sirsa, Haryana, India
e-mail: drrekharani92@gmail.com

Received (23 January 2018)
Revised (5 September 2018)
Accepted (20 November 2018)

The present study deals with a homogeneous and isotropic micropolar porous thermoelastic circular plate by employing eigenvalue approach in the three phase lag theory of thermoelasticity due to thermomechanical sources. The expressions of components of displacements, stresses, volume fraction field, temperature distribution, normal stress, shear stress, couple stress and stress are obtained in the transformed domain by employing the Laplace and Hankel transforms. The resulting quantities are obtained in the physical domain by employing the numerical inversion technique. Numerical computations of the resulting quantities are made and presented graphically to show the effects of void, phase lag, relaxation time with and without energy dissipation.

Keywords: micropolar porous, thermoelasticity, eigenvalue approach, Laplace and Hankel transforms, three phase lag model.

1. Introduction

The linear theory of micropolar thermoelasticity was developed by Nowacki [1] and Eringen [2]. Tauchert, Claus and Ariman [3] also examined the linear theory of micropolar coupled thermoelasticity. Dost and Tabarrok [4] represented the theory of generalized micropolar thermoelasticity taking into account Green Lindsay theory [5] of thermoelasticity. The theory of micropolar thermoelasticity including heat flux among constitutive variables was investigated by Chandrasekharaiah [6].

International Journal of Theoretical and Applied Mechanics
http://www.iaras.org/iaras/journals/ijtam

Axisymmetric Problem of a Microelongated Thermoelastic Medium due to Thermomechanical Sources

RAJNEESH KUMAR
Department of Mathematics
Kurukshetra University, Kurukshetra, Haryana
INDIA
rajneesh_kuk@rediffmail.com

ASEEM MIGLANI
Department of Mathematics
Ch. Devi Lal University, Sirsa, Haryana
INDIA
miglani_aseem@rediffmail.com

REKHA RANI
Department of Mathematics
Ch. Devi Lal University, Sirsa, Haryana
INDIA
rekharani024@gmail.com

Abstract:- An axisymmetric problem of a microelongated thermoelastic medium by considering an infinite circular plate under the influence of thermomechanical sources has been solved by employing the eigenvalue approach. The solution in the form of the components of displacement, stresses and temperature distribution is obtained in the transformed domain by using the Laplace and the Hankel transforms. A numerical inversion technique has been used to get the results in the physical domain, numerically, for a particular model. The results are presented graphically to show the effect of microelongation on various field components. The results are discussed graphically.

Key-words:- Axisymmetric, Microelongation, Thermoelastic, Eigenvalue, Thermomechanical sources; Numerical Inversion.

1 Introduction

The theories for the microcontinuum i.e. the micromorphic continuum fields were introduced by A. C. Eringen and these differ from classical (linear and non-linear) field theories by the fact that each material particle is endowed with additional degrees of freedom. That means, in contrast to classical continuum mechanics (rational mechanics), where the motion (macromotion) of a material particle is fully described by a vector function called deformation function, micromorphic material particles undergo an additional micromotion, corresponding to the rotation and deformation of the material particle at the microscale. In the most general case of micromorphic continua, there are nine additional degrees of freedom (three for microrotation and six for microdeformation). In principle, micromorphic continua are almost universal but, due to its complexity, the practical usefulness of this theory is inversely proportional to its generality.

A special case is that of microstretch continua. Here, the isotropic expansion or contraction of the material particle is permitted in addition to rotation. Shearing motions are not allowed in microstretch continua. That means the particles of microstretch materials have seven degrees of freedom, three for displacements, three for microrotations and one for microstretch. Microstretch theory adequately model the bubbly liquids. A more special is the theory of micropolar continua, in which only the microrotations of material particles, described by three degrees of freedom, are allowed in micropolar continua in addition to the motion at macroscale. The theory of microstretch elastic bodies or Micropolar theory of elasticity with stretch is a generalization of the micropolar theory of elasticity for which the theory was given by Eringen [1]. Eringen [2] also

Journal of Solid Mechanics Vol. 11, No. 1 (2019) pp. 1-1
DOI: 10.22034/JSM.2019.666213

A Problem of Axisymmetric Vibration of Nonlocal Microstretch Thermoelastic Circular Plate with Thermomechanical Sources

R. Kumar [1,*], K. Rani [2], A. Miglani [2]

[1] Department of Mathematics, Kurukshetra University, Kurukshetra, India
[2] Department of Mathematics, Chandigarh University, Gharuan, Mohali, India

Received 1 September 2018; accepted 1 November 2018

ABSTRACT

In the present manuscript, the investigation of free axisymmetric vibrations of nonlocal microstretch thermoelastic circular plate subjected to thermomechanical sources is carried out. Laplace and Hankel transforms technique is proposed to analyze the problem. Laplace and Hankel transforms are used to obtain the transformed solutions for the displacements, stress, rotation, microstretch, temperature and microstress. The results are obtained in the physical domain by using numerical inversion technique of transforms. The frequency equations are obtained numerically for clamped and simply supported plates. The effect of nonlocal parameter, thermomechanical sources, thermal relaxation times (GL) and Coupled Thermoelastic (CT) on the [illegible] are computed numerically and presented graphically in the form of [illegible]. Some special cases are also discussed.

Keywords: Nonlocal elasticity, Thermoelasticity, Laplace and Hankel transforms, Eigenvalue approach, Circular plate

1 INTRODUCTION

THE nonlocal elasticity theory [1] for elastic materials with long range cohesive forces was developed by Eringen [2]. Eringen and Edelen [6] developed the nonlocal elasticity theory [7] and Eringen and Kim [7] developed the nonlocal elasticity theory for elastic solids in such a way that the nonlocal effect is incorporated in the constitutive relations only and the elastic problem is simplified in the sense that the governing differential equations remain same as in the classical elasticity. Eringen [8] developed the nonlocal theory for elastic solids with microstructure. Eringen [9] developed the nonlocal theory for elastic solids with microstructure. Eringen [10] developed the nonlocal theory for elastic solids with microstructure. Eringen [11] developed the nonlocal theory for elastic solids with microstructure. Eringen [12] developed the nonlocal theory for elastic solids with microstructure. Eringen [13] developed the nonlocal theory for elastic solids with microstructure. Eringen [14] developed the nonlocal theory for elastic solids with microstructure. Eringen [15] developed the nonlocal theory for elastic solids with microstructure. Eringen [16] developed the nonlocal theory for elastic solids with microstructure. Eringen [17] developed the nonlocal theory for elastic solids with microstructure. Eringen [18] developed the nonlocal theory for elastic solids with microstructure. Eringen [19] developed the nonlocal theory for elastic solids with microstructure. Eringen [20] developed the nonlocal theory for elastic solids with microstructure. Eringen [21] developed the nonlocal theory for elastic solids with microstructure. Eringen [22] developed the nonlocal theory for elastic solids with microstructure. Eringen [23] developed the nonlocal theory for elastic solids with microstructure. Eringen [24] developed the nonlocal theory for elastic solids with microstructure. Eringen [25] developed the nonlocal theory for elastic solids with microstructure. Eringen [26] developed the nonlocal theory for elastic solids with microstructure. Eringen [27] developed the nonlocal theory for elastic solids with microstructure. Eringen [28] developed the nonlocal theory for elastic solids with microstructure. Eringen [29] developed the nonlocal theory for elastic solids with microstructure. Eringen [30] developed the nonlocal theory for elastic solids with microstructure. Eringen [31] developed the nonlocal theory for elastic solids with microstructure. Eringen [32] developed the nonlocal theory for elastic solids with microstructure. Eringen [33] developed the nonlocal theory for elastic solids with microstructure. Eringen [34] developed the nonlocal theory for elastic solids with microstructure. Eringen [35] developed the nonlocal theory for elastic solids with microstructure. Eringen [36] developed the nonlocal theory for elastic solids with microstructure. Eringen [37] developed the nonlocal theory for elastic solids with microstructure. Eringen [38] developed the nonlocal theory for elastic solids with microstructure. Eringen [39] developed the nonlocal theory for elastic solids with microstructure. Eringen [40] developed the nonlocal theory for elastic solids with microstructure. Eringen [41] developed the nonlocal theory for elastic solids with microstructure. Eringen [42] developed the nonlocal theory for elastic solids with microstructure. Eringen [43] developed the nonlocal theory for elastic solids with microstructure. Eringen [44] developed the nonlocal theory for elastic solids with microstructure. Eringen [45] developed the nonlocal theory for elastic solids with microstructure. Eringen [46] developed the nonlocal theory for elastic solids with microstructure. Eringen [47] developed the nonlocal theory for elastic solids with microstructure. Eringen [48] developed the nonlocal theory for elastic solids with microstructure. Eringen [49] developed the nonlocal theory for elastic solids with microstructure. Eringen [50] developed the nonlocal theory for elastic solids with microstructure. Eringen [51] developed the nonlocal theory for elastic solids with microstructure. Eringen [52] developed the nonlocal theory for elastic solids with microstructure. Eringen [53] developed the nonlocal theory for elastic solids with microstructure. Eringen [54] developed the nonlocal theory for elastic solids with microstructure. Eringen [55] developed the nonlocal theory for elastic solids with microstructure. Eringen [56] developed the nonlocal theory for elastic solids with microstructure. Eringen [57] developed the nonlocal theory for elastic solids with microstructure. Eringen [58] developed the nonlocal theory for elastic solids with microstructure. Eringen [59] developed the nonlocal theory for elastic solids with microstructure. Eringen [60] developed the nonlocal theory for elastic solids with microstructure. Eringen [61] developed the nonlocal theory for elastic solids with microstructure. Eringen [62] developed the nonlocal theory for elastic solids with microstructure. Eringen [63] developed the nonlocal theory for elastic solids with microstructure. Eringen [64] developed the nonlocal theory for elastic solids with microstructure. Eringen [65] developed the nonlocal theory for elastic solids with microstructure. Eringen [66] developed the nonlocal theory for elastic solids with microstructure. Eringen [67] developed the nonlocal theory for elastic solids with microstructure. Eringen [68] developed the nonlocal theory for elastic solids with microstructure. Eringen [69] developed the nonlocal theory for elastic solids with microstructure. Eringen [70] developed the nonlocal theory for elastic solids with microstructure. Eringen [71] developed the nonlocal theory for elastic solids with microstructure. Eringen [72] developed the nonlocal theory for elastic solids with microstructure. Eringen [73] developed the nonlocal theory for elastic solids with microstructure. Eringen [74] developed the nonlocal theory for elastic solids with microstructure. Eringen [75] developed the nonlocal theory for elastic solids with microstructure. Eringen [76] developed the nonlocal theory for elastic solids with microstructure. Eringen [77] developed the nonlocal theory for elastic solids with microstructure. Eringen [78] developed the nonlocal theory for elastic solids with microstructure. Eringen [79] developed the nonlocal theory for elastic solids with microstructure. Eringen [80] developed the nonlocal theory for elastic solids with microstructure. Eringen [81] developed the nonlocal theory for elastic solids with microstructure. Eringen [82] developed the nonlocal theory for elastic solids with microstructure. Eringen [83] developed the nonlocal theory for elastic solids with microstructure. Eringen [84] developed the nonlocal theory for elastic solids with microstructure. Eringen [85] developed the nonlocal theory for elastic solids with microstructure. Eringen [86] developed the nonlocal theory for elastic solids with microstructure. Eringen [87] developed the nonlocal theory for elastic solids with microstructure. Eringen [88] developed the nonlocal theory for elastic solids with microstructure. Eringen [89] developed the nonlocal theory for elastic solids with microstructure. Eringen [90] developed the nonlocal theory for elastic solids with microstructure. Eringen [91] developed the nonlocal theory for elastic solids with microstructure. Eringen [92] developed the nonlocal theory for elastic solids with microstructure. Eringen [93] developed the nonlocal theory for elastic solids with microstructure. Eringen [94] developed the nonlocal theory for elastic solids with microstructure. Eringen [95] developed the nonlocal theory for elastic solids with microstructure. Eringen [96] developed the nonlocal theory for elastic solids with microstructure. Eringen [97] developed the nonlocal theory for elastic solids with microstructure. Eringen [98] developed the nonlocal theory for elastic solids with microstructure. Eringen [99] developed the nonlocal theory for elastic solids with microstructure. Eringen [100] developed the nonlocal theory for elastic solids with microstructure.

* Corresponding author
Email address: rajneesh_kuk@hotmail.com (R. Kumar)

2

introducing an imaginary nonlocal strain [illegible] and the stress tensor in the modified nonlocal theory, free vibration of functionally graded nonhomogeneous [illegible] plates with simply supported boundary conditions based on the first order plate theory and time dependent [illegible] are investigated. Peng, Li, Tang and Shen [16] presented the influence of nonlocal size parameter on the deflection of a nonlocal Nano beam and crack growth. Sumelka, Zaera and Fernández-Sáez [17] [illegible] nonlocal elasticity theory. Vazirkov and Lurie [18] presented the nonlocal theory of [illegible] vibration of rods described in terms of functions [illegible] the nonlocal elasticity and [illegible] theory. Vazirkov and Lurie [18] presented the nonlocal theory of [illegible] distinct fields, gradient elasticity theories and [illegible] nonlocal lattice particle method for their [illegible] Kaur and Tomar [20] investigated the propagation [illegible] Eringen [21] obtained the constitutive relations [illegible] of thermoelastic solids together with the balance laws [illegible] developed the nonlocal generalized thermoelasticity theory [illegible] mechanics. Allan [23] introduced the rigid equations of [illegible] problems for nonlocal linear thermoelasticity [illegible] generalized nonlocal thermoelasticity and also [illegible] Zenkour and Abouelregal [24] [illegible] subjected to a harmonically varying heat [illegible] Thermoelastic model with one relaxation time [illegible] sinusoidal pulse varying heat [illegible] order sample material by solving the [illegible] arbitrarily thermal sources and [illegible] In the present investigation, [illegible] homogeneous nonlocal elastic [illegible] approach. The Laplace and Hankel [illegible]

EDUINDEX

PUBLICATION CERTIFICATE

This publication certificate has been issued to

Sita Ram

For publication of research paper titled

औद्योगिक विकास में कृषि की भूमिका

Published in

Drishtikon with ISSN 0975-119X

Vol:*12* Issue: *9* Month: *June* Year: *2020*

Impact factor:*5.4*

The journal is indexed, peer reviewed and listed in UGC Care

Editor

Editor

www.edurindex.org
editor@edurindex.org

Note: This eCertificate is valid with published papers and the paper must be available online at the website under the network of EDUindex.

Printing Area®

Peer Reviewed International Refereed Research Journal

At.Post.Limbaganesh,Tq.Dist.Beed Pin-431126 (Maharashtra)

Certificate Of Publication

This is to certify that the review board of our research journal accepted the research paper/article titled भारत के आर्थिक विकास को रोकती सामाजिक चुनौतियां of Dr./Mr./Miss/Mrs. SITA RAM (Asst. Prof.) Deptt. of Economics

It is peer reviewed and published in the Issue 62 Vol. 03 in the month of February 2020.

Thank you for sending your valuable writing for printing area Journal

Indexed (IIJIF) | Impact Factor 7.387 | Govt.of India, Trade Marks Registry Regd.No.3419602

ISSN 2394-5303

Editor in chief
Dr.Bapu G.Gholap

J Mater Sci: Mater Electron (2023) 34:1947

Effect of La^{3+} doping concentration on the structural, electrical, dielectric, and magnetic properties of α-Fe_2O_3 nanoparticles

Vijay Kumar[1,2], Dharamvir Singh Ahlawat[1,*], Amrik Singh[1], and RadheShyam[3]

[1] *Department of Physics, Chaudhary Devi Lal University, Sirsa 125055, Haryana, India*
[2] *Department of Physics, Govt. College Bhattu Kalan, Fatehabad 125053, Haryana, India*
[3] *Department of Physics, Malaviya National Institute of Technology Jaipur, J L N Marg, Jaipur 302017, Rajasthan, India*

Received: 3 April 2023
Accepted: 10 September 2023

ABSTRACT

Lanthanum (La)-substituted α-Fe_2O_3 (pure, 2%, 5%, 8%, and 10%) nanopowder with altering concentration was fabricated using the sol–gel technique. The effect of trivalent La^{3+} ions on the microstructural, electrical, dielectric, and magnetic properties of the hematite nanopowder was investigated. X-ray diffraction (XRD) pattern of pure and La-doped samples was indexed as a rhombohedral phase with the $R\bar{3}c$ space group of hematite having crystallite size ranging from 13.5 to 33.4 nm. The existence of La^{3+} ions in the α-Fe_2O_3 matrix was confirmed by the EDS spectra. Furthermore, XRD findings are in-line with FTIR observation. The resistivity plots demonstrated two different regions corresponding to two dissimilar kinds of conduction mechanisms. Investigation of resistivity data indicates the variable-range hopping and nearest-neighbor hopping conduction mechanisms are present in the 100–300 K and 300–400 K temperature slots, respectively. The dielectric analysis of undoped & La-substituted α-Fe_2O_3 was carried out in the temperature range 100–400 K and followed the variation in lattice parameters and morphology of samples. Magnetic study reveals that magnetic properties were significantly modified with the addition of La^{3+}ions in the hematite lattice.

1 Introduction

In the last few decades, magnetic materials captured the researcher's attention because of their prospective applications such as magnetic memories, targeted drug delivery systems, magnetic imaging, and sensing in different technical aspects [1–5]. Magnetic materials have become the center of interest because of their thermal stability, low cost, and their eco-friendly behavior. Among these magnetic oxides, iron oxide (Fe_2O_3) nanoparticles gain popularity due to their widespread applications such as adsorbents, catalysts, magnetic fluids, and high resistance to corrosion [6–9]. Fe_2O_3 is generally observed to exist in four crystalline phases such as α-Fe_2O_3, β-Fe_2O_3, γ-Fe_2O_3, and ε-Fe_2O_3. Out of these phases, the hematite (α-Fe_2O_3) is the best stable phase of iron oxide having characteristics of an n-type semiconductor with a bandgap of ~ 2.1 eV

Address correspondence to E-mail: dahlawat66@gmail.com

https://doi.org/10.1007/s10854-023-11300-1

[10–13] and always exhibits a hexagonal structure with $R\bar{3}c$ space group. It is always fascinating to modulate the material properties through the addition of suitable impurities and the more exciting rather challenging is to make these material modifications suitable for use in desired applications. Like a p-type or n-type semiconductor is just made by the addition of suitable trivalent or a pentavalent impurity, respectively. These semiconductors have revolutionized the world and present age may be called as age of semiconductors. So this becomes the main application and motivation to pursue a material and introduce a suitable impurity and to explore any possibilities of enhancement in properties for almost any person working on materials. The existing reports reveal that the substitution of transition metals at the Fe-site in the α-Fe_2O_3 crystal structure is favored in tunning the structural, electrical, optical, dielectric, and magnetic properties of hematite nanoparticles [14–22]. The incorporation of La^{3+} ion in α-Fe_2O_3 was observed to induce semiconducting nature along with the increase in dielectric constant (ε′) and crystallite size while decreasing the dielectric loss ($X = 0.10$).Furthermore, it has been investigated that doping of lanthanide (Ln^{3+}) ions strongly influences the structural, electrical, dielectric, and magnetic properties [23–27]. The increased value of electrical resistivity was observed with La^{3+} ion substitution attributed to the hopping conduction mechanism. Besides, Ce doping is also observed to significantly influence the electrical, structural, dielectric, and magnetic properties of hematite nanoparticles[28, 29]. The substitution of Gd^{3+} ions in α-Fe_2O_3 was observed to improve the magnetic properties [30]. Seham K. Abdel-Aal et al. synthesized the Perovskite-graphene nanocomposites of rare-earth $LaFeO_3$-rGO and $LaFeO_3$ nanoparticles by citrate sol–gel method, and the effect of graphene has been observed where it decreases the particle size and energy band gap values by ≈ 10 nm and 0.03 eV, respectively, with increased value of saturation magnetization [31]. Cu doping of the NiZnCu-based ferrite system assists in the modification of the matrix owing to the difference in the ionic size of Ni^{2+} which can alter the electrical and magnetic properties. The substitution of copper was observed to decrease the firing temperature[32]. Seham K. Abdel-Aal et al. successfully prepared Cu hybrid perovskites diammonium series $[(NH_3)_2(CH_2)_3]CuCl_4$& $[(NH_3)_2(CH_2)_4]CuCl_2Br_2$ by the evaporation method and reported that Cu-based hybrid perovskites show strong absorption in UV region according to the optical absorption study. The energy gap of C_3CuCl and $C_4CuClBr$ are equal to 2.85 and 3.9 eV, respectively [33].Seham Kamal Abdel-Aal et al. designed a new series of 2D hybrid perovskites of the formula $NH_3(CH_2)nNH_3MX_4$ n = 3 – 9, M = Mn, Cu, Co, Bi. X = Cl, Br and obtained a promising result concerning photovoltaic application of 2D perovskite hybrid. The primary results of the band gap energies are (1.75 eV–2.65 eV). Regarding to its stability and safety, it is highly recommended to emerge Bi alkyl ammonium as hybrid perovskite lead-free, low cost, and environmental friendly material for solar cells applications [34]. To date, the doping of only a few elements from the lanthanide series was reported. The doping of La ions among other lanthanides is observed to perfect substitution for the Fe-site without occupying the interstitial sites and tailored the structural, electrical, and both the direct and indirect bandgap in α-Fe_2O_3 [35–37]. To the best of our knowledge, the investigation of microstructural, electrical, dielectric, and magnetic properties of La^{3+} ions substituted in α-Fe_2O_3 nanoparticles remains unexplored. Therefore, the present report describes the tailoring of structural, electrical(temperature-dependent resistivity), dielectric, and magnetic properties of La^{3+}doped α-Fe_2O_3 nanoparticles.

2 Experimental details

2.1 Materials and synthesis

Lanthanum-doped hematite samples with different compositions were fabricated using the sol–gel technique with formula $Fe_{2-2X}La_{2X}O_3$ ($X = 0.00$, 0.02, 0.05, 0.08 & 0.10). The iron (III) nitrate nonahydrate, $Fe(NO_3)_3.9H_2O$ (Sigma-Aldrich, 99.95%), and Lanthanum (III) nitrate hexahydrate La $(NO_3)_2.6H_2O$ (Sigma-Aldrich, 99.99%) salts were taken in their stoichiometric ratio and dissolved in deionized (DI) water with the formation of a solution. The obtained solution was heated to 80 °C with continuous stirring until it converted into gel form. Thus the formed gel was heated at 120 °C for 2 h to solidify it. Further to remove any existing moist content, this solidified gel was heated at 200 °C temperature for 3 h. Now, agate mortar-pestle is used for hand grinding this solidified gel with required homogeneity. After 3 h of continuous hand grinding, this homophasic powder was pelletized in 10 mm diameter dye using a hand-operated hydraulic press under 5 tons of pressure. Eventually,

the produced pellets were sintered at 600 °C in the air for 6 h.

2.2 Characterizations

La-substitutedα-Fe_2O_3samples were characterized using various techniques such as X-ray diffraction (XRD), Fourier transform infrared spectroscopy (FTIR), field emission scanning electron microscopy (FESEM), energy-dispersive X-ray spectroscopy (EDS), temperature-dependent resistivity, dielectric constant, and vibrating sample magnetometer (VSM). The crystal structure of the samples was determined by the Bruker-AXSD8 advance diffractometer with wavelength (λ = 1.540 Å) using Cu K_α source. The morphology study and elemental composition of samples were carried out using FESEM with EDS instrument model Nova Nano FE-SEM 450 (FEI). FTIR measurements were taken by Perkin-Elmer 580B IR spectrophotometer using the KBr pellet technique between 4000 and 500 cm^{-1} for 16 scans at a resolution of 4 cm^{-1} at room temperature. The resistivity measurements of samples were carried out by Keithley electrometer-6517B in the temperature range of 100 to 400 K. Furthermore, the dielectric and magnetic properties of all samples were studied by Agilent 4285A precision LCR meter and Lake Shore-7410 Series VSM, respectively.

3 Results and discussion

3.1 XRD analysis

The XRD patterns of $Fe_{2-2X}La_{2X}O_3$ (X = 0.00, 0.02, 0.05, 0.08, and 0.10) nanoparticles are displayed in Fig. 1. The XRD patterns of pure and La-doped hematite show rhombohedral phase in the $R\bar{3}c$ space group and the peaks are assigned to (012), (104), (110), (113), (024), (116), (018), (214),and (300) planes referring to JCPDS card No. 84–0311[38–40].

The addition of more La content (after X = 0.08) into α-Fe_2O_3 lattice triggers the reduction of the intensity of peaks which indicate that crystallinity of samples has been decreased [41, 42]. This specifies the solubility limit of La ions in α-Fe_2O_3 lattice where saturation is observed at X = 0.08 La doping concentration. This scenario provides evidence of insolubility at higher La doping concentrations, which has already been reported by different research groups [43–46]. The formation of

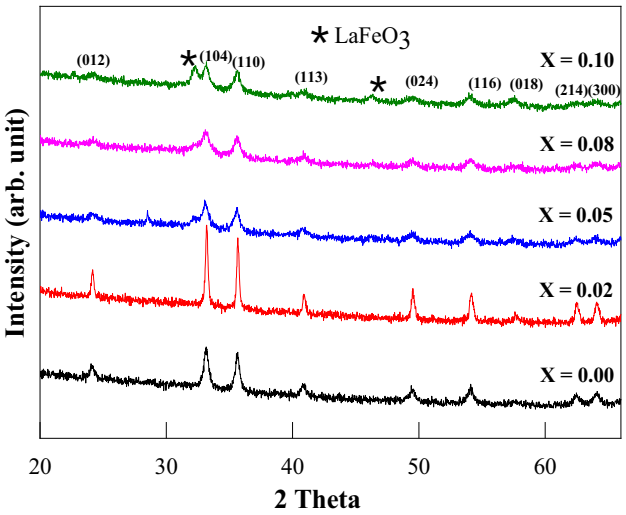

Fig. 1 XRD patterns of $Fe_{2-2X}La_{2X}O_3$ (X=0.00, 0.02, 0.05, 0.08,0.10) nanoparticle samples

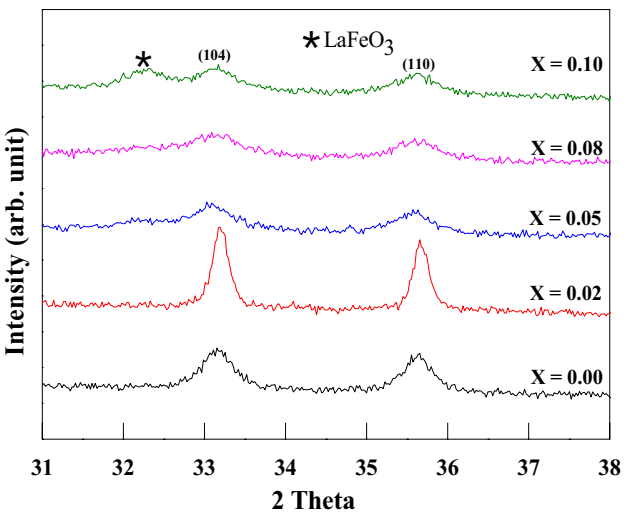

Fig. 2 XRD patterns of $Fe_{2-2X}La_{2X}O_3$ (X=0.00, 0.02, 0.05, 0.08, 0.10) samples indicating peak shifts toward lower angle

a secondary phase of $LaFeO_3$ (JCPDS No. 96–154-2033) at higher concentration along with the primary α-Fe_2O_3 phase may be due to a greater radius of La^{3+} (1.6061 Å) than Fe^{3+} (0.645 Å), as La^{3+} well incorporated between interstitial location in Fe^{3+} below X = 0.08 of La doping. But above a particular concentration (X = 0.10), the hoarding of La ions begins over the lattice surface. The additional peaks of the secondary phase are noticed for X = 0.10 of La doping, as evident from Fig. 2 [47]. Interestingly, the peak intensities of the α-Fe_2O_3 phase get increased

for the low-concentration doping of La content ($X = 0.02$), which favored the growth of the parent crystal. Moreover, the crystallite size (D) of all the synthesized samples has been estimated with the help of Debye-Scherer's formula [48].

$$D = \frac{0.89\lambda}{\beta \cos\theta}, \quad (1)$$

where the wavelength of the X-ray is taken as $\lambda = 1.54$ Å, while β and θ represent the fullwidth at half maximum (FWHM) and Bragg angle, respectively [45, 49]. The crystallite size of the pure α-Fe_2O_3 sample is ~ 18.1 nm which is increased drastically when doping of La content at low concentration. On further increasing the doping concentration, the crystallite size decreases significantly. However, it increases slightly at a high doping La concentration ($X = 0.10$) at saturation. The calculated value of crystallite size and lattice parameter is summarized in Table 1, which indicates an enhancement in the FWHM of the diffraction peaks with increasing La concentration in the host lattice of α-Fe_2O_3 leads to a reduction in crystallite size [50]. The incorporation of La ions into the Fe-site of α-Fe_2O_3 results in the enhancement of lattice parameter values ($a = b$ and c) below $X = 0.08$, after that (at $X = 0.10$) an indiscriminate variation is inspected. The structural anomaly indicated by non-uniform variation in crystallite size and lattice parameters in Table 1 may be attributed to the occurrence of secondary phase [51, 52].

Furthermore, it is also seen that peaks are shifted toward the lower angle side, as shown in Fig. 2. This shifting of diffraction peaks toward the lower Bragg angle indicates the presence of strain produced due to La doping in the α-Fe_2O_3 lattice (Fig. 3).

Table 1 Crystallites size, lattice parameters, and particle size of $Fe_{2-2X}La_{2X}O_3$ nanoparticles at different compositions

Compositions (X)	Crystallite size (nm)	Lattice parameters (Å)		Particle size (nm)
		a (= b)	c	
$X = 0.00$	18.1	5.039	13.215	51.42
$X = 0.02$	33.4	5.037	13.211	73.69
$X = 0.05$	15.3	5.040	13.226	68.92
$X = 0.08$	13.5	5.061	13.232	54.93
$X = 0.10$	16.7	5.063	13.250	141.57

3.2 FESEM and EDS analysis

FESEM micrographs of $Fe_{2-2X}La_{2X}O_3$ (X = 0.00, 0.02, 0.05, 0.08, and 0.10) are shown in Fig. 4. The average particle size of the pure sample and La-doped hematite samples was analyzed using IMAGE-J software. The estimated particle size of the pure sample is ~ 51 nm, while it lies between ~ 54 and ~ 141 nm for α-$Fe_{2-2X}La_{2X}O_3$ samples. It can be observed from the micro-images (Fig. 4) that undoped hematite microstructure is comparatively fine and uniform, as compared to that of higher La doping concentration, which may be due to an increase in the average value of particle size on account of larger ionic radii of the La^{3+} than the host Fe^{3+} ions [53–55].

Additionally, EDS analysis is used to confirm the La incorporation in the synthesized sample, as displayed in Fig. 5. The EDS spectrum of pure hematite (Fig. 5(a)) shows only the peaks corresponding to the elements iron (Fe) and oxygen (O) [56]. Conversely, EDS spectra of La-doped hematite samples (Fig. 5(b-e)) show the additional peaks of La along with Fe and O. The experimental weight percentage is shown in Table 2.

3.3 FTIR analysis

The Vibrational study using infrared absorption has been carried out to gain more information on the crystal structure. FTIR plots of $Fe_{2-2x}La_{2x}O_3$ samples ranging from 400 cm^{-1} to 4000 $cm^{-1}$are shown in Fig. 3. The O–H bending mode of hydroxyl group is represented by bands emerging at 3448.8, 2924.2, and 2850.9 cm^{-1} but asymmetric as well as symmetric vibration of -CH_3 kind groups are represented by the bends at 1629.9 cm^{-1} [57–59]. The FTIR bands emerging at 1109.1 and 1383.0 cm^{-1} are assigned for –CH_2 and outstanding hydroxyl group C–OH, respectively[60, 61]. However, the bands appearing at 457.7 and 547.8 cm^{-1} are corresponding to E_u and A_{2u}, two characteristic modes in α-Fe_2O_3 [62]. The overlapping of A_{2u} and E_u vibrations in transverse direction to the c-axis can be correlated with the band at 547.8 cm^{-1}which may attribute to the elongated Fe–O vibration. The two vibration modes A_{2u} and E_u can be overlapped because they loss the inversion point simultaneously. Also, both are antisymmetric to inversion. The energies of these states are close due to slight change in polarization change.

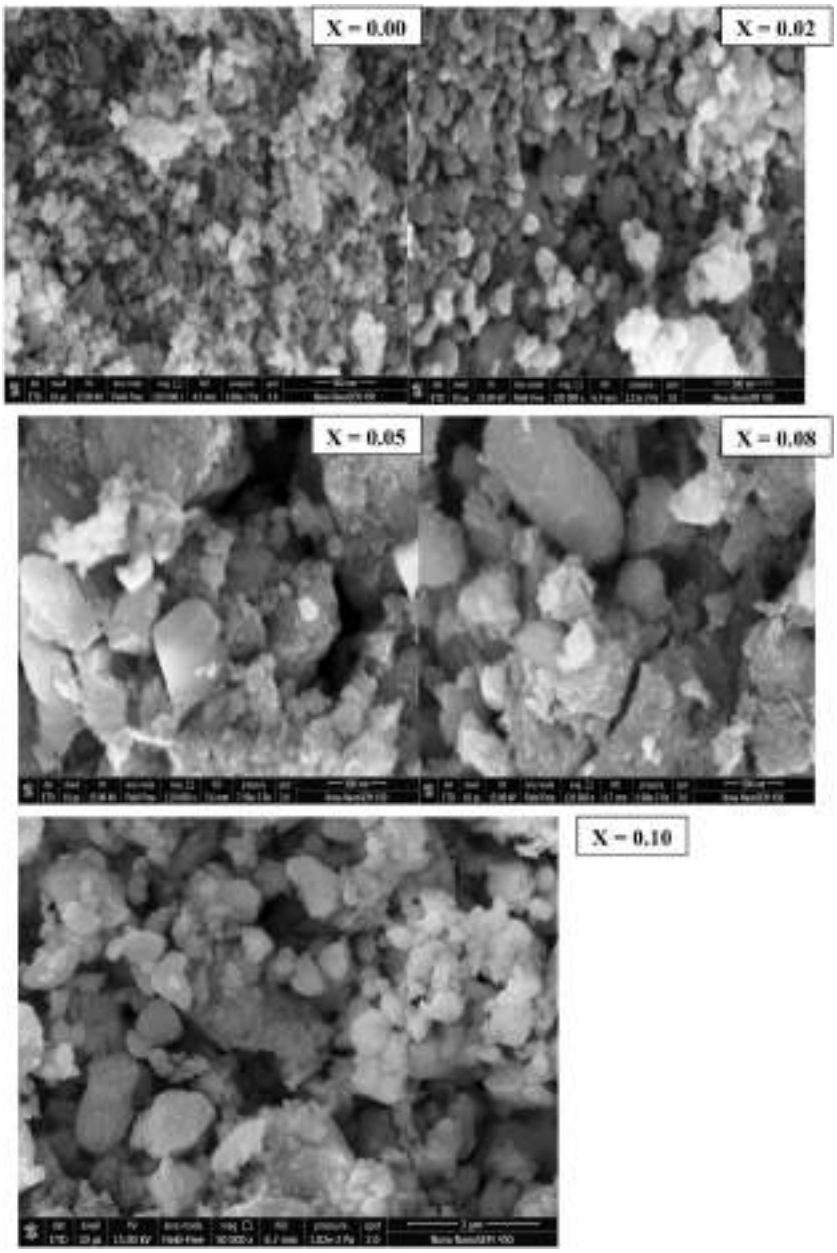

Fig. 3 FE-SEM micrograph of α-$Fe_{2-2X}La_{2X}O_3$ ($X = 0.00$, 0.02, 0.05, 0.08,0.10) samples

Furthermore, from Fig. 3, it is also examined that with the incorporation of La into the hematite lattice at $X = 0.02$, an increase in peak intensity indicates an enhancement in crystalline nature at this composition, but for higher doping concentration[63], the intensity of E_u and A_{2u} modes is observed to reduce the peaks intensity which reveal that crystallinity of the α-Fe_2O_3 degrading with a higher doping level of La. FTIR spectroscopy investigation and XRD prediction are in good agreement to predict the crystalline nature of synthesized samples. The assignment of the observed bands are given in Table 3.

3.4 Temperature-dependent resistivity analysis

The variation of resistivity for La-doped α-Fe_2O_3 nanoparticles in the temperature range 100–400 K is shown in Fig. 6. There is not much significant variation in the resistivity of α-$Fe_{2-2x}La_{2x}O_3$ up to 300 K but above 300 K resistivity is observed to decrease exponentially with

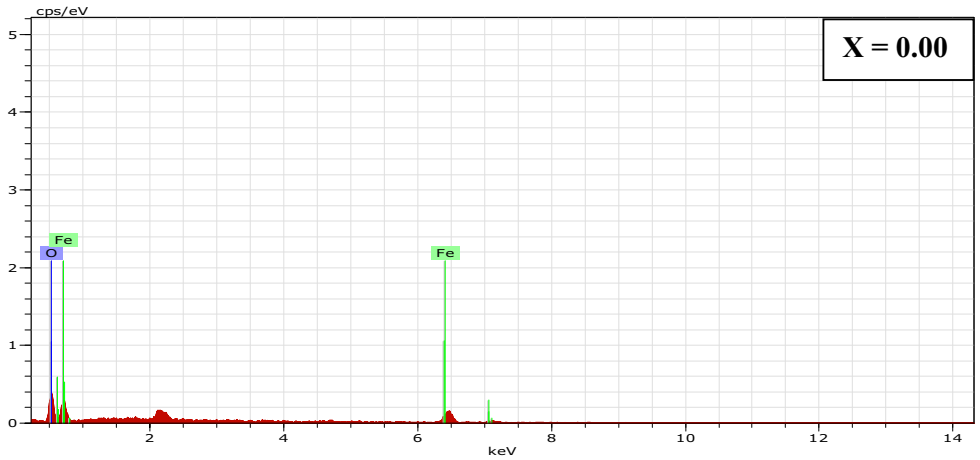

(a)

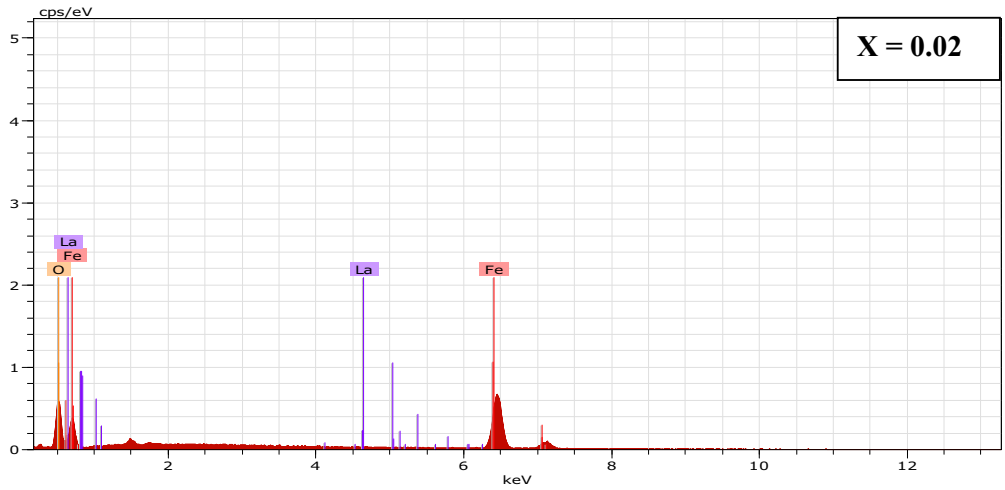

(b)

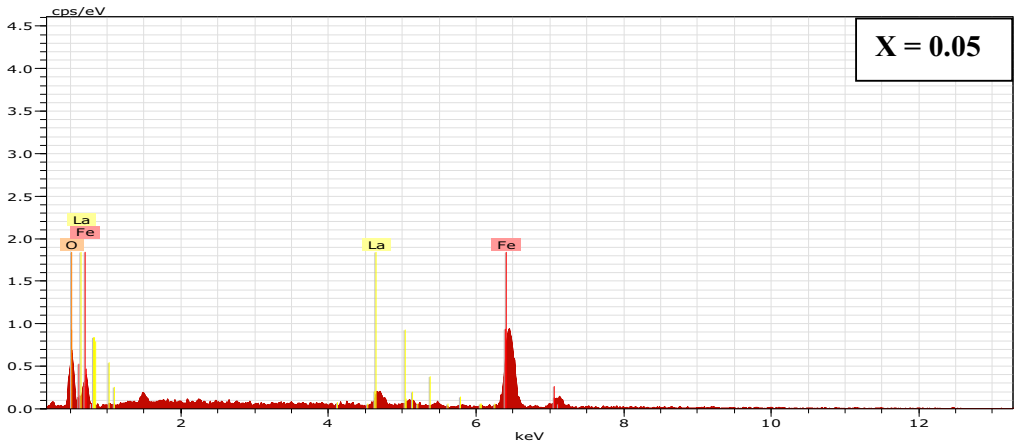

(c)

Fig. 4 **a–e** EDS spectrographs of $Fe_{2-2X}La_{2X}O_3$ ($X = 0.00, 0.02, 0.05, 0.08, 0.10$) respectively

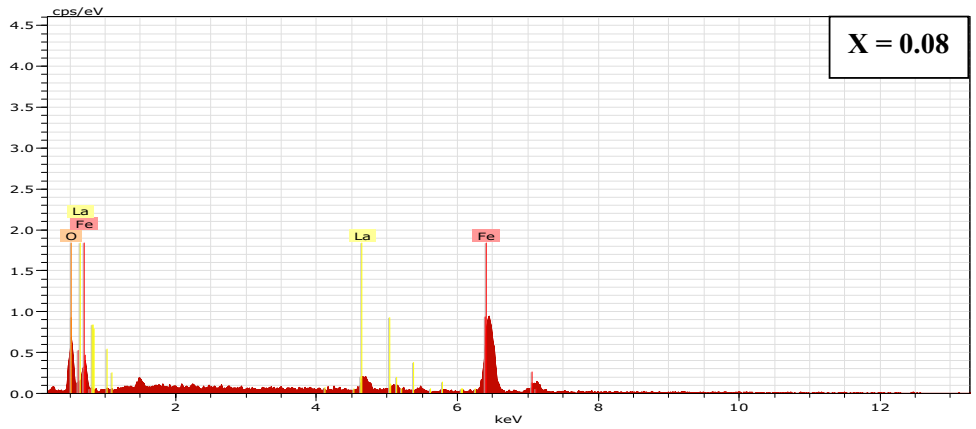

(d)

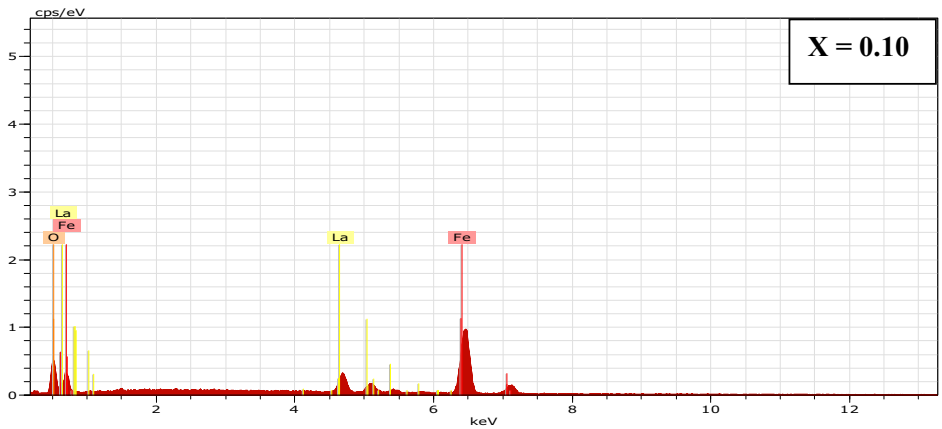

(e)

Fig. 4 continued

increasing temperature that can be explained based on improved drift velocity charge carriers due to thermal energy which confirms the semiconducting behavior of the synthesized materials [64]. These two resistivity variation regions (100–300 K and 300–400 K) may be attributed to two kinds of conduction mechanisms variable-range hopping and nearest-neighbor hopping, respectively. At lower temperature, the charge carriers cannot contribute to conduction due to a lack of thermal energy but at higher temperature charge carriers gain sufficient thermal to cross-grain boundaries and contributes to conduction resulting in reduced electrical resistivity. It is observed from Fig. 6, the resistivity plots that the substitution of La ions in Fe_2O_3 lattice leads to an increase in resistivity due to a decrease in the Fe^{3+} ions concentration on La substitution which in turn reduces the rate of electron transport hopping. The resistivity values of samples are summarized in Table 3. The elevated resistivity indicates the high insulating behavior, which can be well linked with our observation regarding the increase in dielectric constant with increasing La concentration. [65–67].

3.5 Dielectric analysis

Figure 7 illustrates the variation of dielectric constants with temperatures ranging from 100 to 400 K of $Fe_{2-2X}La_{2x}O_3$ ($X = 0.00$, 0.02, 0.05, 0.08, and 0.10) nanoparticles at selected frequencies range (0.1 to 0.4 MHz). The value of real dielectric constant of pure and La-doped hematite nanoparticles was determined with the help of Eq. (2) given as follows:

$$\varepsilon' = C_p d/\varepsilon_0 A \tag{2}$$

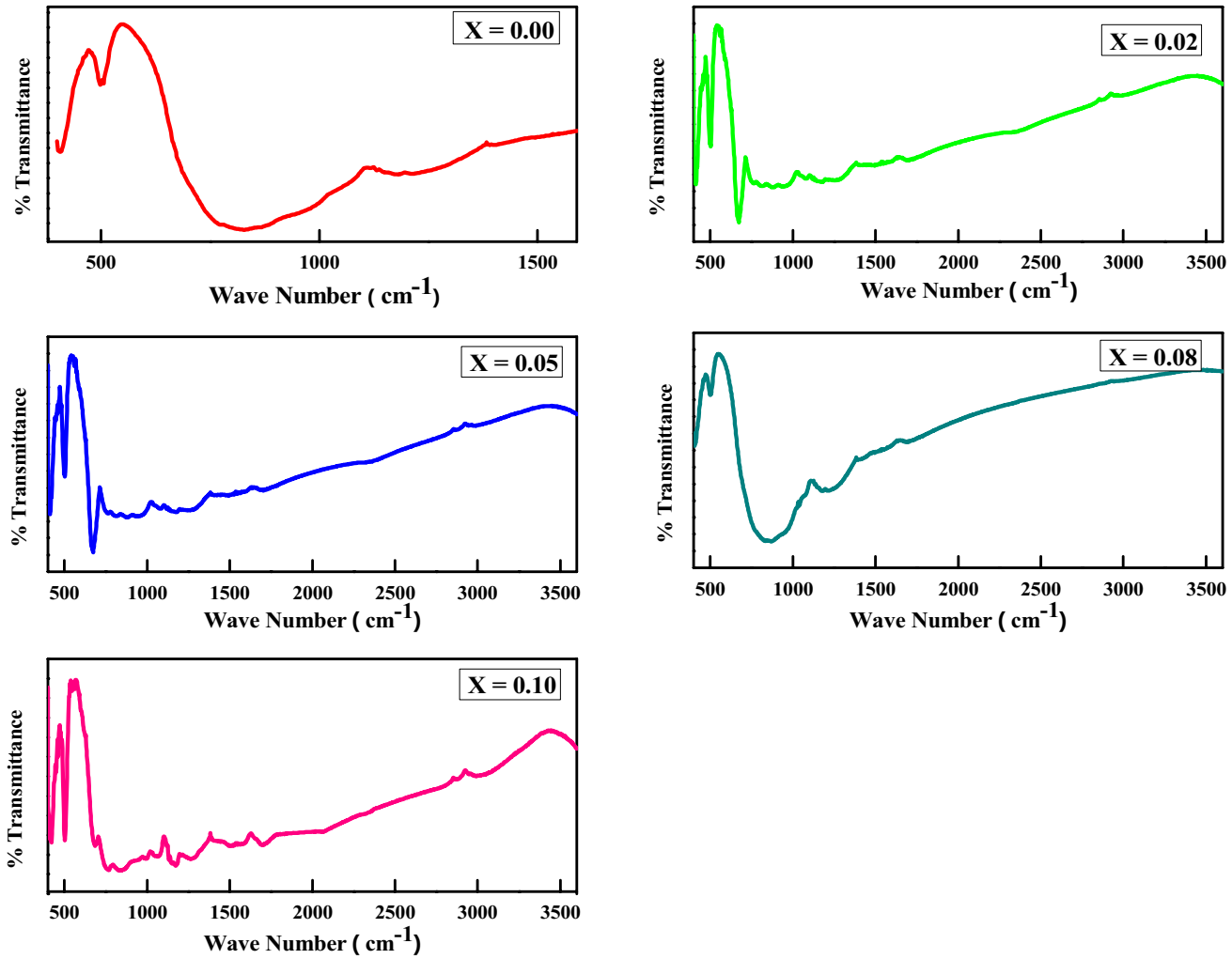

Fig. 5 FTIR-spectra of $Fe_{2-2X}La_{2X}O_3$ ($X = 0.00$, 0.02, 0.05, 0.08 and 0.10) samples

where ε_0 is the free space permittivity, d denotes the distance between the plates, and '*A*' is used for the area of plates [68].

The dielectric constant observed to exhibit weak frequency dispersion along with low temperature dependence for all samples below ~ 200 K which may be attributed to the inability of dipoles to orient themselves in field direction due to lack of thermal energy. Contrary to this, the thermal energy triggers space-charge polarization with increasing temperature ($T > 220$ K) due to the liberation of more localized dipoles. All these factors result in the increased value of ε′ in the high-temperature region which is a general behavior in the case of the ionic solids [69, 70]. The dependence of the dielectric constant on frequency can be correlated and explained with help of cole–cole model [71] as well as Maxwell–Wagner type model [72] of interfacial polarization with the help of Koop's theory [73, 74]. The high value of dielectric constant at lesser frequencies side exhibits grain boundaries contribution. While with the increase of frequency of the applied field, the involvement of grains predominates hence resulting in lowering the dielectric constant. The electrons hopping inside grains causes them to pile up on grain boundaries leading to space-charge polarization, and thereby, the dielectric constant gets elevated at low frequencies. But with increasing frequency, a decrease in orientation polarizability can be observed, due to the exchange of electrons between ions Fe^{2+} and Fe^{3+} and start lagging behind the applied field. This reduced the probability of electrons shifting on grain boundary and hence dielectric constant drop at a higher frequency. The all-over increased dielectric constant with increasing La concentration may be

Table 2 Weight % of Fe, O, and La in α-$Fe_{2-2x}La_{2x}O_3$ ($X = 0.00$, 0.02, 0.05, 0.08, and 0.10) nanoparticles

La doping concentration	Elements	Experimental (weight %)
$X = 0.00$	Fe	74.62
	O	25.38
$X = 0.02$	Fe	58.77
	O	40.68
	La	0.54
$X = 0.05$	Fe	56.76
	O	38.35
	La	04.89
$X = 0.08$	Fe	62.97
	O	32.45
	La	04.58
$X = 0.10$	Fe	66.98
	O	25.45
	La	07.57

attributed to doping induced non-Centro symmetric nature ferrite lattice, resulting in improved atomic polarizability and formation of $LaFeO_3$ secondary phase distributed on the grain boundaries resulting in the piling space charges there [65, 75]. Since polarization and unit cell volume is inversely proportional to each other [70]. The value of dielectric constant first increases for $X = 0.02$ concentration of La due to the reduction in lattice cell parameters and then decreases from $X = 0.05$ to $X = 0.10$ of La doping concentration due to its increased lattice parameter and unit cell volume. Dielectric constant values (selected frequencies) at 100 K are summarized in Table 3.

Dielectric loss (tanδ of the samples has been obtained in the frequency range 0.1 MHz to 0.4 MHz as a function of temperature ranging from 100 to 400 K. The plots between dielectric loss and temperature are shown in Fig. 8. Initially, at 400 K, the dielectric loss of $Fe_{2-x}La_{2x}O_3$ ($X = 0.00$, 0.02, 0.05, 0.08, and 0.10) synthesized samples increases with 0% to 8% concentration in the host lattice and decreases with 10% concentrations of La at 400 K.

This type of variation can be explained with the help of the Cole–Cole model [69] and Debye's relation, $\tan\delta = \omega\tau/1+\omega^2\tau^2$ where ω denotes angular frequency of applied field and τ is used for relaxation time. With the increase of ω, factor tanδ decreases accordingly. Further at a particular frequency, the variation in tanδ plot can be attributed to the relaxation time [76, 77]. At low temperature, relaxation time is more and its value decreases with the increase in temperature which may be related to Koop's phenomenological theory. At higher concentration ($X = 0.100$), the loss has been decreased due to secondary phase of $LaFeO_3$ [65]. The calculated value of Dielectric loss (tanδ from graph at

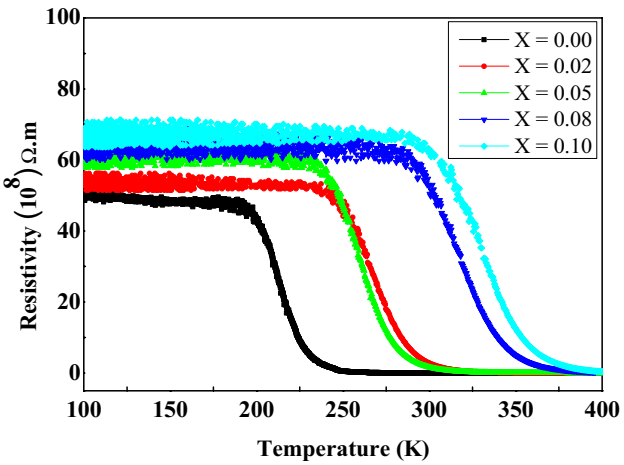

Fig. 6 Electrical resistivity versus temperature of $Fe_{2-2x}La_{2x}O_3$ ($X = 0.00$, 0.02, 0.05, 0.08, and 0.10) samples

Table 3 The assignment of the observed bands of IR for of $Fe_{2-2X}La_{2X}O_3$ ($X = 0.00$, 0.02, 0.05, 0.08, and 0.10) samples

IR bands in cm^{-1}	Assignment	References
3448.8	O–H Bending (hydroxyl group)	[57–59]
2924.2	O–H Bending (hydroxyl group)	[57–59]
2850.9	O–H Bending (hydroxyl group)	[57–59]
1629.9	$–CH_3$Symmetric & Asymmetric vibrations	[57–59]
1109.1	$–CH_2$ Mode	[60, 61]
1383.0	C-OH (hydroxyl group)	[60, 61]
457.7	E_u Characteristic modes	[62]
547.8	A_{2u} Characteristic modes,	[62]
547.8	The overlapping of A_{2u} and E_u vibrations band (elongated Fe–O vibration)	[62]

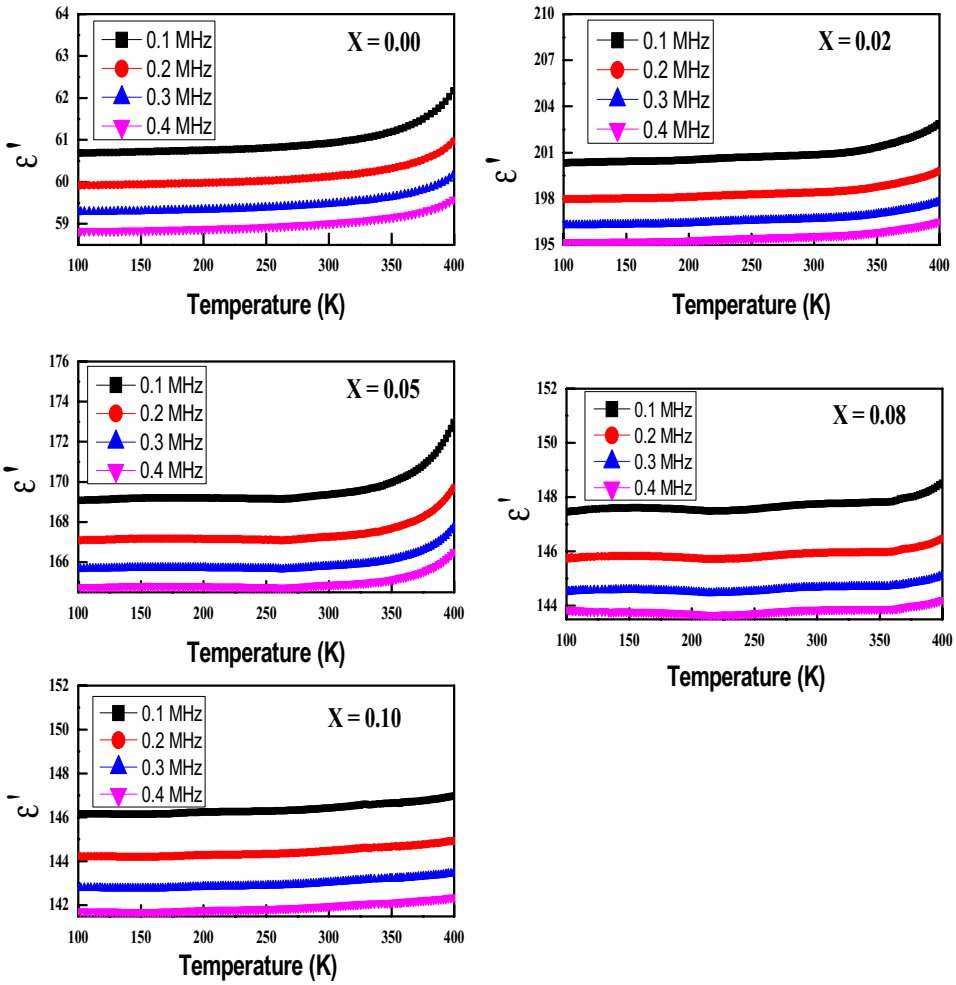

Fig. 7 Variation of dielectric constant with temperature at different frequencies of $Fe_{2-2x}La_{2x}O_3$ ($X = 0.00$, 0.02, 0.05, 0.08, and 0.10) nanoparticles

selected frequencies (0.1 MHz and 0.4 MHz) and temperature (400 K) are summarized in Table 4.

3.6 VSM analysis

The magnetic behavior of synthesized La-doped hematite nanoparticle samples was understood through M-H loops at room temperature, as depicted in Fig. 8, 9. The observed different magnetic parameters such as coercivity (H_c), remanence magnetization (M_R), and maximum magnetization (M_S) are summarized in Table 4. From all M-H traces at room temperature, we observed that there is no saturation magnetization up to a field strength of 20,000 Oe which reveals that there is a presence of superparamagnetic particles. Furthermore, it has been also revealed that the presence of these non-saturated hysteresis loops at different concentrations means the wide distribution of particle size in the system [28]. Consequently, it may be concluded that the system not only consists of superparamagnetic particles, but agglomeration also contributes to the hysteresis behavior [78] (Table 5).

From this hysteresis curve, it is observed for the coercivity (H_C) that it decreases at $X = 0.02$ due to small particle size; however, this curve shows the high value of coercivity (H_C) at higher concentrations, which may be due to an increase in the particle size [79].

4 Conclusions

Enhanced value of dielectric constant and magnetic properties for $Fe_{2-2X}La_{2X}O_3$ ($X = 0.00$,0.02,0.05,0.08,0.10) in comparison to pure hematite was observed and accredited to the microstructural variation encouraged by the incorporation of La^{3+} ions for Fe^{3+} ions. Increasing La^{3+} concentration to $X = 0.10$ migration of La^{3+} ion results in the

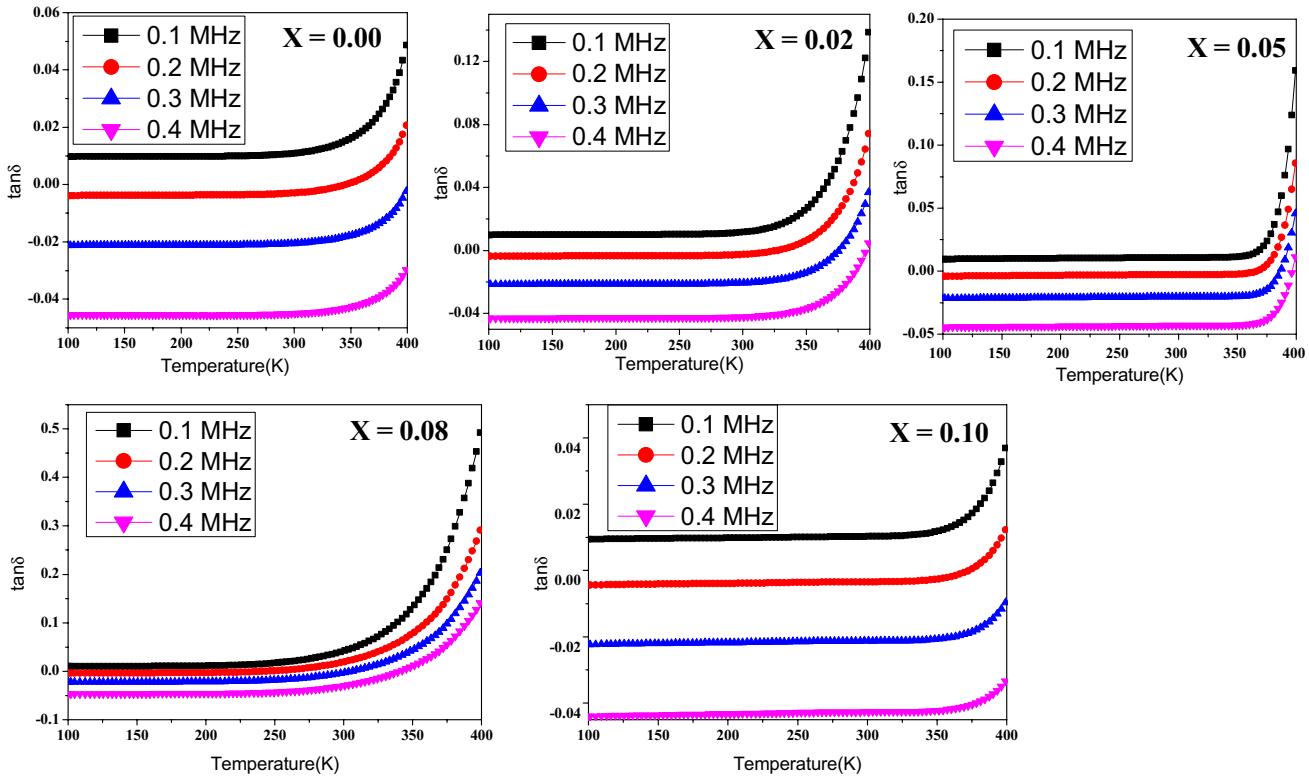

Fig. 8 Dielectric loss versus temperature at different frequencies for$Fe_{2-2x}Y_{2x}O_3$ (X=0.00, 0.02, 0.05, 0.08, and 0.10) nanoparticles

Table 4 Resistivity and dielectric constants (at selected frequencies) of pure and La-doped hematite nanoparticles at 100 K

Doping concentration (X)	Resistivity at 100 K ($\times 10^8$ Ωm)	Dielectric constant (100 K)			
		0.1 MHz	0.2 MHz	0.3 MHz	0.4 MHz
X=0.00	54.06	60.76	59.96	59.30	58.83
X=0.02	66.69	200.32	197.95	196.31	195.22
X=0.05	63.64	169.11	167.16	165.76	164.65
X=0.08	60.11	147.51	145.86	144.62	143.80
X=0.10	56.57	146.20	144.29	142.89	141.74

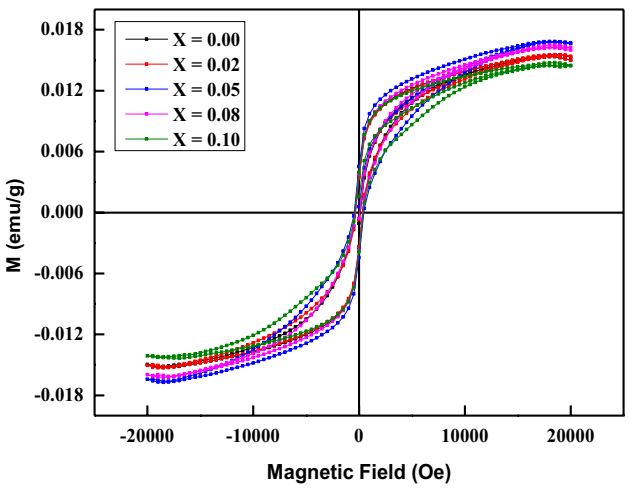

Fig. 9 M-H curves of $Fe_{2-2x}La_{2x}O_3$ (X=0.00,0.02,0.05,0.08, and 0.10) samples at room temperature

development of impurity phases of $LaFeO_3$. The dielectric constant observed increases with increasing La concentration in comparison to pure α-Fe_2O_3 mainly due to the non-centrosymmetric nature of the ferrite lattice, improved atomic polarizability, and formation of $LaFeO_3$ phase at the grain boundaries. But the value of dielectric constant decreases for higher La concentration (X = 0.05 to X = 0.10) due to increased lattice parameter and hence unit cell volume. Investigation of resistivity data indicates the variable-range hopping and nearest-neighbor hopping conduction mechanisms that are effective in the 100 to 300 K and 300 to 400 K temperature slots, respectively. The frequency dependency of the

Table 5 Coercivity (H_C), remanence magnetization (M_R) & maximum magnetization (M_S) of pure and La-doped hematite nanoparticles

Samples doping concentration (X)	M_R (emu/g)	M_S (emu/g)	H_C (O_e)	(M_R/M_S)
$X=0.00$	0.0037	0.0153	365.54	0.241
$X=0.02$	0.0033	0.0154	339.20	0.214
$X=0.05$	0.0044	0.0167	459.03	0.263
$X=0.08$	0.0036	0.0162	371.46	0.222
$X=0.10$	0.0039	0.0144	402.04	0.270

dielectric constant may also be understood based on the space-charge polarization mechanism by using Koop & Maxwell–Wagner's models. Furthermore, it has also been noticed that the average value of coercivity (H_C) and remanence magnetization (M_R) are enhanced for hematite materials doped with Lanthanum.

Acknowledgements

The authors are grateful to Dr. K. Asokan and R. C. Meena, IUAC, New Delhi for providing facilities for the measurement of resistivity and dielectric properties. IIT, Roorkee(India) is also acknowledged for help in the VSM measurements.

Authors contribution

All authors contributed to the investigation design and conception. Material preparation, data collection, and first draft were performed by VK under the supervision ofDSA. Analysis and discussion contributed by VK, DSA, AS, and RS.All authors read, improved, and approved the final manuscript.

Funding

This work was supported by Chaudhary Devi Lal University, Sirsa, and UGC, New Delhi by providing JRF & contingency to VK under supervisor DSA.

Declarations

Conflict of interest The authors declare no competing interests.

Data availability The authors declare that the data supporting the findings are available within the paper and supplementary information files not available.

References

1. T.S. Ahmadi, Z.L. Wang, T.C. Green, A. Henglein, M.A. Elsayed, Shape controlled synthesis of colloidal platinum nanoparticles. Sci. **272**, 1924 (1996)
2. H. Mattoussi, L.H. Radzilowski, B.O. Dabbousi, E.L. Thomas, M.G. Bawendi, M.F. Rubner, Electroluminescence from heterostructures of poly (phenylenevinylene) and inorganic CdSe nanocrystals. J. Appl. Phys. **83**, 7965 (1998)
3. W.U. Huynn, J.J. Dittmer, A.P. Alivisatos, Hybrid nanorod-polymer solar cells. Sci. **295**, 2425 (2002)
4. N.C. Pramanik, T.I. Bhuiyan, M. Nakanishi, T. Fujii, J. Takada, S. Seok, Synthesis and characterization of cerium substituted hematite by sol-gel method. Mater. Lett. **59**, 3783 (2005)
5. C. Burda, X. Chen, R. Narayanan, M.A. El-Sayed, Chemistry and properties of nanocrystals of different shapes. Chem. Rev. **105**, 1025 (2005)
6. P. Tartaj, M. Del Puerto Morales, S. Veintemillas-Verdaguer, T. Gonzalez-Careno, C.J. Serna, The preparation of magnetic nanoparticles for applications in biomedicine. J. Phys. D Appl. Phys. **36**, 182 (2003)
7. A.K. Gupta, M. Gupta, Synthesis and surface engineering of iron oxide nanoparticles for biomedical applications. Biomater. **26**, 3995 (2005)
8. J. Murbe, A. Rechtenback, J. Topfer, Synthesis and physical characterization of magnetite nanoparticles for biomedical applications. Mater. Chem. and Phys. **110**, 426 (2008)
9. A.S. Teja, P.Y. Koh, Synthesis, properties, and applications of magnetic iron oxide nanoparticles. Prog Crystal Growth Charact. Mater. **55**, 22–45 (2009)
10. S. Mitra, S. Das, K. Mandal, S. Chaudhuri, Synthesis of α-Fe_2O_3 Nanocrystalline its different morphological attributes: Growth, mechanics, optical and magnetic properties. Nanotech. **18**, 275608 (2007)
11. J. Jacob, M.A. Khadar, VSM and Mossbauer study of nanostructured hematite. J. Magn. Magn. Mater. **322**, 614 (2010)

12. R. Yao, C. Cao, Self-assembly of α-Fe_2O_3 mesocrystals with high coercivity. RSC Adv. **2**, 1979 (2012)
13. V. Malik, S. Sen, D.R. Getting, M.G. Josifovska, M. Schmidt, P. Guptasarma, Field-enhanced magnetic moment in ellipsoidal nano-hematite. Mater. Res. Express **1**, 026114 (2014)
14. W.B. Ingler, J.P. Baltrus, S.U.M. Khan, Photoresponse of p-type zinc-doped iron(iii) oxide thin films. J. Am. Chem. Soc. **126**, 10238 (2004)
15. V.R. Satsangi, S. Kumari, A.P. Singh, R. Shrivastav, S. Dass, Nanostructure hematite for photoelectrochemical generation of hydrogen. Int. J. Hydrogen Energ. **33**, 312 (2008)
16. A.K. Shwarsctein, Y.S. Hu, A.J. Forman, G.D. Stucky, E.W. McFarland, Electrodeposition of α-Fe_2O_3 doped with Mo or Cr as photoanodes for photocatalytic water splitting. J. Phys. Chem. C **112**, 15900 (2008)
17. H. Kockar, M. Bayirli, M. Alper, A new example of the diffusion-limited aggregation: Ni–Cu film patterns. Appl. Surf. Sci. **256**, 2995 (2010)
18. Y. Koseoglu, F. Kurtulus, H. Kockar, H. Guler, O. Karaagac, S. Kazan, B. Aktas, Magnetic characterizations of cobalt oxide nanoparticles. J. Supercond. Nov. Magn. **25**, 2783 (2012)
19. Y. Lin, Y. Xu, M.T. Mayer, Z.I. Simpson, G. McMahon, S. Zhou, D. Wang, Growth of p-type hematite by atomic layer deposition and utilization for improved solar water splitting. J. Am. Chem. Soc. **134**, 5508 (2012)
20. P. Liao, J.A. Keith, E.A. Carter, Water oxidation on pure and doped hematite (0001) surfaces prediction of Co and Ni as effective dopants for electrocatalysis. J. Am. Chem. Soc. **134**, 13296 (2012)
21. F. Ozel, H. Kockar, S. Beyaz, O. Karaagac, T. Tanrisever, Superparamagnetic iron oxide nanoparticles: effect of iron oleate precursors obtained with a simple way. J. Mater. Sci. Mater. Electron. **24**, 3073 (2013)
22. O. Karaagac, B. Bilir, H. Kockar, Superparamagnetic cobalt ferrite nanoparticles: Effect of temperature and base concentration. J. Supercond. Nov. Magn. **28**, 1021 (2015)
23. F. Bodker, M.F. Hansen, C.B. Koch, K. Lefmann, S. Morup, Magnetic properties of hematite nanoparticles. Phys. Rev. B **61**, 6826 (2000)
24. M.F. Hansen, C.B. Koch, S. Morup, Magnetic dynamics of weakly and strongly interacting hematite nanoparticles. Phys. Rev. B **62**, 1124 (2000)
25. C. Frandsen, C.R.H. Bahl, B. Lebech, K. Lefmann, L.T. Kuhn, L. Keller, N.H. Andersen, M.V. Zimmermann, E. Johnson, S.N. Klausen, S. Morup, Oriented attachment and exchange coupling of α-Fe_2O_3 nanoparticles. Phys. Rev. B **72**, 214406 (2005)
26. C.R. De Silva, S. Simth, I. Shim, J. Pyun, T. Guta, J. Jiao, Z. Zheng, Lanthanide (III)-doped magnetite nanoparticles. J. Am. Chem. Soc. **131**, 6336 (2009)
27. L.E. Mathevula, L.L. Noto, B.K. Mothudi, M.S. Dhlamini, Structural and optical properties of α-Fe_2O_3nanoparticles influence by holmium ions. Physica B **535**, 258 (2018)
28. R. Bhat, B. Want, A. Firdous, G.N. Dar, Probing of electric and magnetic properties of holmium doped iron oxide nanoparticles. J. Mater. Sci. Mater. Electron. **29**, 19472 (2018)
29. V. Kumar, D.S. Ahlawat, S.A. Ul Islam, A. Singh, Ce doped induced modifications in the structural, electrical and magnetic behavior of hematite nanoparticles. Mater. Sci. Eng. B **272**, 115327 (2021)
30. H. Wan, P. Rong, X. Liu, L. Yang, Y. Jiang, N. Zhang, R. Ma, S. Liang, H. Wang, G. Qiu, Morphological evolution and magnetic property of rare-earth-doped hematite nanoparticles: promising contrast agents for T1-weighted magnetic resonance imaging. Adv. Funct. Mater. **27**, 1606821 (2017)
31. S.K. Abdel-Aal, A.S. Abdel-Rahman, Graphene influence on the structure, magnetic, and optical properties of rare-earth perovskite. J Nanoparticle Res **22**, 267 (2020)
32. M. Houshiar, L. Jamilpanah, Effect of Cu dopant on the structural, magnetic and electrical properties of Ni-Zn ferrites. Mater. Res. Bull. **98**, 213–218 (2018)
33. S.K. Abdel-Aal, M.F. Kandeel, A.F. El-Sherif, A.S. Abdel-Rahman, Synthesis, characterization, and optical properties of new organic–inorganic hybrid perovskites [(NH3)2(CH2)3]CuCl4 and [(NH3)2(CH2)4]CuCl2Br 2. Phys. Status Solidi A (2021). https://doi.org/10.1002/pssa.202100036
34. S.K. Abdel-Aal, A.S. Abdel-Rahman, G.G. Kocher-Oberlehner, A. Ionov, R. Mozhchil, Structure, optical studies of 2D hybrid perovskite for photovoltaic applications. Acta Cryst **A70**, C1116 (2017). https://doi.org/10.1107/S2053273317084583
35. T.T. Ahmed, I.Z. Rahman, M.A. Rahman, Study on the properties of the copper substituted Ni-Zn ferrites. J. Mater. Process. Technol. **153**, 797 (2004)
36. J.S. Justus, S.D.D. Roy, A.M.E. Raj, Influence of lanthanum doping on the structural and optical properties of hematite nanopowders. J. Appl. Sci. Eng. Methodol. **2**, 272 (2016)
37. D. Ravinder, M. Hashim, A. Upadhyay, M.M. Ismail, S. Kumar, R. Kumar, S.S. Meena, A. Khalilullah, Investigation of structural and magnetic properties of La doped Co–Mn ferrite nanoparticles in the presence of α-Fe_2O_3 phase. Solid State Commun. **342**, 114629 (2022)

38. X.-L. Cheng, J.-S. Jiang, C.-Y. Jin, C.-C. Lin, Yi. Zen, Q.-L. Zhang, Cauliflower-like α-Fe_2O_3 microstructures, Toluene-water interface-assisted synthesis, characterization and applications in wastewater treatment and visible-light photocatalysis. Chem. Eng. J. **216**, 139 (2014)
39. A. Lassoued, B. Dkhil, A. Gadri, S. Ammar, Control of the shape and size of iron oxide (α-Fe_2O_3) nanoparticles synthesized through the chemical precipitation method. Results Phys. **7**, 3007 (2017)
40. S. Surjeet Chahal, K. Ashok, K. Parmod, Zn doped α-Fe_2O_3: an efficient material for UV driven photocatalysis and electrical conductivity. Crystals **10**, 273 (2020)
41. G. Neri, A. Bonavita, G. Rizzo, S. Galvango, P. Siciliano, Methanol gas sensing properties of CeO_2 α-Fe_2O_3 thin films. Sens. Actuators B Chem. **114**, 687 (2006)
42. Y. Liu, D. Sun, Effect of CeO_2 doping on catalytic of Fe_2O_3 / γ-Al_2O_3 catalyst for catalytic wet peroxide oxidation of azo dyes. J. Hazard. Mater. **143**, 448 (2007)
43. K. Rama Krishna, K. Vijaya Kumar, D. Ravinder, Structural and electrical conductivity studies in nickel-zinc ferrite. Adv. Mater. Phys. Chem. **2**, 185 (2012)
44. V.V. Awati, S.M. Rathod, S.E. Shirsath, M.L. Mane, Fabrication of Cu^{2+} substituted nanocrystalline Ni–Zn ferrite by solution combustion route: Investigations on structure, cation occupancy and magnetic behavior. J. Alloys Compound **553**, 157 (2013)
45. P. Kumar, V. Singh, V. Sharma, G. Rana, H.K. Malik, K. Asokan, Investigation of phase segregation in yttrium doped zinc oxide Ceram. Intern. **41**, 6734 (2015)
46. F. Gao, G. Qin, Y. Li, Q. Jiang, L. Luo, K. Zhao, One-pot synthesis of La-doped SnO_2 layered nanoarrays with an enhanced gas-sensing performance toward acetone. RSC Adv. **6**, 10298 (2016)
47. AsmaAslama, Atta Ur Rehmana, Nasir Amin, M. Ajaz un Nabi, Quratul ain Abdullah, N. A. Morley, Muhammad Imran Arshad, Hafiz T. Ali, Mohammad Yusuf, ZartashiaLatif, KiranMehmood, Lanthanum doped $Zn_{0.5}Co_{0.5}La_XFe_{2-X}O_4$ spinel ferrites synthesized via co-precipitation route to evaluate structural, vibrational, electrical, optical, dielectric, and thermoelectric properties, **154**, 110080 (2021)
48. H. Magnan, D. Stanescu, M. Rioult, E. Fonda, A. Barbier, Enhanced photoanode properties of epitaxial Ti-doped α-Fe_2O_3 (0001) thin films. Appl. Phys. Lett. **101**, 133908 (2012)
49. G. Rana, U.C. Jhori, A study on structural and magnetic properties of Ni-substituted magnetite nanoparticles. J. Alloy. Compd. **577**, 376 (2013)
50. M. Mohapatra, S.K. Sahoo, C.K. Mohanty, R.P. Das, S. Anand, Effect of Ce (IV) doping on the formation of goethite and its transformation to hematite. Mater. Chem. Phys. **94**, 417 (2005)
51. Y. Al Angari, Magnetic properties of La-substituted $NiFe_2O_4$ via egg-white precursor route. J. Magnet. Magnet. Mater. **323**, 1835 (2011)
52. N. Singh, A. Agarwal, S. Sanghi, P. Singh, Effect of magnesium substitution on dielectric and magnetic properties of Ni–Zn ferrite. Physica B **406**, 687 (2011)
53. T.I. Bhuiyan, M. Nakanishi, Y. Kusano, T. Fujii, Synthesis, morphology and color tone properties of the lanthanum substituted hematite. Mater. Lett. **61**, 3774 (2007)
54. K. Suzuki, E. Oho, Special raster scanning for reduction of charging effects in scanning electron microscopy. J. Scann. Microscopies **36**, 327 (2014)
55. S.A. Ul Islam, F.A. Andrabi, F. Mohmed, K. Sultan, M. Ikram, K. Asokan, Ba doping induced modifications in the structural, morphological and dielectric properties of double perovskite La_2NiMnO_6 ceramics. J. Solid State Chem. **290**, 121597 (2020)
56. R. Bhat, M. Qayoom, G.N. Dar, B. Want, Improved dielectric, conductivity and magnetic properties of erbium-doped α-Fe_2O_3 nanoparticles. J. Mater. Sci. Mater. Electron. **30**, 20914 (2019)
57. P.I.P. Soares, A.M.R. Alves, L.C.J. Pereira, J.T. Coutinho, I.M.M. Ferreira, C.M.M. Novo, J.P.M.R. Borges, Effects of surfactants on the magnetic properties of iron oxide colloids. J. Colloid Interface Sci. **419**, 46 (2014)
58. S. Liu, K. Yao, L. Fu, M. Ma, Selective synthesis of Fe_3O_4, γ-Fe_2O_3, and α-Fe_2O_3 using cellulose-based composites as precursors. RSC Adv. **6**, 2135 (2016)
59. M.F. Kandeel, S.K. Abdel-Aal, A.F. El-Sherif, H.S. Ayoub, A.S. Abdel-Rahman, Crystal structure and optical properties of 1D-bi based organic-inorganic hybrid perovskite. IOP Conf Series (2019). https://doi.org/10.1088/1757-899X/610/1/012063
60. S.K. Abdel-Aal, A.S. Abdel-Rahman, W.M. Gamal, M. Abdel-Kader, H.S. Ayoub, A.F. El-Sherif, M.F. Kandeel, S. Bozhko, E.E. Yakimovd, E.B. Yakimovd, Crystal structure, vibrational spectroscopy and optical properties of a one-dimensional organic–inorganic hybrid perovskite of $[NH_3CH_2CH(NH_3)\text{-}CH_2]bicl_5$. Acta Cryst B (2019). https://doi.org/10.1107/S2052520619011314
61. Y.P. Fu, C.H. Lin, C.S. Hsu, Preparation of ultrafine CeO_2, powders by microwave-induced combustion and precipitation. J. Alloys Compd. **391**, 110 (2005)
62. Y. Wang, A. Muramatsu, T. Sugimoto, FTIR analysis of well-defined α-Fe_2O_3 particles. Colloids Surf. A **134**, 281 (1998)
63. A.S. Abdel-Rahman, Many-body reduced vector solution and water vibrations (2022). Forthcoming, Nonlinear

Optics, Quantum Optics: Concepts in Modern Optics ISSN: 1543–0537 (print) url: https://www.oldcitypublishing.com/journals/nloqo-home/nloqo-forthcoming-papers/21104-2/, Available at SSRN: https://ssrn.com/abstract=4254290 or https://doi.org/10.2139/ssrn.4254290.

64. K. Bindu, K.M. Ajith, H.S. Nagaraja, Electrical, dielectric and magnetic properties of Sn-doped hematite (α-$Sn_XFe_{2-X}O_3$) nanoplates synthesized by microwave-assisted method. J. Alloy. Compd. **735**, 847 (2017)
65. K. Kamala Bharathi, C.V. Ramana, Improved electrical and dielectric properties of La-doped Co ferrite. J. Mater. Res. **26**, 584 (2011)
66. P. Kumar, G. Rana, G. Dixit, A. Kumar, V. Sharma, R. Goyal, K. Sachdev, S. Annapoorni, K. Asokan, Structural, electrical and magnetic properties of diluted Y doped $NiFe_2O_4$nanoparticles. J. Alloys Compd. **685**, 492 (2016)
67. Parmod Kumar, Vikas Sharma, Jitendra P. Singh, Ashish Kumar, Surjeet Chahal, K. Sachdev, K.H. Chae, Ashok Kumar, K. Asokan, D. Kanjilal, Journal of Magnetism and Magnetic Materials **489**, 165398 (2019).
68. M. Qayoom, K.A. Shah, A.H. Pandit, A. Firdous, G.N. Dar, Dielectric and electrical studies on iron oxide (α-Fe_2O_3) nanoparticles synthesized by modified solution combustion reaction for microwave applications. J. Electroceram. **45**, 7 (2020)
69. J. Liu, Y. Bin, M. Matsuo, Magnetic behavior of Zn-doped Fe_3O_4 nanoparticles estimated in terms of crystal domain size. J. Phys. Chem. C **116**, 134 (2012)
70. R. Geeta, C.J. Umesh, K. Asokan, Correlation between structural and dielectric properties of Ni-substituted magnetite nanoparticles. EPL **103**, 17008 (2013)
71. S. Holm, Time domain of characterization of the cole-cole dielectric model. J. Electr. Bioimp. **11**, 101 (2020)
72. K.W. Wagner, "ZurTheorie der UnvollkommenenDielektrika. Ann. Phys. **345**, 817 (1913)
73. J.P. Singh, S. Gautam, P. Kumar, A. Tripathi, J.M. Chen, K.H. Chae, K. Asokan, Correlation between the dielectric properties and local electronic structure of copper doped calcium titanate. J. Alloys Compd. **572**, 84 (2013)
74. L. Phor, V. Kumar, Structural, magnetic and dielectric properties of lanthanum substituted. Ceram. Int. **45**, 22972 (2019)
75. J.C. Anderson, *Dielectrics, Spottiswoode* (Ballantyne & Co., Ltd., London, 1964), p.177
76. S.K. Abdel-Aal, A.S. Abdel-Rahman, Fascinating physical properties of 2D hybrid perovskite, [(NH3)(CH2)7(NH3)] CuClxBr 4–x, x = 0, 2 and 4. J. Electron. Mater. **48**, 1686 (2019)
77. P. Kumar, P. Kumar, A. Kumar, R.C. Meena, R. Tomar, F. Chand, K. Asokan, Structural, morphological, electrical and dielectric properties of Mn doped CeO2. J. Alloy. Compd. **672**, 543–548 (2016)
78. M.K. Bharti, S. Chalia, P. Thakur, A. Thakur, Effect of lanthanum doping on microstructural, dielectric and magnetic properties of $Mn_{0.4}Zn_{0.6}Cd_{0.2}La_xFe_{1.8-x}O_4$ ($00 \leq x \leq 04$). J. Supercond. Nov. Magn. **34**, 2591 (2021)
79. B.D. Cullity, Introduction to magnetic material, 2ndedn. (Addison-Wesley, Reading) 568 (2008).

Nanocomposites

ISSN: (Print) (Online) Journal homepage: https://www.tandfonline.com/loi/ynan20

Effect of heat treatment on the microstructural properties of silica embedded cobalt ferrite nanocomposites

Meenakshi Bansal, Dharamvir Singh Ahlawat, Amrik Singh, Vijay Kumar & Shish Pal Rathee

To cite this article: Meenakshi Bansal, Dharamvir Singh Ahlawat, Amrik Singh, Vijay Kumar & Shish Pal Rathee (2020) Effect of heat treatment on the microstructural properties of silica embedded cobalt ferrite nanocomposites, Nanocomposites, 6:4, 158-164, DOI: 10.1080/20550324.2020.1865711

To link to this article: https://doi.org/10.1080/20550324.2020.1865711

Published online: 30 Dec 2020.

NANOCOMPOSITES
2020, VOL. 6, NO. 4, 158–164
https://doi.org/10.1080/20550324.2020.1865711

Taylor & Francis
Taylor & Francis Group

RESEARCH ARTICLE

OPEN ACCESS Check for updates

Effect of heat treatment on the microstructural properties of silica embedded cobalt ferrite nanocomposites

Meenakshi Bansal[a], Dharamvir Singh Ahlawat[a], Amrik Singh[a], Vijay Kumar[a] and Shish Pal Rathee[a,b]

[a]Department of Physics, Chaudhary Devi Lal University, Sirsa, India; [b]Department of Physics, A.I.Jat H.M. College, Rohtak, India

ABSTRACT

Silica coated cobalt ferrite ($CoFe_2O_4$:SiO_2) nanocomposites were synthesized by co-precipitation technique using metal nitrates as precursors. The as-prepared samples were heat treated at different temperatures of 250, 500 and 750 °C for 24 h. Structural, thermal, and morphological behavior of nanocomposites are investigated by XRD, FTIR, TGA-DTG, and SEM characterization results, useful in biomedical applications. With increasing calcinations temperature from 250 to 500 °C and 750 °C an increase in crystallite size of $CoFe_2O_4$:SiO_2 nanocomposites has been determined from 20.26 to 28.95 nm and 38.76 nm by Williamson–Hall method, respectively. Furthermore, by increasing the temperature from 250 to 750 °C the lattice parameter and strain values have been found to increase from 8.0321 to 8.0691 Å and 1.01×10^{-2} to 3.75×10^{-3}, respectively. Analysis of TGA results found no weight loss when the sample was heated beyond 700 °C and thus complete decomposition of precursors has led to the formation of stable nanocomposite structures at high temperatures. SEM analysis of synthesized samples at 750 °C revealed well developed nanoparticles of $CoFe_2O_4$: SiO_2 with inter-granular porosity.

GRAPHICAL ABSTRACT

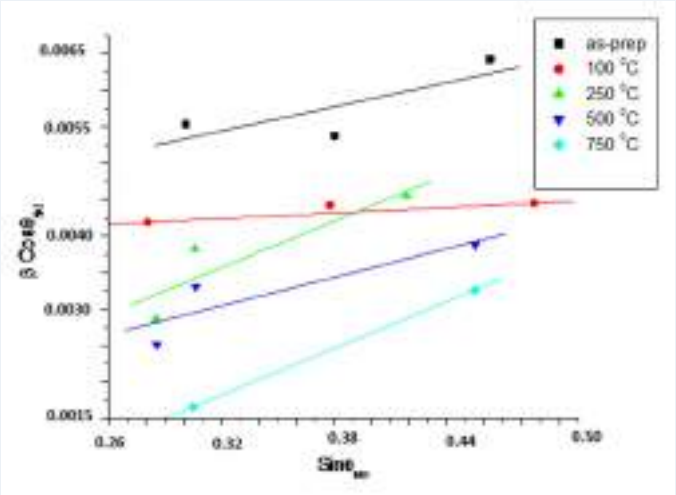

ARTICLE HISTORY
Received 21 April 2020
Accepted 14 December 2020

KEYWORDS
Silica; cobalt ferrite; coating; nanocomposites; co-precipitation

1. Introduction

Ferrite nanoparticles have received significant attention of researchers in recent years due to their specific magnetic and electrical properties [1]. More importantly, nanoferrites have shown gas sensing capability [2,3]. Moreover, they may be used in transformer cores, high speed digital tapes, photocatalytic activity toward the degradation of organic materials and oxidative nature of reactions in the presence of reducing gases [4,5]. Ferrites multifunctional character with super-paramagnetic properties makes them an interesting candidate for magnetic data storage, magnetic imaging, drug delivery, and microwave devices [6–8]. Among spinel ferrites, cobalt ferrite ($CoFe_2O_4$) has long been of great importance in fundamental sciences and technological applications due to its special magnetic properties such as high coercivity (Hc), moderate saturation magnetization (Ms), good chemical stability, and high mechanical hardness [9].

CONTACT Dharamvir Singh Ahlawat dahlawat66@gmail.com Department of Physics, Chaudhary Devi Lal University, Sirsa 125055, Haryana, India

Cobalt ferrite has an inverse spinel structure represented by $(Co_{1-X}Fe_X)$ $A(Co_XFe_{2-X})BO_4$ where X denotes the degree of inversion, A denotes tetragonal sites, and B represents octahedral sites. However, cobalt ferrite usually has a strong tendency to agglomerate, which makes them very different and difficult to reveal their unique physical properties. One way to overcome this difficulty is to disperse nanoparticles in a matrix as this method allows stabilization of the nanoparticles [10]. Research in nanocomposites having magnetic particles embedded in a silica insulating matrix widely has grown considerably in recent years due to the unique magnetic properties of these materials [11]. Silica provides protection to cobalt ferrite particles from harmful neighboring environment, needed for many technological applications. A number of methods have been used to obtain nanoparticles such as reverse micelle preparation [12], sol–gel method [13], hydrothermal [14], low temperature auto combustion [15], microemulsion [16], reduction–oxidation route [17], continuous-flow micro-reactors. etc. [18]. There are many limitations of these methods like: toxic nature and costly reagents, high temperatures, and long time consuming processes. However, an efficient method of preparation to avoid these ambiguities is the co-precipitation method as compared to other methods. The advantages of the co-precipitation method are the high yield, high product purity, the lack of necessity to use organic solvents, good reproducibility, and low cost. Silica embedded cobalt ferrites are promising candidates for biomedical applications like cell separation, purification, bactericide, and magneto hyperthermia of tumor cells [6–8]. The silica embedded cobalt ferrites may be proposed as the suitable materials for delivery of targeted nanomedicine in most harmful environments. Magnetic investigations of silica coated cobalt–ferrite nanocomposites have earlier been reported [19] and the retentivity, saturation magnetization, and coercivity revealed a strong dependence on their crystallite size. Our results suggest the potential applications of these silica embedded magnetic nanoparticles in the biomedical field, especially for hyperthermia treatment [6–8,19]. This paper reports novel data on the properties, synthesis and structure using XRD, FTIR, SEM, and thermal stability by TGA–DTG of silica embedded cobalt ferrite ($CoFe_2O_4$:SiO_2) nanocomposites prepared by co-precipitation method and heat treated at 250, 500, and 750 °C for 24 h.

2. Materials and methods

2.1. Sample preparation

Preparation and synthesis of samples were carried out mainly in three steps by the co-precipitation technique.

Firstly, synthesis of $CoFe_2O_4$ was carried out by using high purity reagents: cobalt nitrate hexahydrate ($Co(NO_3)_2{\cdot}6H_2O$), ferric nitrate nonahydrate ($Fe(NO_3)_3{\cdot}9H_2O$), ammonia hydroxide (NH_4OH) (Sigma-Aldrich), and double distilled water. In this method, solution mixture of $Co(NO_3)_2{\cdot}6H_2O$ and $Fe(NO_3)_3{\cdot}9H_2O$ with a $[Co^{2+}]/[Fe^{3+}]$ molar ratio 1:2 was dissolved in double distilled water and stirred vigorously for 3 h at 70 °C. Double distilled water was used as a solvent in order to avoid the production of impurities in the final product. Now a brown colored clear solution was obtained by equally blending the mixture. Then ammonia hydroxide (NH_4OH) solution was used as a base so as to get the precipitates of $CoFe_2O_4$ solution. After that the obtained solution was filtered with double distilled water and ethanol many times to remove impurities if any. Thus, a suspension solution containing dark brown precipitates was obtained.

In the second step, synthesis of SiO_2 was carried out. For this, typical molar ratio of precursors TEOS:C_2H_5OH:HNO_3:H_2O:NH_4OH was taken as 1:3:0.01:1:0.016, respectively. Initially, the first three chemicals were dissolved in double distilled water as per their given ratios. Then, NH_4OH was added drop wise in the solution mixture of TEOS, C_2H_5OH, and HNO_3. Addition of NH_4OH turned the solution mixture from transparent to milky. Now the obtained suspension was stirred for 2 h at 60 °C.

In the third step, synthesis of $CoFe_2O_4$:SiO_2 was carried out. For this, the obtained suspension solution in the first and second steps was mixed together and stirred for 6 h. Temperature of the system was kept constant at 70 °C during stirring. Then the resultant precipitates were filtered out and washed many times with double distilled water. After that the precipitates so obtained were dried at 80 °C in a vacuum oven for 24 h. The dried sample was grind to a very fine powder. This fine powder was divided among five parts. One of these five parts was kept as the as-prepared sample. The other fine powdered identical samples were heated at 250, 500, and 750 °C separately using a programmable furnace.

2.2. Instrumentation

XRD: X-ray diffraction (XRD) patterns of samples were recorded by an X-ray diffractometer (Philips PW/1710) with Cu filter using mono-chromatic Cu Kα radiation of wavelength1.548 Å at 50 kV and 40 mA. The scanning range by 2θ angle was kept 10°–80°. XRD pattern gives information regarding crystallite size, strain, and lattice constant.

FTIR: To investigate the compositional characteristics like phase transformation and bonding of constituents from optical excitation of vibrational

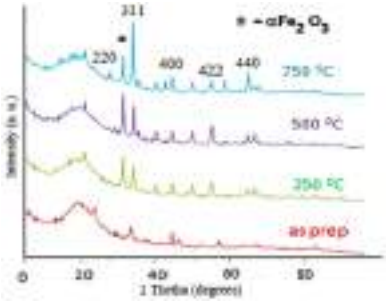

Figure 1. XRD patterns of $CoFe_2O_4$:SiO_2 samples (a) as-prepared, (b) 250 °C, (c) 500 °C, and (d) 750 °C.

modes, infra-red spectra were recorded in the range 4000–400 cm^{-1} using Fourier transform infrared (FTIR) spectrometer (Perkin-Elmer 1600). For FTIR characterization, pellets were obtained by homogeneously mixing the samples with KBr powder and then pressing.

SEM: Surface morphology was analyzed by scanning electron microscopy (SEM-JSM6610LV) with a maximum applied voltage of 30 kV.

TGA-DTG: Change in mass of sample as a function of temperature and decomposition of precursors was studied by Thermogravimetric Analysis (TGA)-Derivative Thermogravimetry (DTG) curve in temperature range 25–1100 °C (FRS1 R-Type).

3. Results and discussion

3.1. XRD analysis

The XRD patterns of the as-prepared sample and that annealed at different temperatures varying from 250 to 750 °C are shown in Figure1. The presence of amorphous silica in all the samples was confirmed by the broad hump seen in X-ray patterns at $2\Theta \sim 18°–23°$. The presence of weak diffraction peaks in the as-prepared $CoFe_2O_4$:SiO_2 sample suggests agglomeration of the nanocomposites. The weak peaks that appeared at 250 °C suggest that the particles of $CoFe_2O_4$ had been nucleated in the silica matrix and thus the XRD pattern show poor crystallinity. In order to achieve better crystallinity, the as-prepared sample was further heat treated at 500 and 750 °C. On comparing the XRD pattern with the JCPDS PDF card No. 22-1086, the formation of cobalt ferrite nanocomposites is confirmed. From analysis of Figure 1, it could be clearly seen that the rise in temperature from 250 to 500 °C leads to higher crystallinity of the sample. In the diffractogram of samples thermally treated from 250 to 500 °C two significant peaks centered at $2\Theta \sim 33.20°$ and 35.41° are noticed. The peak centered at $2\Theta \sim 33°$ indicates about the formation of hematite phase (α-Fe_2O_3) [20] and the peak noticed at $2\Theta \sim 35°$ could be indexed as the characteristic peak of

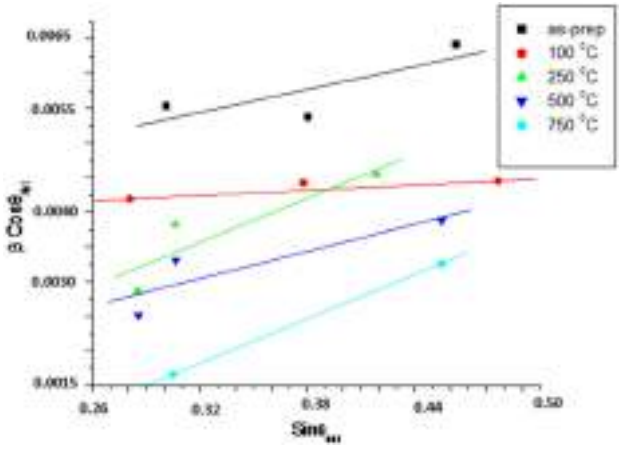

Figure 2. Williamson–Hall (W–H) plot of as-prepared and thermally treated $CoFe_2O_4$:SiO_2 nanocomposites at different temperatures.

$CoFe_2O_4$:SiO_2. By comparing with JCPDS PDF card no. 22-1086 peaks could be easily indexed to a cubic spinel structure (Fd3M). Here, the intensity of the peak indicating hematite phase ($2\Theta \sim 33.20°$) is found higher than that of the peak of $CoFe_2O_4$ phase ($2\Theta \sim 35.41°$). This indicates that $CoFe_2O_4$ phase was not developed fully and in this case related literature suggests that ferrite silica phase is mostly calcined in the temperature range 300–700 °C [21]. Further, heat treatment of sample to 750 °C, results in a sharp increase in the intensities of peaks which suggests that crystallinity of particles has increased. Moreover, it may also be noticed that the intensity of the peak corresponding to $CoFe_2O_4$ phase is increased while that indicating hematite phase has decreased. This shows dominance of $CoFe_2O_4$ phase over hematite phase indicating that $CoFe_2O_4$ particles are now been nucleated in the silica matrix.

The crystallite size, $D_{D\text{-}S}$ of the nanostructured material has been estimated from the broadening of the XRD peaks using the Scherrer equation [22] with the size-strain plot shown in Figure 2

$$D_{D-S} = K\lambda/\beta\cos\theta \tag{1}$$

where λ is the of X-ray wavelength, K is a structure constant, θ denotes diffraction angle, β represents the full width at half maxima.

The size–strain plot also known as W–H plot considers about the effect of stress broadening on the nanostructure size (D_{W-H}) and is calculated by using the Williamson–Hall method

$$\beta = k\lambda/D_{W-H}\cos\theta + 4\varepsilon \ \mathrm{Sin}\,\theta \tag{2}$$

where ε measures stress coefficient and its value is measured from the slope of the fitted line. This stress broadening coefficient leads to an increase in grain size as compared to that measured by Debye–Scherrer equation given in Table 1.

The lattice parameter '*a*' is calculated for most intense reflection (3 1 1) from Bragg's equation

Table 1. Crystallite size, strain and lattice parameter with increasing temperature.

Temperature (°C)	Crystallite size 'D_{D-S}' (nm)	Average crystallite size 'D_{W-H}' (nm)	Strain 'ε'	Lattice parameter 'a' (Å)
250	19.80	20.26	1.01×10^{-2}	8.0321
500	27.15	28.95	2.72×10^{-3}	8.0625
750	35.34	38.76	3.75×10^{-3}	8.0691

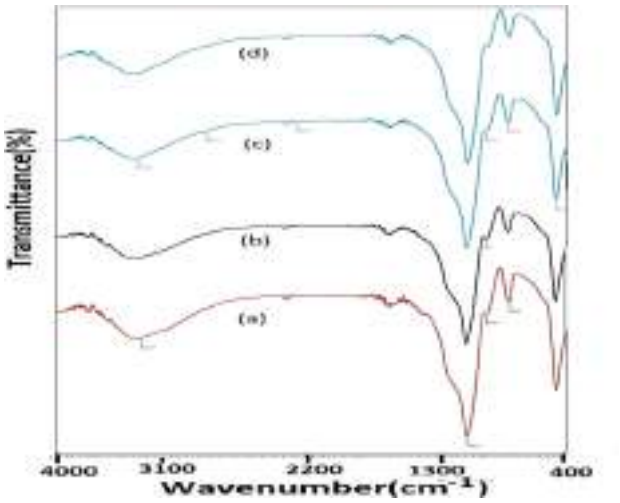

Figure 3. FTIR spectra of $CoFe_2O_4$:SiO_2 nanocomposites calcined at different temperatures: (a) as-prepared, (b) 250 °C, (c) 500 °C, and (d) 750 °C.

$$a = d\sqrt{h^2 + k^2 + l^2} \quad (3)$$

Calculated values of crystallite size using the Debye–Scherrer equation (D_{D-S}) and Williamson–Hall method (D_{W-H}), strain and lattice parameter with increasing temperature are listed in Table 1. In our earlier communication, we have reported the magnetic properties of these samples and retentivity, saturation magnetization and coercivity revealed a strong dependence on the crystallite size and showed promise as a material for magnetic hyperthermia [19].

3.2. FTIR analysis

The FTIR spectra of (a) as-prepared sample and samples calcined at (b) 250 °C, (c) 500 °C, and (d) 750 °C for 2 h in the wave number range of 4000–400 cm^{-1} is shown in Figure 3. The spectra of as-prepared sample of $CoFe_2O_4$:SiO_2 shows bands at 3398.5 and 3404 cm^{-1} which are denoted to stretching vibration of H–O–H and surface silanol group (Si–OH), respectively. This spectrum confirms about the band of water overlaps with surface hydroxyl group vibrations that results in band broadening. Furthermore, the strong absorptions at 1095.57, 798.53 and 464.84 cm^{-1} indicate the formation of silica network [23], while the presence of a band found at 956.69 cm^{-1} has been assigned to Si–O–Fe. The presence of Si–O–Fe vibrations indicates some interaction between the highly isolated Fe^{3+} ions and the nearest silica matrix. The presence of Si–O–Fe and Co–O bonds reflects about the chemical nature of the transition metals. As, transition metal ions do not participate directly into the sol–-gel chemistry even though they have been introduced into the starting solutions [24]. In the spectra of the as-prepared sample and the sample calcined at 250 °C, the band at 1650 cm^{-1} could be assigned to the deformation of molecular water having a strong presence in these samples. For the samples thermally treated at temperature of 500 °C, the absorption band at 1095.57 cm^{-1} for Si–O–S is of the SiO_4 tetrahedron has further broadened, while that for O–Si–O symmetric bond stretching vibrations at 464.84 $cm^{-1}$and vibrational mode of Si–O–Si bond present at 800 cm^{-1} becomes much weaker. This corresponds to a resettlement process of the silica network [25]. However, the presence of a broad hump at 3425 cm^{-1} indicates Si–OH vibrations. Correspondingly, the band centered around 956 cm^{-1} shows for the absorption of the Fe–O stretching in Fe–O–Si bonds which has increased in intensity. These facts reflect the formation of $CoFe_2O_4$ clusters that are accompanied with the rearrangement of the silica network and the enhancement of the Si–O–Fe bond between the $CoFe_2O_4$ clusters and the surrounding silica network. Furthermore, for the samples heat treated at 750 °C, the IR spectrum changes greatly as compared with that of samples heat treated at lower temperatures. The absorption at 1095 cm^{-1} for Si–O–Si of the SiO_4 tetrahedron grows narrower and stronger, while a band corresponding to 956 cm^{-1} appeared [22,26]. The poor development of ferrite structure in as-prepared sample is evidenced by the weakening of the characteristic band of ferrite (590 cm^{-1}). This fact is in agreement with our XRD results, which has showed poor crystallinity in the as-prepared sample. Moreover, at high temperature, elimination of water molecules and Si–OH volatiles from the sample leads to densification of $CoFe_2O_4$:SiO_2 and hence justifying about the formation of nanocomposites which is confirmed by the XRD results.

3.3. SEM analysis

The micrograph of $CoFe_2O_4$:SiO_2 nanocomposites thermally treated at 250, 500, and 750 °C are shown in Figure 4. SEM micrograph of the samples thermally treated at 250 °C indicates agglomeration of particles due to the presence of magnetic inter-

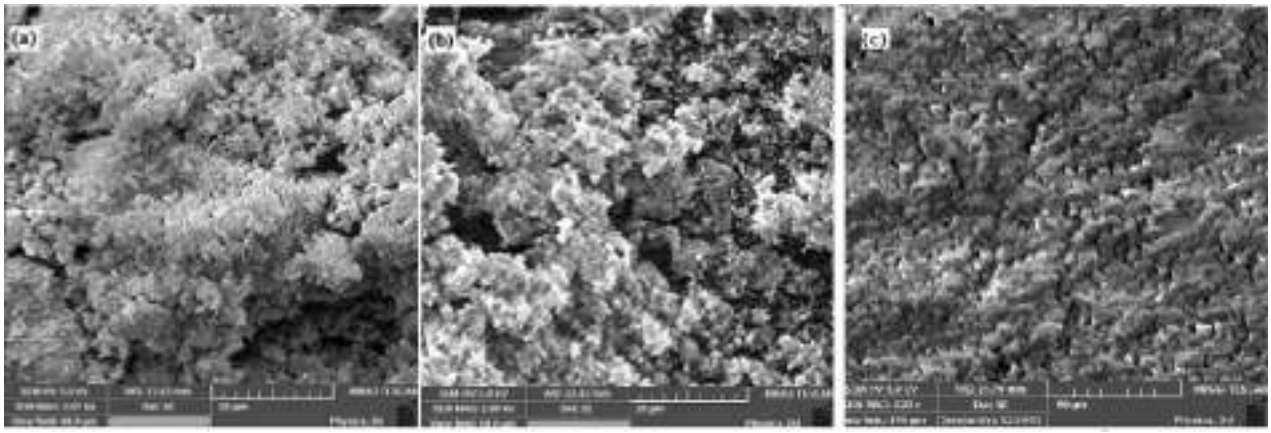

Figure 4. SEM micrograph of $CoFe_2O_4$:SiO_2 nanocomposites heat treated at (a) 250 °C, (b) 500 °C, and (c) 750 °C.

particles and Van der Waal's interactions as shown in Figure 4(a).Micrograph of $CoFe_2O_4$:SiO_2 thermally treated at 500 °C is shown in Figure 4(b) and indicates that particles are still agglomerated but with decreasing agglomerate size at 500 °C as compared to that at 250 °C [26]. Silica embedded CoFe2O4 nanoparticles are well developed having non-uniform morphology along with agglomeration of particles which is supported by the SEM results of grown $CoFe_2O_4$ nanoparticles reported by Raval et al. [27]. Although, SEM analysis of the sample at 750 °C shown in Figure 4(c) demonstrates about well-developed nanoparticles of $CoFe_2O_4$:SiO_2. Inter-granular porosity was also observed at 750 °C. It can be clearly seen that SiO_2 is coated on the $CoFe_2O_4$ surface. A clear trend of microstructural change is found with temperature. Our magnetic findings of these silica coated cobalt–ferrite nanocomposites indicate [19] that retentivity, saturation magnetization, and coercivity can vary with crystallite size and is strongly depended on temperature. Hence, our results indicate the individual appearance of silica embedded nanoparticles has been enhanced in the case of higher temperatures and they may be suitably designed for maximum heating efficiency in magnetic hyperthermia for cancer treatment [6–8].

3.4. TGA–DTG analysis

The thermal decomposition behavior of precursors was investigated by TGA–DTG analysis. TGA–DTG curves of the as-prepared powdered samples are shown in Figure 5. Change in mass of sample as a function of temperature and decomposition of precursors was studied by TGA–DTG curve in temperature range 25–1100 °C. Thermogravametric analysis of precursors revealed that a total weight loss of −24% occurred at four different temperature ranges 50–200, 201–350, 351–600, 601–750 °C. When the powdered sample was heated from 50 to 200 °C (first stage), around 7% weight loss occurred

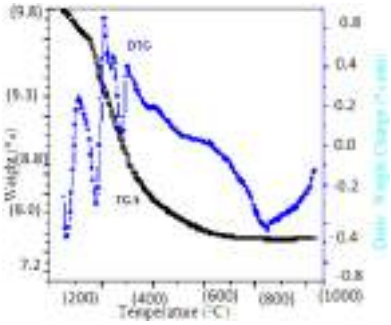

Figure 5. TGA–DTG curve of as-prepared silica coated cobalt ferrite nanocomposites.

due to the loss of moisture from the sample. This loss of moisture is also reflected in the DTG curve by the presence of a peak at 114 °C. In the second stage (201–350 °C) nearly 11% weight loss has been observed. This weight loss might be due to the oxidative decomposition of precursors. The presence of a strong peak around 208 °C attributes to the decomposition of precursors in the DTG curve [28,29]. In the third stage (351–600 °C), a constant weight loss is observed leading to the formation of an intermediate structure. In the temperature range 601–750 °C, the negligible weight loss implies strengthening of the intermediate structure of $CoFe_2O_4$:SiO_2 nanocomposites. Analysis of TGA results found no weight loss when the sample was heated beyond 700 °C. This actually confirmed the complete decomposition of precursors and existence of a stable structure of $CoFe_2O_4$:SiO_2 nanocomposites even at high temperatures. Consequently, silica embedded cobalt ferrite nanoparticles are protected from harmful environments as needed for many technological applications such as magnetic data storage, magnetic imaging, microwave devices.

4. Conclusions

Silica embedded cobalt ferrite nanocomposites were successfully prepared by co-precipitation method and heat treated at different temperatures of 250,

500, and 750 °C. With increasing calcinations temperature from 250 to 500 °C and 750 °C an increase in crystallite size of $CoFe_2O_4$:SiO_2 (nanocomposites) has been determined from 20.26 to 28.95 nm and 38.76 nm, respectively by W–H method. By increasing the temperature from 250 to 750 °C the lattice parameter and strain values have been found to increase from 8.0321 to 8.0691 Å and 1.01×10^{-2} to 3.75×10^{-3} respectively. The XRD and SEM results indicated that there is an increase in particle size, crystallinity, surface morphology and microstructure of the nanocomposites with increasing calcination temperature. The characterization showed a clear trend between heat treatment temperature and resulting microstructures. The presence of Si–O–Fe vibrations in the FTIR spectra suggests some interactions between highly isolated Fe^{3+} ions and nearest silica matrix. TGA–DTG results indicate no weight loss by heating the samples beyond 700 °C and confirmed the complete decomposition of precursors and formation of a stable structure of $CoFe_2O_4$:SiO_2 nanocomposites at high temperatures. Individual appearance of silica embedded nanoparticles has been enhanced for the case of higher temperatures and may be suitably designed to obtain maximum heating efficiency in magnetic hyperthermia for cancer treatment and other technological use.

Acknowledgement

The University of Delhi, New Delhi and IIT, Rurkee are gratefully acknowledged for providing experimental facilities to characterize the samples.

Disclosure statement

No potential conflict of interest was reported by the authors.

Notes on contributors

Meenakshi Bansal as a Research Scholar, Deptt. of Physics, CDLU, Sirsa (Hry.) India has prepared and characterized the silica coated cobalt ferrites samples for her Ph.D. degree.

Dharamvir Singh Ahlawat as an Associate Professor, Deptt. of Physics, CDLU, Sirsa (Hry.) India has guided this research work for Ph.D. degree.

Amrik Singh, Assistant Professor in the same department has contributed for quality improvement of figures and citation of references.

Vijay Kumar working as a Research Scholar in the same department has contributed in FTIR discussion.

Shish Pal Rathee was a Research Scholar in the same department and currently working as an Assistant Professor of Physics, A.I. Jat H.M. College, Rohtak (Hry.) India. His contribution in this work is for discussion part of thermal properties.

References

1. Gunther L. Quantum tunneling of magnetization. Phys World. 1990;12:28.
2. Kamble RB, Mathe VL. Nanocrystalline nickel ferrite thick film as an efficient gas sensor at room temperature. Sensor Actuat B – Chem. 2008;131(1):205–209.
3. Darshane SL, Suryavansh SS, Mulla IS. Nanostructured nickel ferrite: a liquid petroleum gas sensor. Ceram Int. 2009;35(5):1793–1797.
4. Ajroudi L, Madigou V, Villain S, et al. Synthesis and microstructure of cobalt ferrite nanoparticles. J Cryst Growth. 2010;312(16–17):2465–2471.
5. Papa F, Patron L, Carp O, et al. Catalytic activity of neodymium substituted zinc ferrites for oxidative conversion of methane. J Mol Catal A – Chem. 2009; 299(1–2):93–97.
6. Virden A, Wells S, Grady KO. Cobalt ferrite, a new gas sensing material. J. Magn Magn Mater. 2007; 316:768–771.
7. Ding J, Miao WF, Cormick PG, et al. High-coercivity ferrite magnets prepared by mechanical alloying. J Alloys Compd. 1998;281(1):32–36.
8. Mazaleyrat F, Varga LK. Ferromagnetic nanocomposites. J Magn Magn Mater. 2000;215:253–259.
9. Cullity BD. Elements of X-ray diffraction. Reading (MA): Addison-Wesley; 1959.
10. Huang X, Chen J. Preparation and characterization of $CoFe_2O_4/SiO_2$ nanocomposites. J Magn Magn Mater. 2004;280(1):37–43.
11. García-Cerda LA, Torres-García VA, Matutes-Aquino JA, et al. Magnetic nanocomposites: preparation and characterization of Co-ferrite nanoparticles in a silica matrix. J Alloy Compd. 2004;369(1–2):148–151.
12. Calero-DdelC VL, Rinaldi C. Synthesis and magnetic characterization of cobalt-substituted ferrite ($Co_xFe_{3-x}O_4$) nanoparticles. J Magn Magn Mater. 2007;314(1):60–67.
13. Silva JB, Diniz CF, Ardinson JD, et al. Cobalt ferrite dispersed in a silica matrix prepared by sol-gel process. J Magn Magn Mater. 2004;272:1851–1853.
14. Li XH, Xu CL, Han XH, et al. Synthesis and magnetic properties of nearly monodisperse $CoFe_2O_4$ nanoparticles through a simple hydrothermal condition. Nanoscale Res Lett. 2010;5(6):1039–1044.
15. Xiao SH, Jiang WF, Li LY, et al. Low-temperature auto-combustion synthesis and characterization of cobalt ferrite nanopowder. Mater Chem Phys. 2007; 106(1):82–87.
16. Lee Y, Lee J, Bae CJ, et al. Large-scale synthesis of uniform and crystalline magnetite nanoparticles using reverse micelles as nanoreactors under reflux conditions. Adv Funct Mater. 2005;15(3):503–509.
17. Gu ZJ, Xiang X, Fa GI, et al. Facile synthesis and characterization of cobalt ferrite nanocrystals via a simple reduction–oxidation route. J Phys Chem C. 2008;112(47):18459–18466.
18. Hassan AA, Neveu S, Dupuis V, et al. Synthesis of cobalt ferrite nanoparticles in continuous flow microreactors. RSC Adv. 2012;2(30):11263–11266.

19. Bansal M, Aghamkar P, Ahlawat DS. Structural and magnetic investigations of silica coated cobalt-ferrite nanocomposites. Orient J Chem. 2018;34(4): 2060–2067.
20. Xavier S, Thankachan S, Jacob BP, et al. Effect of sintering temperature on the structural and magnetic properties of cobalt ferrite nanoparticles. Nanosystems: Phys Chem Math. 2013;4:430–437.
21. Duhan S, Aghamkar P, Kishore N, et al. Effect of growth temperature on the structural of Nd-doped silica prepared by the chemical method. Mater Chem Phys. 2009;114(1):103–106.
22. Shinde TJ, Gadkari AB, Vasambekar PN. Saturation magnetization and structural analysis of $N_{i0.6}Zn_{0.4}NdyFe_{2-y}O_4$ by XRD, IR and SEM techniques. J Mater Sci: Mater Electron. 2010;21(2):120–124.
23. Rohilla S, Kumar S, Aghamkar P, et al. Investigations on structural and magnetic properties of cobalt ferrite/silica nanocomposites prepared by the coprecipitation method. J Magn Magn Mater. 2011;323(7):897–902.
24. Garcia Cerda LA, Montemayor SM. Synthesis of $CoFe_2O_4$ nanoparticles embedded in a silica matrix by the citrate precursor technique. J Magn Magn Mater. 2005; 294:e43–e46.
25. Coey JMD. Noncollinear spin arrangement in ultrafine ferrimagnetic crystallites. Phys Rev Lett. 1971;27(17):1140–1142.
26. William E, Lee W, Mark R. Ceramic microstructures: property control by processing. London, New York: Chapman & Hall; 1994.
27. Raval A, Panchal N, Jotania R. Structural properties and microstructure of cobalt ferrite particles synthesized by a sol–gel auto combustion method. Int J Mod Phys Conf Ser. 2013;22:558–563.
28. Xiao SH, Xu HJ, Hu J, et al. Influence of calcination temperature on structural and magnetic properties of nanocomposites formed by Co-ferrite dispersed in sol–gel silica matrix using tetrakis(2-hydroxyethyl) orthosilicate as precursor. Physica E. 2008; 40(10):3064–3067.
29. Rajput AB, Hazra S, Ghosh NN. Synthesis and characterization of pure singlephase $CoFe_2O_4$ nanopowder via a simple aqueous solution based EDTA-precursor route. J Exp Nanosci. 2013;8(4):629–639.

Journal of Magnetism and Magnetic Materials 474 (2019) 505–511

Contents lists available at ScienceDirect

Journal of Magnetism and Magnetic Materials

journal homepage: www.elsevier.com/locate/jmmm

Research articles

Structural, thermal and magnetic investigations of cobalt ferrite doped with Zn^{2+} and Cd^{2+} synthesized by auto combustion method

Harpreet Kaur, Amrik Singh, Vijay Kumar, Dharamvir Singh Ahlawat*

Department of Physics, Chaudhary Devi Lal University, Sirsa 125055, Haryana, India

ARTICLE INFO

Keywords:
Auto combustion
Cobalt ferrite
$CoZnFe_2O_4$
$CoCdFe_2O_4$
VSM analysis
TEM

ABSTRACT

The nanoparticles of Cobalt-ferrite ($CoFe_2O_4$), $CoZnFe_2O_4$ and $CoCdFe_2O_4$ have been synthesized by Auto-combustion method. In this method, nitrates of Co, Fe, Zn and Cd were used as the starting materials, while citric acid has been used as a fuel for the preparation of the samples of $CoFe_2O_4$, $Co_{0.9}Zn_{0.1}Fe_2O_4$ and $Co_{0.9}Cd_{0.1}Fe_2O_4$. Further, the effect of Zn^{2+} and Cd^{2+} doping on the structural, thermal and magnetic properties of Cobalt-Ferrite ($CoFe_2O_4$) were also investigated as a useful data. Thermal decomposition is confirmed by fast weight loss nearly up to 580.0 °C due to removal of hydroxyl group and after that weight loss has been observed almost negligible up to 1000 °C from the analysis of the TGA plot. In powder XRD results, pure cubic spinel structure of all the composition has been found. With the help of W-H method using XRD data, the crystallite size has been found to be lying in the range from 46.20 nm to 53.30 nm and strain values are obtained from −0.0003 to 0.0008. The FTIR spectra confirmed the presence of M−O bond and ferrite in our prepared samples. It may be mentioned on the basis of analysis of results for particle size by two XRD and TEM methods which indicate about the formation of nano materials and doping of cobalt ferrites. Moreover, TEM results have also indicated the presence of nano-sized spherical shape of prepared particles with agglomeration. From analysis of VSM results, the obtained values of coercivity (H_c) have been found for these ferrites between 263.45 Oe and 1408.93 Oe. By the substitution of cobalt magnetic ions with Zn^{2+} and Cd^{2+}, it is possible to tune the magnetic properties of cobalt ferrite as a promising material for various technological applications.

1. Introduction

Research work on nanoparticles has recently become an important field of investigations since almost two decades because of their unique properties for various technological applications [1]. The nanoparticles have many advantages in health care like they can be used to deliver drugs to the targeted animal cells directly. They have more stability as compared to bulk form of material with less toxic effects. Further, magnetic nanoparticles have been used in many others applications like information technology, storage systems and ferro fluids for magnetic drug delivery and hyperthermia for cancer treatment [2]. As, these nano sized magnetic materials are useful due to their high magnetization and magneto resistivity. Furthermore, among magnetic nanoparticles metal ferrites have been generally found more useful. Because, ferrites are relatively more stable against oxidation and belong to non-toxic category. The properties of magnetic nanoparticles depend upon their chemical structure and their methods of preparation. Some nano magnetic materials have the specialty that they change their dimensions when magnetic field is applied. Magnetic nanoparticles are single domain having large magnetic moment. Due to high chemical stability, ferrite materials have many more interesting properties like optical, electrical, chemical and magnetic properties [3]. Spinel ferrites have the general formula $M^{2+}(Fe^{3+})_2O_4$ (M^{2+} = Ni^{2+},Co^{2+},Cu^{2+}, Mn^{2+}), where M^{2+} and Fe^{3+} ions can occupy either tetrahedral (A^-) or octahedral (B^-) sites and oxygen has a face centered cubic (fcc) close packing arrangement. In these materials, 8A sites and 16B sites are occupied by metallic ions [4–8]. The Fe is equally distributed in both octahedral and tetrahedral sites. Therefore, magnetic moment of Fe get cancel out each other, hence magnetization is due to cobalt only. Depending on cations distribution on A and B sites, it shows ferrimagnetic, antiferromagnetic, spin (cluster) and paramagnetic behavior. The properties of ferrite nanoparticles also depend upon their composition, microstructure, dopants and various preparation methods [9].

Cobalt ferrite is an important material among all the ferrites, because it has some special properties. It is a hard-magnetic material having high coercivity, moderate magnetization, high mechanical hardness and high chemical stability at nanoscale size of material. Because of its high coercivity and stability, the sensors and actuators

* Corresponding author.
E-mail address: dahlawat66@gmail.com (D.S. Ahlawat).

https://doi.org/10.1016/j.jmmm.2018.11.010
Received 22 March 2018; Received in revised form 30 October 2018; Accepted 2 November 2018
Available online 03 November 2018
0304-8853/

made by cobalt ferrite are more durable and of high use. Therefore, it is also used in high density storage, transformer core, high quality filters and phase shifters [10]. The $CoFe_2O_4$ has an inverse spinel structure with Co^{2+} ions mainly placed on B sites and Fe^{3+} ions distributed, almost equally between A and B sites [11]. The doping of diamagnetic ion Zn and Cd in $CoFe_2O_4$ brings about interesting change in the magnetic properties of cobalt ferrite. As, cobalt ferrite is ferrimagnetic below 790 K, means magnetic interactions in this ferrite are very strong. However, when Co^{2+} is replaced by Zn^{2+} in $Co_{1-x}Zn_xFe_2O_4$, then Zn^{2+} occupies the tetrahedral site and Fe^{3+} ions are displaced to the octahedral sites. Thus, by increasing concentration of x, the Fe_A-O-Fe_B interactions become weak and T_n is expected to decrease. $ZnFe_2O_4$ is a normal spinel, it is antiferromagnetic due to $Fe_B - Fe_B$ interactions only. However, T_n of $ZnFe_2O_4$ is very small, 9 K [12]. In this article, we have reported the properties of cobalt ferrite ($CoFe_2O_4$), cobalt zinc ferrite ($CoZnFe_2O_4$) and cobalt cadmium ferrite ($CoCdFe_2O_4$) synthesized by auto-combustion method. Cobalt zinc ferrite is one of the promising soft ferrite used in electronic devices such as transformer core, electric motors and generators, because Zn has high resistivity, low losses, high mechanical hardness, high Curie temperature and good chemical stability [13–15]. In fact, Co-Zn mixed ferrites have been selected under this research due to their high sensitivity of magnetization needed for above mentioned applications. Further, one more material like doping of cadmium ion into the spinel lattice ($CoCdFe_2O_4$) has prominent effect on the magnetic properties such as spin canting effect and hence many researchers have conducted investigations on these ferrites [16–18].

2. Materials and methods

2.1. Synthesis of $Co_{1-x}Zn_xFe_2O_4$ and $Co_{1-x}Cd_xFe_2O_4$ Ferrites

Among various methods of synthesis, the auto combustion method is versatile as it is comparatively a time saving, low cost and simple easy procedure method [19]. It gives pure, ultrafine, nanoparticles of various shapes and relatively strain free nanoparticles in powder form of material. This method does not produce any type of waste product. Sol–gel auto-combustion synthesis is also known as auto-ignition or self-propagation method for the preparation of spinel type ferrite nanomaterials [20]. Nitrates have been chosen as metal precursor because of their high water solubility and easy combustion by combining the metal nitrate with suitable fuel. Citric acid provides fuel for ignition oxidized by nitrates [21]. Ammonium nitrate is used in combustion reactions to act as an extra oxidant without change in the proportion of other participants under the chemical reaction. Addition of this extra oxidant produced an increase in the combustion gas and thereby effect to expand the micro structures and eventually increase in the surface area of nanoparticles in final powder form product.

$$2NH_4NO_3(s) \rightarrow 2N_2(g) + 4H_2\ O + O_2(g)$$

Nanoparticles of cobalt ferrite were prepared in this research work and general formula of these materials is written as $Co_{1-x}Zn_xCd_xFe_2O_4$, (x = 0, 0.1). Raw materials that have been used in this method are Cobalt nitrate $Co(NO_3)_2{\cdot}6H_2O$ [98%], Ferric nitrate $Fe(NO_3)_3{\cdot}9H_2O$ [98%], Zinc nitrate $Zn(NO_3)_2{\cdot}6H_2O$ [98%] and Cadmium nitrate Cd $(NO_3)_2{\cdot}4H_2O$ [99%]. A stoichiometric ratio of Cobalt nitrate and Ferric nitrate of AR grade were mixed in 50 ml distilled water. Molar ratio of Cobalt nitrate and Ferric nitrate was taken as 1:3. The citric acid (C) was added as a fuel in the metal nitrate (N) in the ratio (C: N) as 1:8 under vigorous stirring conditions. The ferrite samples were successfully prepared by doping of Zn^{2+} and Cd^{2+} having different molar ratios ($Co_{1-x}Zn_xFe_2O_4$, x = 0.0, 0.1), $Co_{1-x}Cd_xFe_2O_4$ (x = 0, 0.1) to $CoFe_2O_4$. The amount 1.189 gm of Zinc nitrate has been added to the metal nitrate solution and 1.22gm of cadmium nitrate was added to the metal nitrate solution. To adjust the pH value equal to 7, the Ammonium hydroxide equal to 20 ml was also added drop by drop.

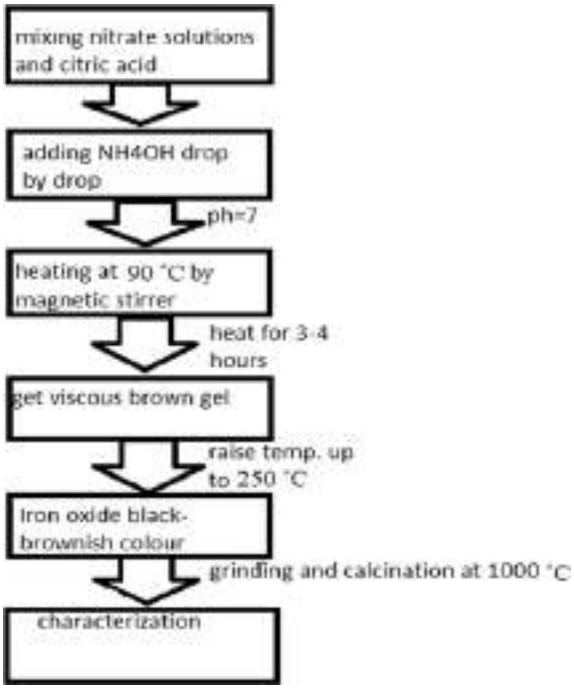

Fig. 1. Schematic representation of auto-combustion method.

After that, the solution was heated at 90 °C for 3–4 h on the magnetic stirrer. Water present in the solution then slowly started to decrease by evaporation. During evaporation process solution becomes viscous and consequently gel was started to form, as shown in Fig. 1. Then, by increasing the temperature up to 250 °C, gel was ignited. This was the actual noted temperature inside the solution by using a separate thermometer, however automatic temperature by the magnetic stirrer has been shown at 300 °C. It has been observed that entire heat has not been transferred from stirrer plate to the solution, in this method. In fact, at 250 °C the combustion process started very rapidly in a violent manner until the entire gel gets burnt out completely. After that the remaining iron oxide black-brownish color material was grinded to prepare ash and then TGA/DTA has been tested only for $CoFe_2O_4$ sample upto 1000 °C to estimate thermal stability. Finally, ash was processed for calcinations at 1000 °C for all these three samples. Hence, as the end product samples of $CoFe_2O_4$, $Co_{0.9}Zn_{0.1}Fe_2O_4$ and $Co_{0.9}Cd_{0.1}Fe_2O_4$ were prepared successfully for various characterizations.

2.2. Characterization techniques

The structural characterization of prepared samples of pure cobalt ferrite, zinc doped cobalt ferrite and cadmium doped cobalt ferrite was performed by recording the X-ray diffraction (XRD). The powder form samples were characterized by using Panalytical Xpert-Pro X-ray diffractometer with Cu-Kα (λ = 1.5406A°) radiation at 45KV and 40 mA in the range $15^o > 2\theta > 80^o$.The average crystallite size of nanoparticles of all the ferrite samples $Co_{1-x}Zn_xFe_2O_4$ ($x = 0.0, 0.1$) was calculated from the Debye-Scherrer's formula. Further, the functional groups were also analyzed by using FTIR spectrometer from 4000 to 400 cm^{-1}, Thermofischer (USA). The particle size of ferrite nano powders were obtained by Transmission electron microscope (HITACHI-H-7650(JAPAN). Furthermore, the magnetic properties of the ferrite particles have been recorded by using Vibrating Sample Magnetometer (VSM, PAR 155) having Magnetic field −10 to +10 kOe. In addition to that change in mass of the sample as a function of temperature and decomposition of precursors were also investigated by TGA-DTG curves in the temperature range 25–1000 °C (FRS1 R-Type).

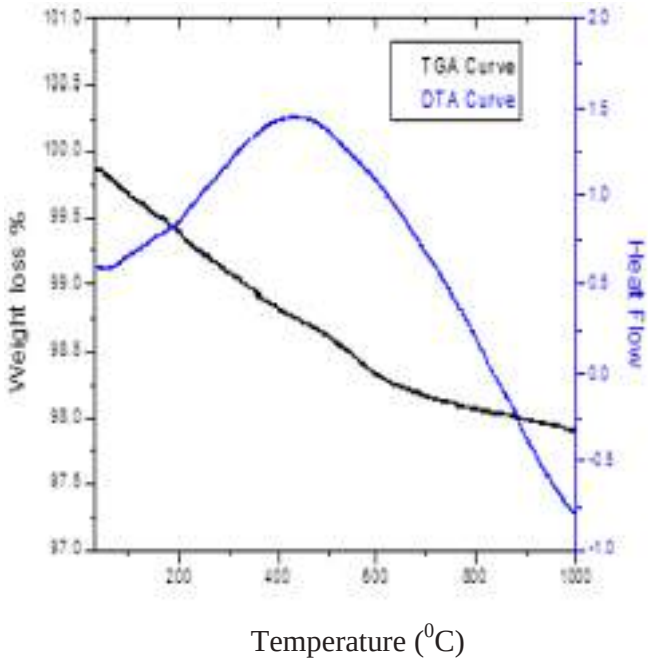

Fig. 2. DTA and TGA curves of cobalt ferrite ($CoFe_2O_4$).

3. Results and discussion

3.1. DTA-TGA analysis

For thermal characterization of sample ($CoFe_2O_4$), the curves of DTA-TGA were recorded as shown in the Fig. 2. The start material for TGA/DTA analysis was taken iron oxide black-brownish color material of $CoFe_2O_4$. The DTA-TGA curves indicate that degradation of dried ferrite nano powder shows some weight loss. The DTA curve explains about the heat required to increase the temperature of the sample and found a negative small value of heat flow approximately between 850 °C to 1000 °C. However, initially the TGA curve indicates weight loss and its analysis confirms about thermal decomposition of the cobalt ferrite nanomaterial under investigation. Thermal decomposition occurred in two steps: (i) first step initially nearly up to 580.0 °C there was high weight loss due to removal of hydroxyl group, moisture, carbon etc. and (ii) the second step, weight loss has been observed almost negligible up to 1000 °C from analysis of the TGA plot. Hence, nearly from 600 °C to 1000 °C there is almost insignificant weight loss by the critical analysis of highly resolved y-axis of the TGA curve. The TGA result confirms that thermal decomposition has completed and in the end, we get thermally stable ferrite powder at 1000 °C [22,23].

3.2. XRD analysis

Fig. 3 shows the XRD patterns of cobalt ferrite nano powder and its doped samples by Zn^{2+} and Cd^{2+} ions which were annealed at 1000 °C. In all these XRD figures, we get (1 1 1), (2 2 0), (3 1 1), (4 0 0), (4 2 2), (5 1 1), (4 4 0) as the prominent peaks and the peak indicated by (3 1 1) has appeared as the most intense prominent peak. Peaks (2 2 2) and (5 3 3) are also appearing in the plots as indicated in the figure for $Co_{0.9}Zn_{0.1}Fe_2O_4$. Moreover from the Fig. 3, the diffraction intensity of almost all the respective peaks has increased in the XRD patterns of Zn and Cd ion doped cobalt ferrites as compared to the peaks obtained for cobalt ferrite sample.

The peaks (4 2 2), (5 1 1) and (4 4 0) indicate face lattice cubic spinel structure with Fd3m space group and formation of single phase in all the three samples [24]. All these peaks indicate solubility of cations in their respective lattice sites. All this reported data of our work

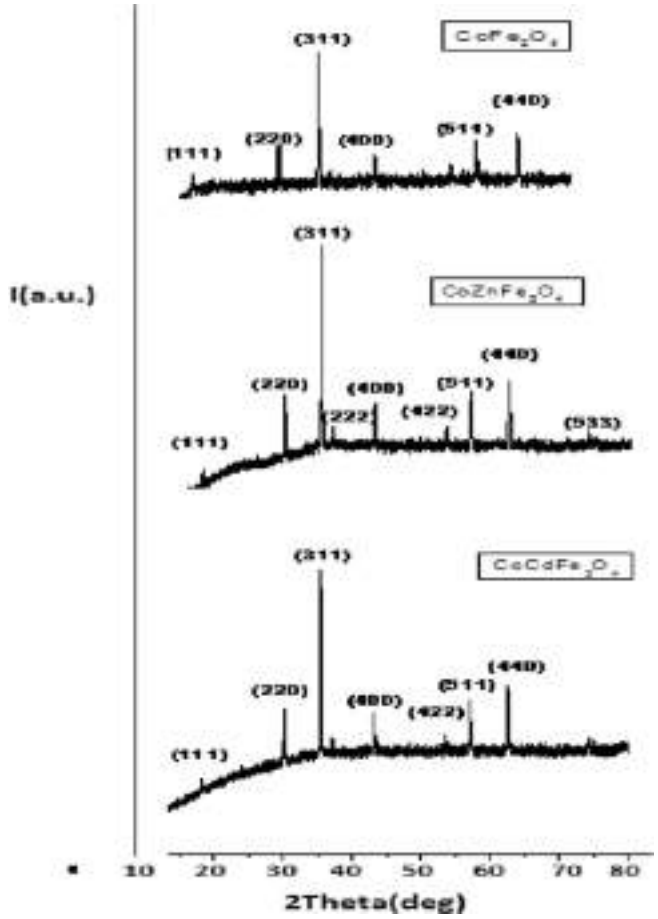

Fig. 3. XRD pattern of ferrite samples.

agrees well with the powder diffraction file of JCPDS 22-1086. At 1000 °C narrower and sharp peaks have been observed that indicate the presence of $Co_{0.9}Zn_{0.1}Fe_2O_4$. There has not been found any trace of extra crystalline phase formation in all these XRD patterns. Particle size is calculated corresponding to the most intense peak (3 1 1) by Debye-Scherrer formula [25].

$$D = \frac{0.9\lambda}{\beta\cos\theta} \quad (1)$$

where, $\lambda = 0.154$ nm. The parameters D and θ are taken as particle size and Bragg's angle respectively. Here β is the full width at half maxima (FWHM) of XRD peaks.

The lattice constant (a) is calculated by:

$$1/d^2 = (h^2 + k^2 + l^2)/a^2 \quad (2)$$

where d is the interplaner spacing and h, k and l are Miller indices. The calculated value of lattice constant and crystallite size of the prepared samples are given in the Table 1. Values of lattice constant varies from 8.37(Å) to 8.40 (Å). Lattice constant increases which indicates about the strong presence of Zn^{2+} and Cd^{2+} ion in our prepared doped

Table 1
Lattice constant, crystallite size and microstrain of $CoFe_2O_4$ and Zn, Cd doped cobalt ferrite samples.

Sample	Lattice constant, a (Å)	$D_{D\text{-}S}$ (nm)	$D_{W\text{-}H}$ (nm)	D_{TEM} (nm)	Strainε
$CoFe_2O_4$	8.37	40.15	46.20	32.57	0.0008
$Co_{0.9}Zn_{0.1}Fe_2O_4$	8.39	50.05	53.30	49.81	0.0003
$Co_{0.9}Cd_{0.1}Fe_2O_4$	8.40	57.78	47.79	58.83	-0.0003

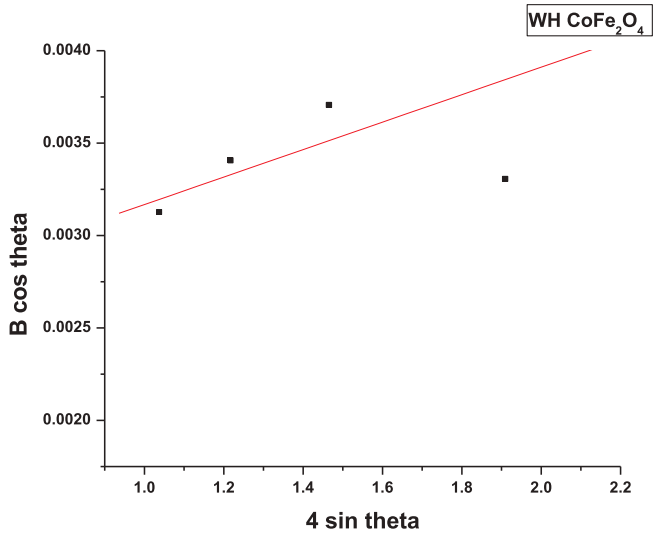

Fig. 4. Plot of βcosθ vs 4sinθ of $CoFe_2O_4$ nanoparticles.

samples. Increase in lattice parameter is due to the reason that ionic radii of Zn^{2+} (0.74 A°) and Cd^{2+} (0.95 A°) are larger than the radius of Co^{2+}(0.70 A°) [26]. The Williamson-Hall (W-H) relation is given by

$$\beta\cos\theta = \frac{K\lambda}{D} + 4\varepsilon Sin\theta \quad (3)$$

where, K = 0.9 for uniform small size crystals, $\lambda$is wavelength of X-ray used, θ is the Bragg's angle, ϵ is strain distribution and D is average crystallite size. For the case of small strain values $\varepsilon = 0$, then W-H relation is reduced to Debye-Scherrer formula. The W-H method is relatively better as compared to the Debye-Scherrer method as it explains about the strain values in the prepared samples.

From the W-H method, crystallite size and strain values have been determined from the intercept on y-axis and slope of the line as shown in the Figs. 4–6 respectively, which are given in the Table 1. The crystallite size has been found to be lying in the range from 46.20 nm to 53.30 nm and strain values are obtained from -0.0003 to 0.0008. As it has been noticed from the Table 1 that strain is decreasing gradually, therefore effect of strain on XRD peak is very-very small. By the doping of cadmium in cobalt ferrite, the crystallite size decreases than for Zn^{2+} doped ferrite because of compressive strain, as we get negative slope in the case of cadmium ion doping. However, we get positive value of slope in the case of zinc ion doping of cobalt ferrite. The positive value

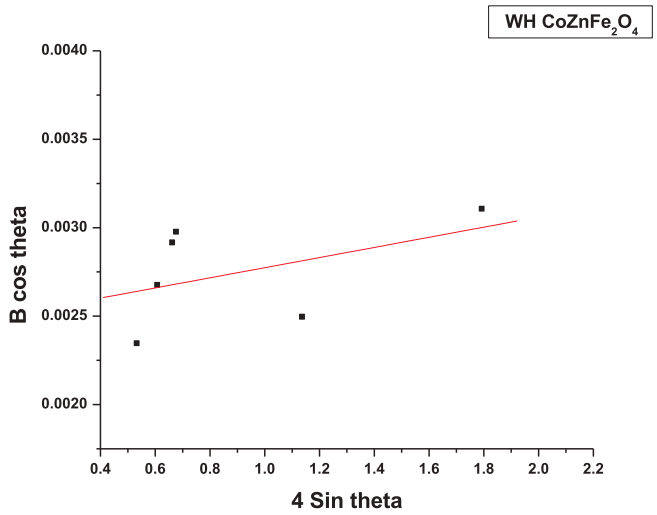

Fig. 5. Plot of βcos θ vs 4sin θ of $Co_{0.9}Zn_{0.1}Fe_2O_4$ nanoparticles.

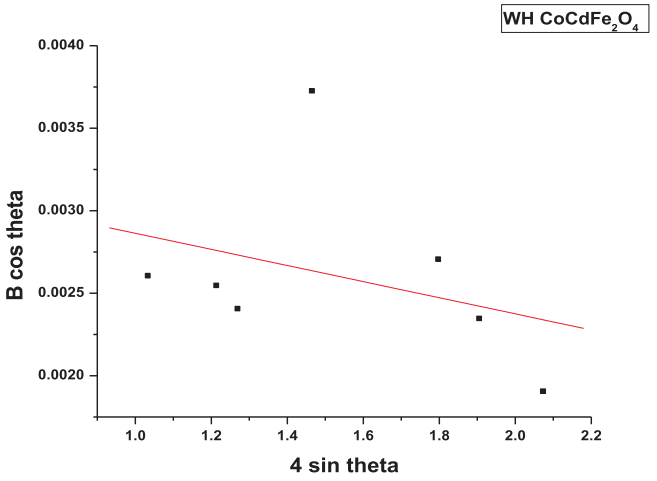

Fig. 6. Plot of βcos θ vs 4sin θ of $Co_{0.9}Cd_{0.1}Fe_2O_4$ nanoparticles.

Table 2
Magnetic properties of $CoFe_2O_4$ and Zn, Cd doped $CoFe_2O_4$ nanoparticles.

Sample	M_s (emu/g)	M_R (emu/g)	H_c (Oe)	Squareness ratio M_R/M_S
$CoFe_2O_4$	72.13	33.74	1408.93	0.46
$CoZnFe_2O_4$	80.84	18.41	263.45	0.227
$CoCdFe_2O_4$	81.60	29.16	620.84	0.357

of slope indicates tensile strain while negative value of slope indicates a compressive type strain. In fact, compressive strain may be believed due to the reason that ionic radii of cadmium ion are larger than zinc ion [27]. Hence, it is may be mentioned from the analysis of results given in Table 2 for particle size by three methods which indicate about the formation of ferrite nano materials and doping of cobalt ferrites.

3.3. FTIR analysis

The Fourier transform infrared spectroscopy (FTIR) plots of all the prepared samples were recorded in the wave number range 4000 cm^{-1}-–400 cm^{-1} as shown in Fig. 7. The FTIR spectroscopy explains about the distribution of cations between the octahedral and tetrahedral sites of cobalt ferrite. In these spectra, bands are existed due to interatomic vibrations. Spectra in the range 400 cm^{-1}-600 cm^{-1} confirmed about the spinel structure of cobalt ferrite and its doped samples by Zn^{2+} and Cd^{2+} ions.

In all these figures of FTIR spectra, it can be noticed that some absorption peaks in finger print region (400 cm^{-1}-–600 cm^{-1}) existed ,which indicate about the M-O stretching that confirms the presence of ferrites in all the prepared samples and indicate spinel structure. Peaks near about 579 cm^{-1}in all samples indicate high frequency band that is due to stretching vibrations of the tetrahedral groups. Lower frequency band obtained near about at 415 cm^{-1} that is due to the stretching mode of the octahedral M-O groups in the ferrites [28–30]. The band around 1052 cm^{-1} explains stretching vibration of C–O [31]. One peak at 1365.1 cm^{-1} indicates the presence of O-H group [32]. The samples have band near around 3450 cm^{-1} and 1630 cm^{-1} respectively show the presence of O-H group as well as some impurities on the surface of ferrite nanoparticles and indicate the existence of O-H group [33–34].

3.4. TEM analysis

Transmission electron microscopy (TEM) images of ferrite samples of $CoFe_2O_4$, $Co_{0.9}Zn_{0.1}Fe_2O_4$ and $Co_{0.9}Cd_{0.1}Fe_2O_4$ are shown in Fig. 8(a–c) respectively. Analysis of the images show high agglomeration of the particles, which may be believed due to nano size effect, magnetic interaction between magnetic nature of nanoparticles and

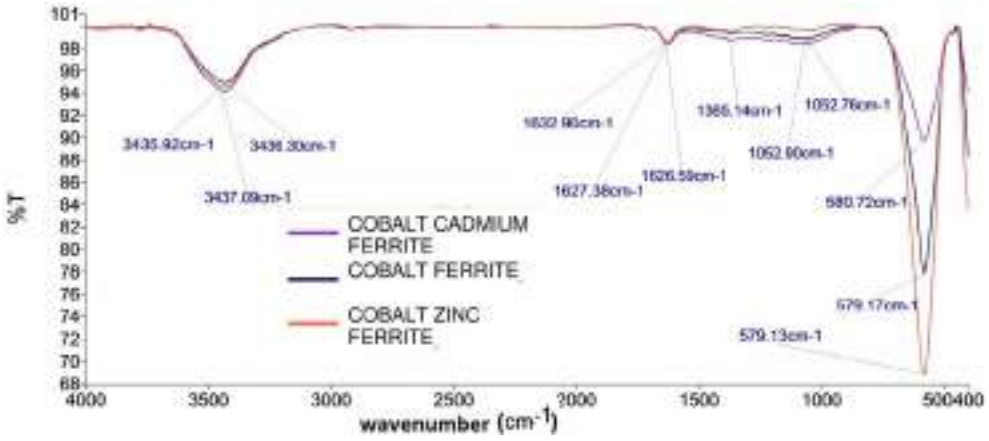

Fig. 7. FTIR spectra for $CoFe_2O_4$ and its doped samples.

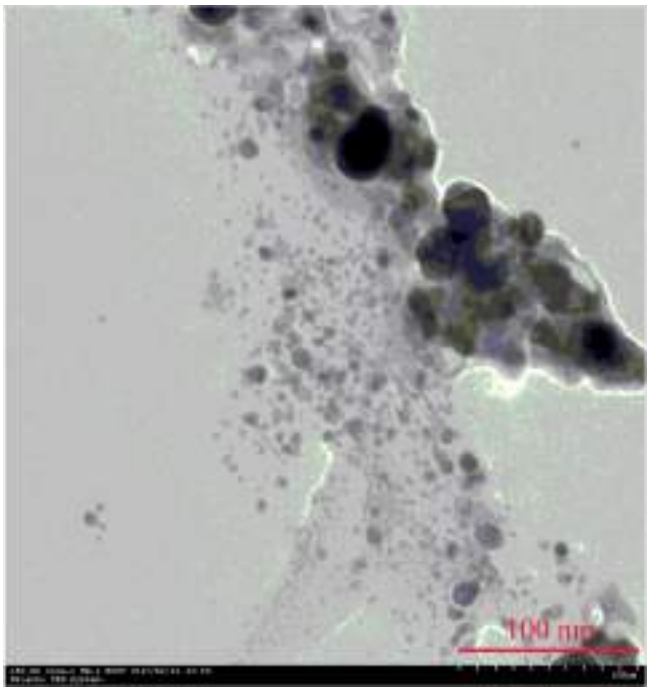

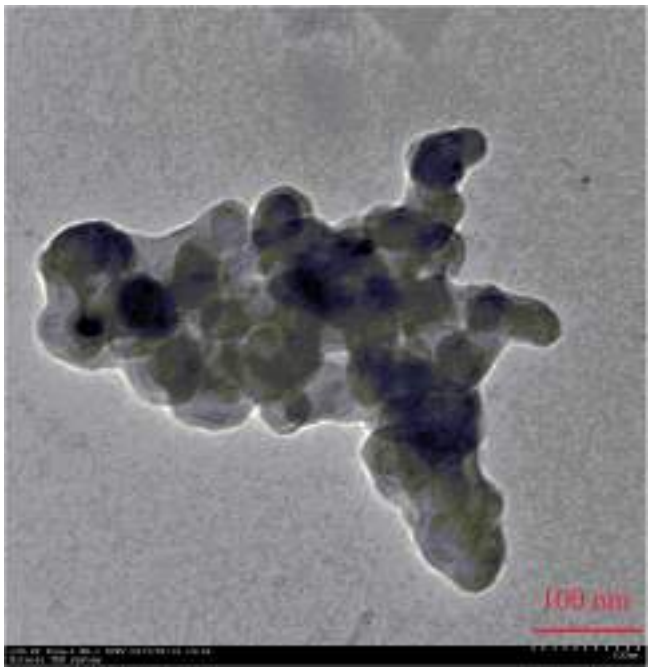

Fig. 8. TEM image of $CoFe_2O_4$. TEM image of $CoZnFe_2O_4$. TEM image of $CoCdFe_2O_4$ nanoparticles.

Fig. 8. (*continued*)

high annealing temperature [35]. Due to high temperature, it is not possible to avoid agglomeration of particles. From the TEM images, it seems like that particles are spherical in shape with crystalline nature. The size of particles was also calculated by the software- Image J. The obtained particle size lies in the range 32.57 nm to 58 nm approximately of cobalt ferrite and its zinc and cadmium doped samples. Particle size of cobalt ferrite nano powder is found approximately 32.51 nm. But with zinc doping particle size increased to 49.81 nm. This could be due to Zn^{2+} ion having zero magnetic moment which has replaced cobalt ion towards the tetrahedral A–sites. Particle size also increases with Cd^{2+} doping as Cd^{2+} ion has similar behavior like Zn^{2+} ion. With cadmium doping particle size increased more from 32.57 nm to 58.83 nm and it is an interesting fact that approximately same range of particle size is obtained for all the prepared samples by XRD method as given in the Table 1 for comparison. Moreover, particles are appearing roughly like irregularly distributed but may be mentioned to have spherical in shape from all the three images.

3.5. VSM analysis

Magnetic properties of the synthesized samples were analyzed by vibrating sample magnetometer (VSM) at room temperature with a maximum applied field of ± 10000Oe. The Figs. 9 to 11 shows the hysteresis loops of cobalt ferrite $CoFe_2O_4$, $Co_{0.9}Zn_{0.1}Fe_2O_4$and $Co_{0.9}Cd_{0.1}Fe_2O_4$ which reveals ferromagnetic behavior of all the samples annealed at 1000 °C. On the basis of the analysis of all these hysteresis loops, it may be mentioned that the ferromagnetic behavior has been modified by the doping of non magnetic ions of Zn and Cd to substitute magnetic cobalt ions in our samples. The magnetic parameters of prepared samples like coercivity (Hc), remanence magnetization (M_R) and squareness ratio (M_R/M_S) have been found to decrease with doping of Zn and Cd ions, as given in the table 2.While saturation magnetization (M_s) is obtained high with doping of Zn and Cd ions in cobalt ferrite which is in fact needed a high value for high-frequency inductors in magnetic materials [36].

By analysis of hysteresis loop from Fig. 9, it is observed that cobalt ferrite has broader loop as compared to other plots in the Figs. 10, 11. However, cobalt ferrite doped with zinc ion has narrower loop as like a soft ferrite. From the Table 2, saturation magnetization values of

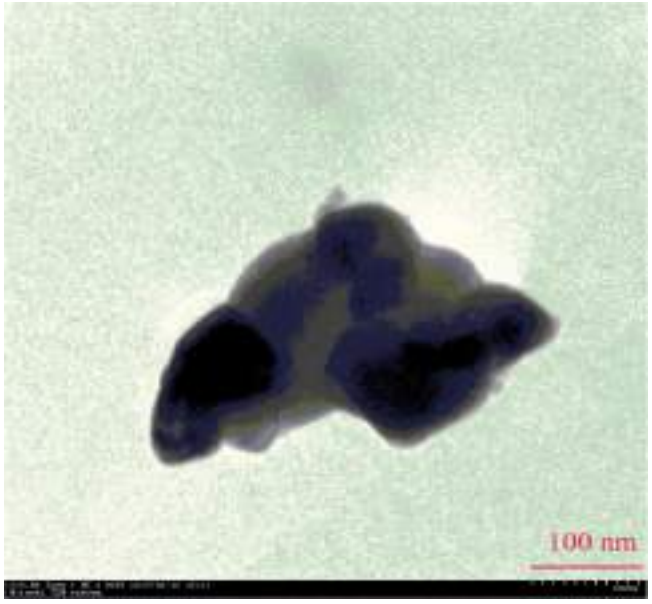

Fig. 8. (*continued*)

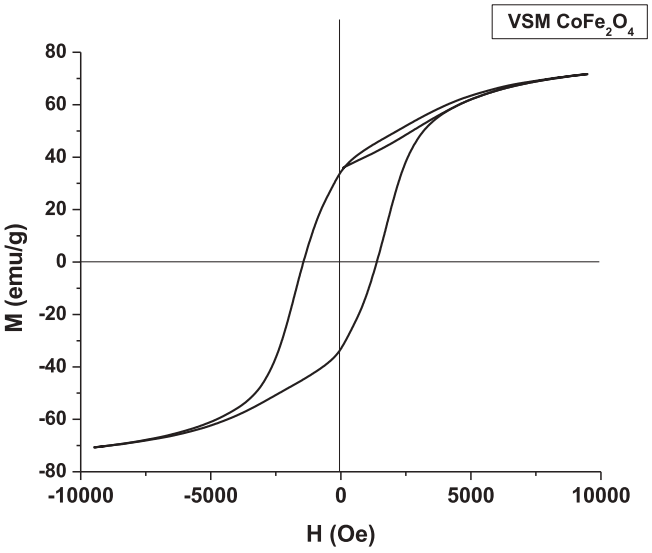

Fig. 9. Magnetic Hysteresis loops of $CoFe_2O_4$.

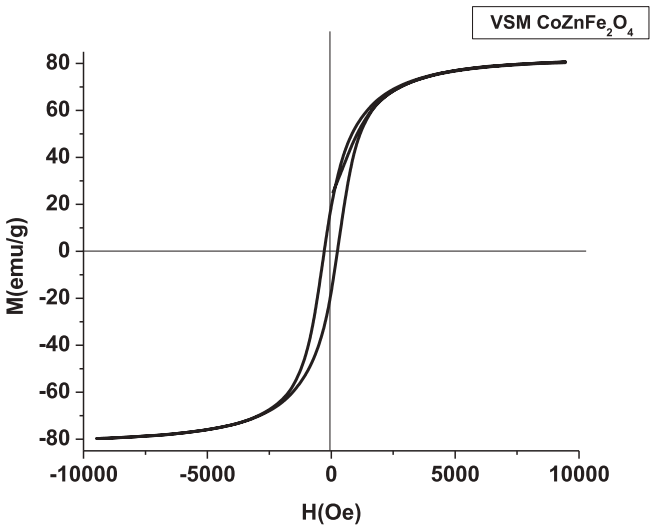

Fig. 10. Magnetic hysteresis loops of $Co_{0.9}Zn_{0.1}Fe_2O_4$.

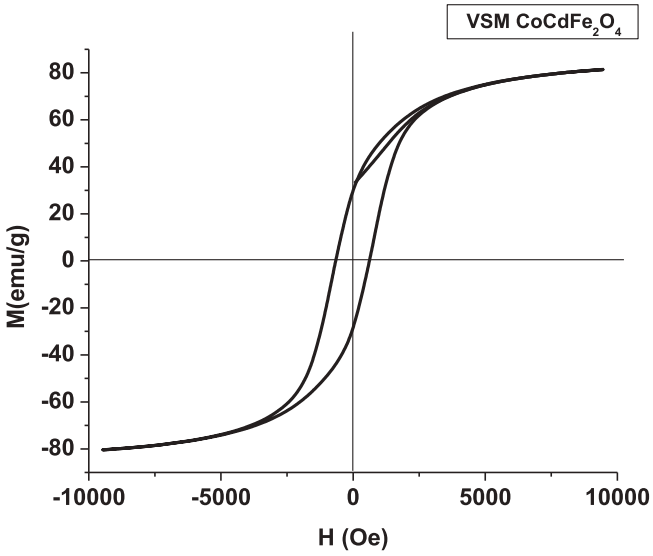

Fig. 11. Magnetic hysteresis loops of $Co_{0.9}Cd_{0.1}Fe_2O_4$.

prepared samples ranges between 72.13 emu/g to 81.60 emu/g. Further, the saturation magnetization (M_s) for cobalt ferrite is observed 72.13 emu/g, which is in good agreement with earlier reported values [37]. Furthermore, M_S values increase with the doping of Zn^{2+} and Cd^{2+}, because $Zn^{2+}$and Cd^{2+} occupies A-site. The dopants has displaced Fe^{3+} towards B-site which increases magnetization, now magnetic moment of A-site decreases because increase in non-magnetic Zn^{2+} ion in the A-site. Hence, concentration of Fe^{2+} ions increases in B-site. Therefore A-B interaction between magnetic ions decreases, which further increases the total magnetization values M_s. An almost similar behavior has also been shown by Cd^{2+} doping in the cobalt ferrite. Increase in the value of M_s by $Zn^{2+}$and Cd^{2+}doping is found in good agreement with the previously reported values by other researchers [38]. The values of coercivity (H_c) found in the range 329.3 Oe to 1408.9 Oe. The H_c value is determined lower 263.4 Oe in the case of cobalt zinc ferrite that is due to the anisotropic nature of spinel cobalt zinc ferrites and due to non- magnetic moments of Zn^{2+} ions [39–41]. The value of saturation magnetization in case of cobalt cadmium ferrite has been found to increase from 72.13 emu/g to 81.60 emu/g with the increase in the temperature due to the gradual increase in crystallinity and particle size [42]. Remanence (M_R) values lies between 18.41 emu/g to 33.74 emu/g, but M_R value is found very less in case of zinc doping hence we obtained soft ferrite sample of $Co_{0.9}Zn_{0.1}Fe_2O_4$ that may be due to the reason that zinc is non- magnetic in nature.

4. Conclusions

The ferrite samples of $CoFe_2O_4$, $Co_{0.9}Zn_{0.1}Fe_2O_4$ and $Co_{0.9}Cd_{0.1}Fe_2O_4$ nanoparticles have been prepared by auto combustion method successfully. Occurrence of thermal decomposition was confirmed by the fast weight loss nearly up to 580.0 °C due to removal of hydroxyl group and after that weight loss has been observed almost negligible up to 1000 °C from the analysis of the TGA plot. From XRD investigations, it is confirmed that all the samples are single phase cubic structure having Fd3m space group of cobalt ferrite samples. The FTIR spectra confirmed the presence of M-O bond that also shows the presence of ferrite in the prepared samples. The crystallite size has been found to be lying in the range from 46.20 nm to 53.30 nm and strain values are obtained from -0.0003 to 0.0008 with the help of W-H method using XRD data. The average crystallite size and lattice parameters of the samples have been found to be larger in the case of Zn and

Cd ion doping in cobalt ferrite, that may be understood due to larger ionic radii of Zn^{2+} and Cd^{2+} as compared to Co^{2+}. The crystallite size in nano range of our prepared samples calculated by Debye - Scherrer formula, Williamson-Hall plot and TEM analysis have been found to be in good agreement with each other. Hence, it is concluded from analysis of results of particle size which indicate about the formation of nano materials and doping of cobalt ferrites. Further, TEM analysis reported spherical shape of ferrite nanoparticles along with the presence of high agglomeration due to magnetic interactions between ferrites particles in our prepared samples. Furthermore, hysteresis loop by VSM analysis confirmed about the ferromagnetic nature along with tuning of magnetic parameters by doping with Zn^{2+} and Cd^{2+} of our prepared cobalt ferrite samples. The values of coercivity (H_c) have been obtained from 263.45 Oe to 1408.93 Oe. The H_c value is determined lower 263.4 Oe in the case of cobalt zinc ferrite that is due to the anisotropic nature of spinel cobalt zinc ferrites and due to non- magnetic moments of Zn^{2+} ions. From the results of all characterization techniques in this paper, it is concluded that magnetic properties of cobalt ferrite nanomaterial can be suitably modified by doping with Zn^{2+} and Cd^{2} ions as a promising material for various technologies useful in many fields like medical, information and communication etc.

Acknowledgement

Thapar University, Patiala and IIT, Roorkiare greatfully acknowledged for providing characterization facilities to our prepared samples.

Appendix A. Supplementary data

Supplementary data to this article can be found online at https://doi.org/10.1016/j.jmmm.2018.11.010.

References

[1] L. Filipponi, D. Sutherland, Nanotechnology - A Brief Introduction (2007).
[2] V. Raghavan, Materials Science and Engineering, Fifth Edition, PHI Learning Private Limited, 2010.
[3] A. Goldman, Modern Ferrite Technology, Van Nostr and Reinhold, New York, 1990.
[4] W. Zhongli, L. Xiaojuan, L. Minfeng, C. Ping, L. Yao, M. Jian, J. Phys. Chem. **112 B** (2008) 11292.
[5] C. Borgohain, K.K. Senapati, K.C. Sarma, P. Phukan, J. Mol. Catal. A: Chem 363 (2012) 495.
[6] C.C. Agrafiotis, C. Pagkoura, A. Zygogianni, G. Karagiannakis, M. Kostoglou, G.A. Konstandopoulos, Int. J. Hydrog. Energy 37 (2012) 8964.
[7] V.S. Kumbhar, A.D. Jagadale, N.M. Shinde, C.D. Lokhande, J. Appl. Surf. Sci 259 (2012) 39.
[8] S.I. Kiselev, J.C. Sankey, I.N. Krivorotov, N.C. Emley, R.J. Schoelkopf, R.A. Buhrman, D.C. Ralph, Nature 425 (2003) 380.
[9] L. Ai, J. Jiang, Curr. Appl. Phys. 10 (2010) 284–288.
[10] W. Chen, W. Zhu, O.K. Tan, X.F. Chen, J. Appl. Phys. 108 (2010) 034101.
[11] G.A. Sawatzky, F. van der Woude, A.H. Morrish, Mössbauer Study of Several Ferrimagnetic Spinels, Phys. Rev. 187 (1969) 747–757.
[12] A.B.V. Groenu, P.F. Bongers, A. L. Stuyts, Mater. Sci. Eng. 3 (1968-69) 317.
[13] G.A. Pettit, D.W. Forester, Mossbauer study of Co-Zn ferrites, Phys. Rev. **4 B** (1971) 3912–3923.
[14] D. Hork, B. Rittich, A. Spanov, D. Horak, A. Spanova, J. Magn. Magn. Mater 311 (2007) 249–254.
[15] B.V. Bhise, M.B. Dongare, S.A. Patil, S.R. Sawant, J. Mater. Sci. Lett. 10 (1991) 922–924.
[16] S. Akhter, M.A. Hakim, J. Mater. Chem. Phys. 120 (2010) 399–403.
[17] A.B. Gadkari, T.J. Shinde, P.N. Vasambekar, J. Alloys Compds. 509 (2011) 966–972.
[18] S.S. Suryawanshi, V.V. Deshpande, U.B. Deshmukh, S.M. Kabur, N.D. Chaudhari, S.R. Sawant, J. Mater. Chem. Phys. 59 (1999) 199–203.
[19] E. Ranjith Kumar, R. Jayaprakash, G. Sarala Devi, P. Siva Prasada Reddy, J. Magn. Magn. Mater 355 (2014) 87–92.
[20] Kopp Alves, Engineering Materials (2013), https://doi.org/10.1007/978-3-642-41275-2_2.
[21] S.T. Aruna, A.S. Mukasyan, Combustion synthesis and nanomaterials, Curr. Opin. Solid State Mater. Sci. 12 (3–4) (2008) 44–50.
[22] M. Srivastava, S. Chaubey, A.K. Ojha, Mater. Chem. Phys. 118 (2009) 174–180.
[23] C. Caizer, M. Stefanescu, J. Phys. D: Appl. Phys. 35 (2002) 3035–3040.
[24] B.D. Cullity, Elements of X-ray Diffraction, Addison-Wesley, London, 1978.
[25] J. Chen, Y. Wang, Y. Deng, J. Alloys Compd. 552 (2013) 65.
[26] A. Manikandan, M. Durka, S. Arul Antony, J. Supercond. Nov. Magn 27 (2014) 2841.
[27] K. Nagamani, M.V. Reddy, Y. Lingappa, K.T.R. Reddy, R.W. Miles, Int. J. Opto electron. Eng 2 (2012) 1–4.
[28] A. Pardeep, G. Chandrasekaran, FTIR study of Ni, Cu and Zn substituted nanoparticles of MgFe2O4, J. Magn. Magn. Mater. 60 (2006) 371–374.
[29] P.N. Vasambekar, C.B. Kolekar, A.S. Vaingankar, Magnetic behaviour of Cd^{2+} and Cr^{3+} substituted cobalt ferrites, J. Magn. Magn. Mater. Chem. Phys. 60 (1999) 282–285.
[30] R.D. Waldron, Infrared Spectra of Ferrites, J. Phys. Rev. 99 (1955) 1727–1735.
[31] Y. Liu, Y. Zhang, J.D. Feng, C.F. Li, J. Shi, R. Xiong, J. Exp. Nanosci. 4 (2) (2009) 159–168.
[32] L. Cui, P. Guo, G. Zhang, Q. Li, R. Wang, M. Zhou, L. Ran, X.S. Zhao, Colloids Surf. A 423 (2013) 170.
[33] M.H. Habibi, H. Parhizkar, J.: Spectrochim. Acta A 127 (2014) 102.
[34] D. Gherca, A. Pui, N. Cornei, A. Cojocariu, V. Nica, O. Caltun, J. Magn. Magn. Mater. 324 (2012) 3906.
[35] C. Upadhyay, H.C. Verma, S. Anand, Cation distribution in nanosized Ni-Zn ferrites, J. Appl. Phys. 95 (2004) 5746–5751.
[36] M. Khairy, S.A. El-Safty, M. Ismael, H. Kawarada, Appl. Catal. 127 B (2012) 1–10.
[37] L. Neel, C.R. Acad. Sci. Paris 230 (1950) 375–377.
[38] Nalla Somaiah, V. Tanjore Jayaraman, P.A. Joy, Dibakar Das, J. Magn. Mater. 324 (14) (2012) 2286–2291.
[39] Y. Koseoglu, Ceram. Int. 39 (2013) 4221.
[40] R.C. Kambale, P.A. Shaikh, N.S. Harale, V.A. Bilur, Y.D. Kolekar, C.H. Bhosale, K.Y. Rajpure, J. Alloys Compd. 490 (2010) 568.
[41] S.P. Yadav, S.S. Shinde, A.A. Kadam, K.Y. Rajpure, J. Alloys Compd. 555 (2013) 330.
[42] S. Morup, Euro. Phys. Lett. 28 (1994) 671–676.

Materials Science and Engineering B 272 (2021) 115327

Contents lists available at ScienceDirect

Materials Science & Engineering B

journal homepage: www.elsevier.com/locate/mseb

Ce doping induced modifications in structural, electrical and magnetic behaviour of hematite nanoparticles

Vijay Kumar [a], Dharamvir S. Ahlawat [a,*], Shah AarifUl Islam [b], Amrik Singh [a]

[a] Deptt. of Physics, Chaudhary Devi Lal University, Sirsa 125055, Hry., India
[b] Solid State Research Lab, Deptt. Of Physics, NIT Srinagar 190006, J&K, India

ARTICLE INFO

Keywords:
Hematite
Ce-doping
Raman
FE-SEM
DC electrical resistivity
VSM

ABSTRACT

In this paper, we investigate effects of Ce-doping on the structural, electrical and magnetic properties of $Fe_{2-2x}Ce_{2x}O_3$ samples synthesized by sol–gel method by varying the composition as (x = 0.00, 0.02, 0.05, 0.08, 0.10). The recorded XRD pattern of synthesized powder samples indicates the formation of hematite phase up to the dopant concentration x = 0.05, thereafter a further increase in doping concentration leads to the existence of secondary phase of cerium oxide (CeO_2) along with the pure phase of hematite. Moreover, XRD results are well supported by FTIR and Raman spectroscopy observations. Variation in grain size as well as the grain growth as revealed from FE-SEM micrographs may be possibly due to Ce ions having different ionic radii than that of the host Fe^{3+}. DC electrical resistivity variation with temperature in the range 150–400 K, reveals the enhancement in electrical conductivity due to the increase of Ce-doping content. Magnetic hysteresis measurements carried out at room temperature (300 K) with a maximum applied field of ±10000Oe reveal that the magnetic parameters i. e. remnant magnetization (M_R) and coercivity (H_C) of $Ce_{2x}Fe_{2-2x}O_3$ increase up to the doping concentration of x = 0.02, thereafter a significant random variation is observed.

1. Introduction

The study of iron nanoparticles has become an interesting topic of research due to their potential applications in various fields of technology such as memory devices, target drug delivery, magnetic imaging and sensors [1–5]. Iron oxides are considered to be extremely useful possessing more stability, being eco-friendly and owing to their low cost. Among the various iron oxides, nanoparticles of Fe_2O_3 are of great interest due to their large variety of applications in the area of adsorbents, catalysis and in storage devices. Fe_2O_3 generally exists in four crystalline phases, α-Fe_2O_3, β-Fe_2O_3, γ-Fe_2O_3 and ε-Fe_2O_3. Out of these four, hematite(α-Fe_2O_3) is the most stable iron oxide that can exhibit interesting chemical, electrical and magnetic properties [6–9] and can also act as one of the raw materials for the iron and steel industry. Furthermore, hematite is environmental-friendly, has a high resistance to corrosion and is also non-toxic nature which makes it a viable material for applications in variety of fields such as storage devices, in bio-applications, catalysis and in magnetic fluids [10–13]. Hematite generally exists in a hexagonal structure with the space group R-3c. Substitutional effect in α-Fe_2O_3 at Fe-site influences the electrical, magnetic and other physical properties. In this direction, a large number of reports are available on the doping of transition metals in hematite and another materials [14–22]. However the reports on rare-earth metal-doping are not exhaustive. Furthermore, it has been found that due to a large magnetic moment, the structural, electrical and magnetic properties have strongly been affected with incorporations of lanthanide (Ln^{+3}) ions [23–27]. Ruqiya et al. [28] reported that there is an increase in saturation magnetisation and decrease in coercivity along with simultaneous decrease in particle size with doping of Ho^{+3} ions in the α-Fe_2O_3 lattice at room temperature. Freyria et al. [29] reported that ferromagnetism has enhanced with incorporation of Europium (Eu^{3+}). Goyal et al. [30] reported the modification in magnetism with Neodymium (Nd) doping in α Fe_2O_3 and correlated the same with reduction in particle size. Wan et al [31] also reported the enhancement in magnetic properties with the incorporation of Gd^{+3} ions in α-Fe_2O_3. For the α-Fe_2O_3, numerous dopants have been employed to tune the catalytic performance for OER (Oxygen evolution reaction), including Si [32–36], Sn [37–41], Pt [42,43], Nb [44,45], Ni [46], Ti [47–49], Al [47], Zn [44], Cr [50,51], Mo [51], and some have been proved to be effective. For instance, single Ti or Sn, and Be/Al co-dopants can increase the photocurrent response of Fe_2O_3 effectively [9]. A defect model was derived to explain this phenomenon. In addition, a temperature independent value for the electron

* Corresponding author.
E-mail address: dahlawat66@gmail.com (D.S. Ahlawat).

https://doi.org/10.1016/j.mseb.2021.115327
Received 12 October 2020; Received in revised form 3 June 2021; Accepted 18 June 2021
Available online 27 June 2021

mobility of 0.01 $cm^2 V^{-1} s^{-1}$ for a donor density of 4.0×10^{20} cm^{-3} (1% Ti) was derived. Indium substitution in hematite also caused a decrease in the crystallite size, an increase in the particle size, a shift in the position of bands in infrared spectra, a decrease in the relative intensity of absorption bands in UV–Vis, NIR spectra and a disappearance of the Morin transition. Maximum substitution was estimated at about 8 mol%. Several chemical and physical methods such as spray pyrolysis, sol–gel, co-precipitation, combustion technique, high energy milling etc. have been used for the fabrication of stoichiometric and chemically pure nano ferrite materials.

However out of these, sol–gel technique is quite robust for the preparation of hematite nanoparticles because stoichiometry of the precursors is precisely maintained and all sorts of impurities and contaminations can be avoided rather efficiently. This versatile method producing high yields of α-Fe_2O_3 nanoparticles useful at the industrial level and more hands-on in terms of size and morphology control. Although it takes a long processing time. By adopting this synthesis method, we have already reported, annealing effect on the structural and dielectric properties of undoped hematite nanoparticles [52]. Furthermore, it will be interesting to know and understand the role played by Ce-doping in hematite for various useful properties [53–55]. Structural, electrical and magnetic properties of Cerium doped hematite have not been reported together for these samples yet, to the best of our knowledge. Ce substitution in the octahedral Fe (1, 2) site of Fe_2O_3 has marked effects on the structural parameters that may strongly enhance electrical properties [56–62]. The magnetic and structural properties of hematite are also affected by particle size [61,63], degree of crystallinity [59], doping [56–60], hence provides new insights and opportunities for technological applications. Because of its low cost, high resistance to corrosion and environment friendly properties, α-Fe_2O_3 nanoparticles have been prepared. As, there is a significant effect of the synthesis method on the properties like structural, microstructural, magnetic and electrical of the hematite (α-Fe_2O_3) nanoparticles. Among the various approaches, doping strategy, typically through incorporating of atoms into the lattice, has been regarded to be an effective approach to improve the photocatalytic activity of metal oxides. Substitutional dopants can affect the electronic properties by increasing the charge carrier density and thus the electrical conductivity. Successful modification of the opto-electronic properties of the hematite are affected by the preparation conditions, chemical composition, temperature and the method of preparation. Among the available chemical methods, the sol–gel technique is an excellent method to synthesize rare earth substituted oxide nanoparticles with maximum purity. As per authors' knowledge, electrical behaviour of cerium doped α-Fe_2O_3 nanoparticles has not yet been understood in correlation with structural, microstructural and morphology at ours selected concentrations. Our new findings by deep insights on electrical conductivity at 5% doping of Ce in α -Fe_2O_3 indicates potentiality in solar cell, sensors, bio-medical and related technology. In this paper we investigate the doping effect of Ce in hematite with varying concentration and also discuss improvement in the DC electrical conductivity versus temperature, enhancement of coercivity and modification in remanence magnetization.

2. Experimental details

2.1. Synthesis

$Fe_{2-2x}Ce_{2x}O_3$ (x = 0.00, 0.02, 0.05, 0.08, 0.10) samples were synthesized by sol–gel method. Iron nitrate $Fe(NO_3)_3 \cdot 9H_2O$ and cerium nitrate $Ce(NO_3)_3 \cdot 6H_2O$ precursors taken in stoichiometric ratio were dissolved in deionised water. After that, the prepared sol was put on heater with rigorous stirring at 80 °C till it got converted into gel and then the obtained gel was transformed to a solid form by heating at 120 °C for 2 h. This solid form was heated at 200 °C for 3 h to remove any moist phase that might otherwise have led to fundamental changes in the structure. Now, in order to attain the homogeneity of mixture the powdered form of samples was mixed and ground thoroughly in an Agatemortar and pestle. After grinding, the powdered samples were pelletized in a hydraulic press using a die of 10 mm diameter and applying a pressure of 5 tonne. The obtained pellets were finally sintered in air at 600 °C for 6 hours to obtain dense samples.

2.2. Characterizations

The prepared samples (pellets) were characterized for various properties such as X-Ray Diffraction (XRD), Raman spectroscopy, FTIR, FE-SEM, temperature dependent resistivity (R-T) and magnetic measurements. Crystal structure of the samples was determined, using a Bruker-AXSD8 advanced diffractometer with Cu K_α (λ = 1.540 Å) source in the range of 30° to 70°. Raman measurement was carried out by using an In-via microscope (Renishaw) with Ar^+ ion laser (λ = 514.5 nm) and 50 mW of laser power [64]. Particle size and morphology of the hematite nanoparticles were obtained by field emission scanning electron microscope (FE-SEM). Variation of DC electrical resistivity with temperature in the range, 150 K to 400 K was measured using Keithley electrometer -6517B interfaced with the lab-view software. Furthermore, the magnetic properties of hematite samples were measured using a vibrating sample magnetometer (VSM), with a varying field of −10KOe to +10 KOe. The hysteresis curves of hematite nanoparticles were obtained for different compositions (x = 0.00, 0.02, 0.05, 0.08, 0.10) at room temperature. The saturation magnetisation (M_{sat}), Remnant magnetisation (M_r) and Coercivity (H_c) of all these compositions were determined and hence the influence of varying Ce-doping concentrations was investigated.

3. Results and discussion

3.1. XRD analysis

The XRD patterns of $Fe_{2-2x}Ce_{2x}O_3$ (x = 0.00, 0.02, 0.05, 0.08, 0.10) nanoparticles are shown in Fig. 1 From these diffraction patterns, $Fe_{2-2x}Ce_{2x}O_3$ (x = 0.00) showing most intense peak at 33.15° corresponding to (1 0 4) plane indicates the pure hematite phase. The addition of Ce ions in the host lattice of α-Fe_2O_3 reduces the intensity of diffraction peaks that corresponds to the formation of nanocrystalline samples with reduced crystallinity [65,66].

The change in the peak intensity is related with the crystallite size (D) which has been estimated with the help of Debye-Scherer's formula

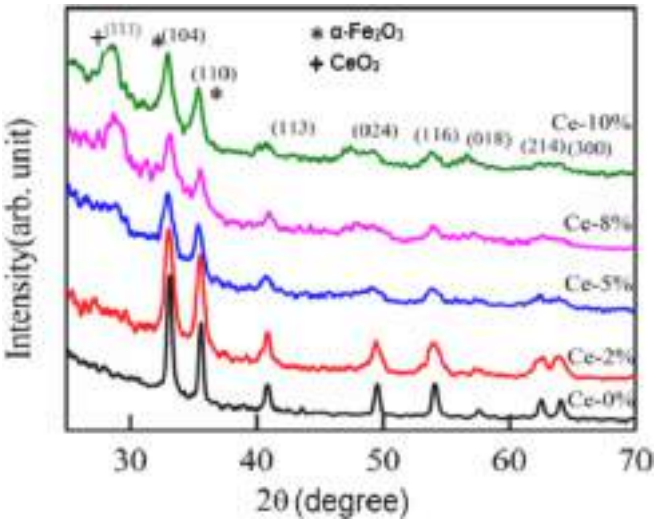

Fig. 1. X-ray diffraction patterns of $Fe_{2-2x}Ce_{2x}O_3$ (x = 0.00, 0.02, 0.05, 0.08, 0.10) nanoparticles showing the decrease in intensity of diffraction peaks with Ce-doping.

[67].

$$D = \frac{0.89\lambda}{\beta\cos\theta} \quad (1)$$

where the parameters in equation (1), i.e. λ = 1.54 Å, β and θ are the wavelength, full width at half maximum (FWHM) [68] and Bragg angle of a particular diffraction peak [69] respectively. From the Table 1, the crystallite sizes for pure α-Fe_2O_3 nanoparticles are observed to be ~21.1 nm. Further, it has been noticed that there is an enhancement in the FWHM of the diffraction peaks with the addition of Ce in host lattice of α-Fe_2O_3. The enhancement in FWHM corresponds to the reduction in crystallite size. The crystallite size reduces to 9.7 nm for 5% Ce-doped α-Fe_2O_3 nanoparticles. The observed decreasing trend for the mean crystallite size (calculated from the most intense peak in XRD pattern) with increasing Ce concentration is in well agreement with the earlier reported work [70]. The Ce ions successfully doped in the hematite may be available in +3 and +4 oxidation states reported by other workers [71]. XRD patterns of cerium-doped hematite clearly show shifting of the centre of the diffraction peaks slightly toward the lower angle on Ce doping in comparison to that of pure hematite. Moreover, the obtained reflections are sharp and high in intensity which reveals that the synthesized samples are well crystalline. In addition, the lattice constants of Cerium doped hematite were found to be slightly larger than those to pure -refer to Table 1. This is consistent with the fact that the ionic radii of Ce^{3+} (1.03 Å) and Ce^{4+} (1.01 Å) are larger than Fe^{3+} (0.64 Å). The shifting of XRD lines with doping simply suggest that Ce ion was successfully substituted into the hematite host structure at the Fe site. The substitution of Ce ions at Fe-site leads to an enhancement in both lattice parameter values (*a* and *c*) for upto 5% doping concentration; however, a random variation has also been observed at higher concentration values of Ce. This indicates that the Ce ions are incorporated in the host lattice of α-Fe $_2O_3$up to 5% doping concentration and above it the solubility limit reaches. The Ce ion fits on the interstitial site of the Fe^{3+} up to 5% doping. Above this concentration, the Ce ions start accumulating over the surface instead of occupying substitution sites in the host lattice resulting in the formation of a secondary phase along with the primary α-Fe $_2O_3$ phase. From the XRD patterns of Fig. 1, some additional peaks have also been noticed for 8% and 10% of Ce ion doping concentration that indicate the formation of secondary phase [72]. These additional peaks for 8% and 10% shift slightly towards left side that means towards lower Bragg angle which indicates some strain is produced due to 8% and 10% Ce doing in α-Fe_2O_3. This type of result directly corresponds to the insolubility of Ce ions within the α-Fe $_2O_3$ crystal lattice [72]. The evidence of insolubility above 5% cerium concentration is in agreement with the already published research work [73]. As given in Table 1, both the crystallite-size and lattice-parameters possess non-uniform variation in their values that may be due to the formation of the secondary phase.

3.2. FTIR analysis

FTIR spectra of $Fe_{2-2x}Ce_{2x}O_3$ (x = 0.00, 0.02, 0.05, 0.08, 0.10) samples in the wave number range from 400 cm^{-1} to 4000 cm^{-1} are shown in Fig. 2. The bands appearing at 3440 cm^{-1}, 1632 cm^{-1} and at 2950 cm^{-1}, 2850 cm^{-1} are the characteristic feature of O–H bending mode of hydroxyl group and asymmetric and symmetric-vibrations of -CH_3 type groups respectively [74,75]. Bands appearing at 1040 cm^{-1} and 1382 cm^{-1} are assigned to-CH_2 and residual hydroxyl group C-OH respectively [76]. Two other bands at 457 cm^{-1} and 539 cm^{-1} referred as Eu and A_{2u} are the characteristic modes of hematite nanoparticles [77]. The presence of a band at 539 cm^{-1} may be related with overlapping of A_{2u} and Eu vibrations in the parallel and perpendicular direction to c-axis and can be attributed to stretching vibration of the Fe–O [6].

Furthermore, it is also noticed in the Fig. 2 that with incorporation of Ce into the pure hematite there is a decrease in the peak intensity of both Eu and A_{2u} modes, resulting in reduction of crystallinity of the α-Fe_2O_3 nanoparticles. However, some enhancement in the peak intensity was recorded for $Fe_{2-2x}Ce_{2x}O_3$ (x = 0.10) that may be due to segregation of ions at this high concentration (x = 0.10). Our observed results of FTIR spectroscopy are found in agreement with the Raman and XRD measurements.

Table 1
Crystallite size, lattice parameters, resistivity and grain size values of $Fe_{2-2x}Ce_{2x}O_3$ (x = 0.00, 0.02, 0.05, 0.08, 0.10) nanoparticles showing the variation arising due to Ce-doping.

Doping Concentration (x)	Crystallite Size (nm)	Lattice Parameters (Å) (a-axis)	(c-axis)	Resistivity at 100 K ($\times 10^8\Omega$m)	Grain Size (nm)
x = 0.00	21.1	5.03	13.22	47.66	427.9
x = 0.02	13.3	5.04	13.25	17.27	402.9
x = 0.05	09.7	5.06	13.26	0.278	103.5
x = 0.08	11.1	5.02	13.21	12.25	365.6
x = 0.10	11.1	5.05	13.27	8.560	367.4

3.3. Raman spectroscopy

Raman spectra of $Fe_{2-2x}Ce_{2x}O_3$ (x = 0.00, 0.02, 0.05, 0.08, 0.10) nanoparticles have been recorded in the range of 200 cm^{-1} to 650 cm^{-1} as shown in Fig. 3. From group theory calculations the recorded Raman spectra shows$A_{1g}$and E_g modes appearing at wave numbers 220cm^{-1}, 490 cm^{-1} and 284cm^{-1}, 402 cm^{-1} & 607 cm^{-1} respectively [77]. Generally, in the Raman spectra we noticed many broad shaped peaks due to reduced particle size in nanoscale region. Hematite belongs to D^6_{3d} point group and there exist five Raman vibration active modes (two of A_{1g} and three of E_g ones) which have also been reported in other studies [78].

From Fig. 3, by careful examination, it has been observed that Raman bands are shifted towards the lower wave-number side with incorporation of Ce ion concentration of up to 8% in the host lattice. This shifting may be related with the reduction in particle size that occurs due to incorporation of Ce ions in the host lattice. As the particle size decreases, the spectral lines become broader and shift towards lower wave number side which is a general characteristic of nanoparticles [79]. The highest value of Full Width at Half Maximum (FWHM) is noticed in A_{1g} mode at about 220 cm^{-1}, due to movement of Fe^{+3} ions along c-axis. However, the peaks shifting towards higher wavenumber side have also been noticed in our results for $Fe_{2-2x}Ce_{2x}O_3$ (x = 0.10) nanoparticles. This type of reverse shifting trend in Raman spectra for x = 0.10, the

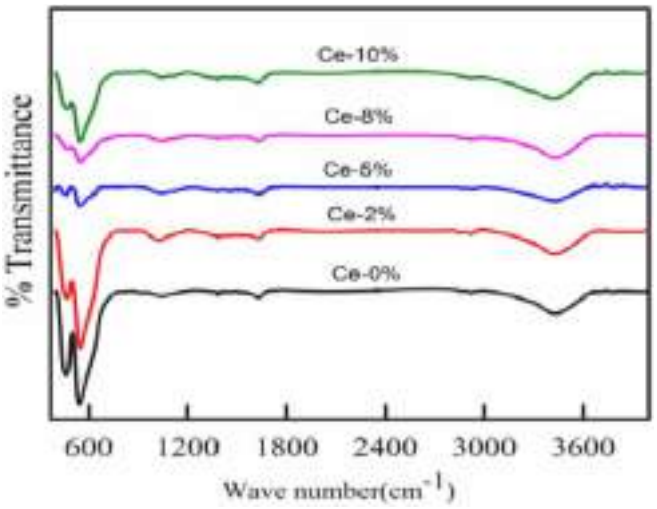

Fig. 2. FTIR spectra of $Fe_{2-2x}Ce_{2x}O_3$ (x = 0.00, 0.02, 0.05, 0.08, 0.10)nanoparticles, revealing various characteristic bands pertaining to different modes.

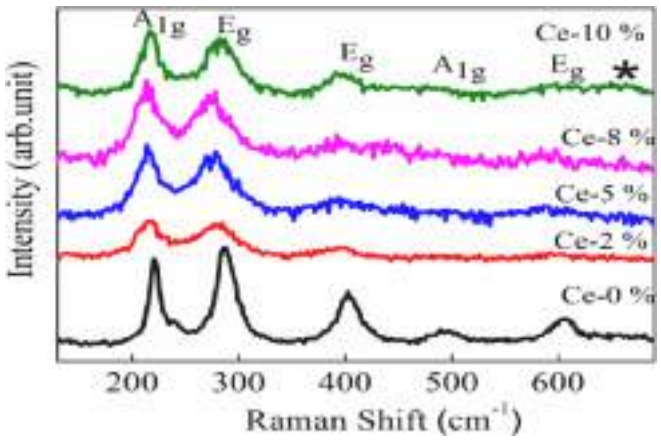

Fig. 3. Raman spectra of $Fe_{2-2x}Ce_{2x}O_3$ (x = 0.00, 0.02, 0.05, 0.08, 0.10) nanoparticles acquired at room temperature, showing the broadening of characteristic peaks due to Ce-doping.

highest concentration, may be due to the segregation of Cerium ions as observed in our XRD measurements.

3.4. FE-SEM analysis

FE-SEM micrographs of pure and Ce-doped hematite samples i.e. $Fe_{2-2x}Ce_{2x}O_3$ (x = 0.00, 0.02, 0.05, 0.08, 0.10) are shown in Fig. 4. These images were taken with the FESEM instrument, model FEI Quanta 200 F SEM, by scanning the surface in raster scan mode which offers resolution in nanometres as well as yields a very low signal to noise ratio [80]. The morphology reveals the grains looking like irregular and flattened spheres having a size variation ranging from 30 to 260 nm in all the compositions. Grain size for all the sample compositions was calculated using IMAGE-J software [81]. The grain growth is observed as getting

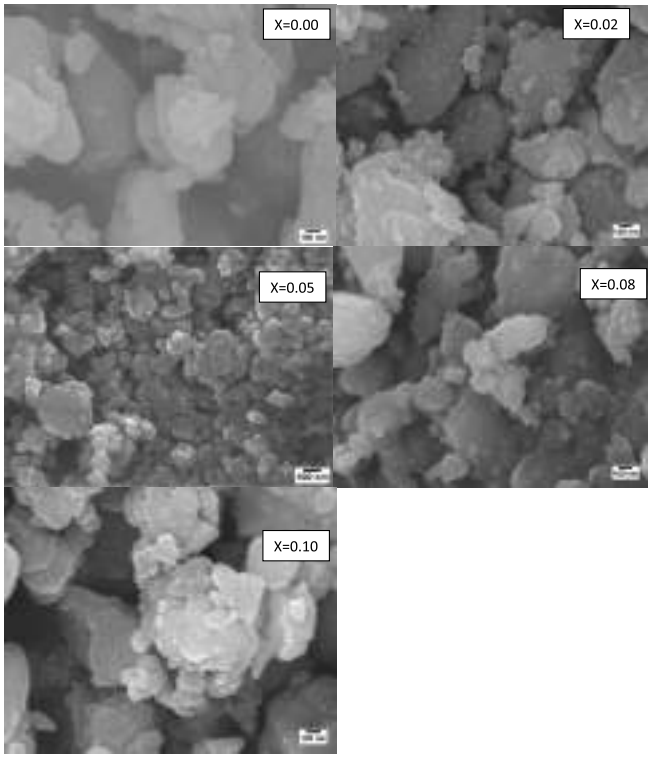

Fig. 4. FE-SEM images of $Fe_{2-2x}Ce_{2x}O_3$(x = 0.00,0.02,0.05,0.08,0.10)nanoparticles, showing the variation in grain size due to Ce-doping.

suppressed by the incorporation of Ce cations substituted for the Fe^{3+} cations, up to the composition with x = 0.05. Beyond this doping concentration, the grains again start to agglomerate and hence the grain growth is enhanced. The variation in grain size as well as grain growth is possibly due to the Ce ions having different ionic radii than the host Fe^{3+} ions [82]. High agglomeration and dispersibility of nanoparticles are observed in the undoped and Ce ion doped hematite samples respectively, same findings reported by J. Ning et al. [71].

3.5. Resistivity measurements

The variation of DC electrical resistivity with temperature (150 K to –400 K) for the prepared samples of $Fe_{2-2x}Ce_{2x}O_3$ (x = 0.00, 0.02, 0.05, 0.08, 0.10) are shown in Fig. 5. The observed behaviour of electrical resistivity with the increase of temperature is an exponential decay type, which has been found in the case of semiconducting materials. The Arrhenius relation [83], explains the variation of electrical resistivity with temperature,

$$\rho_{DC} = Ce^{\left(E_a/kT\right)} \quad (2)$$

where ρ_{DC} is DC electrical resistivity, C is exponential factor, E_a is the conduction activation energy, T is absolute temperature and k is the Boltzmann's constant. Further the variation of electrical resistivity with temperature for $Fe_{2-2x}Ce_{2x}O_3$ (x = 0.05) is shown separately in the Fig. 5 (b) and a similar behaviour can also be resolved separately for other concentrations.

The electrical resistivities of Ce doped hematite samples at 150 K, with doping concentration, x = 0.00, x = 0.02, x = 0.05, x = 0.08 and x = 0.10 are found to be 47.66 × 10^8Ωcm, 17.27 × 10^8Ωcm, 0.278 × 10^8Ωcm,12.25 × 10^8Ωcm and 8.56 × 10^8Ωcm respectively, however it attains a value of the order of 10^7Ωcm at 400K.It is important to note that a decrease in electrical resistivity is noticed up to 5% concentration of Ce and thereafter its random variation has been observed. The charge carrier concentration increases as the cerium doping concentration increases, until it reaches a maximum value at 5% Ce doping and then decreases. However, initially as we increase the Ce concentration, mobility of charge carriers decreases and becomes minimum for 5% Ce doped α-Fe_2O_3. Further increase in doping concentration of Ce beyond solubility limit leads to increase in mobility of charge carriers with the reduction in density of charges, may be due to larger size grain boundary charge segregation as discussed for electrical conductivity of Al doped α-Fe_2O_3 [84]. At x = 0.05 Ce doping the electrical conductivity is highest which may be understood due to microstructural changes with comparatively smallest grain size observed in the FE-SEM of our samples shown in the Fig. 4. Hence in our results lowest value of electrical resistivity at 5% Ce doping of hematite is related with the difference in morphology as compared to other Ce doping values, gives new insights on electrical conductivity may be beneficial in solar cell technology [53]. High resistivity value, below and above 5% Ce doping may be interpreted respectively due to lower charge carrier concentration and Ce ions starting accumulation over the surface rather than substituted at sites in the host lattice forming a secondary phase existing with the primary α -Fe_2O_3 phase [84]. Thus maximum Ce ions concentration, having lowest mobility were substituted in the host lattice sites at 5% Ce doping for our samples supported by XRD analysis. Mobility variation may be understood by dominant ion impurity scattering mechanism [85]. The two oxidation states Ce^{3+} and Ce^{4+} as reported by J. Ning et al. [71] are created as Ce substituted Fe then 3 out of 4 valence electrons were taken by the neighbouring O-atoms and only one electron left with Ce [86]. This extra one electron converts Fe^{3+} ion into Fe^{2+} by creating a donor level just below the Fermi level and hence enhances electron carriers leads to increase in electrical conductivity of α-Fe_2O_3 by Ce doping as per analysis done by M.V. Nikolic in the case of Ti doped α-Fe_2O_3 [86].Hence the electrical conductivity observations may be

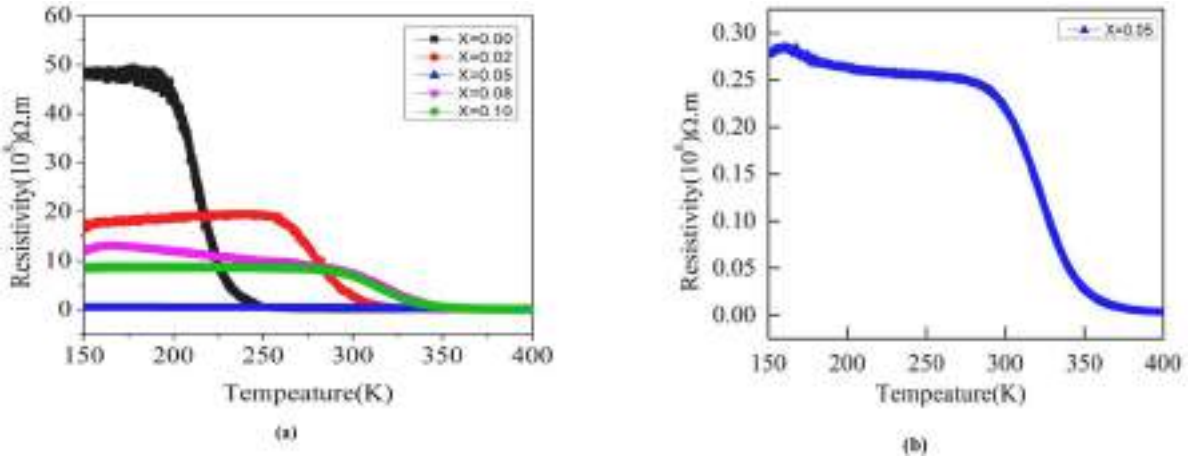

Fig. 5. (a) Resistivity versus Temperature curves of $Fe_{2-2x}Ce_{2x}O_3$(x = 0.00, 0.02, 0.05, 0.08, 0.10) nanoparticles for different doping concentrations of Ce. (b) Resolved curve for Resistivity versus Temperature of $Fe_{2-2x}Ce_{2x}O_3$ (x = 0.05) nanoparticles.

believed to strengthen the two oxidation states of doped Ce in hematite as reported by XPS data [71].

3.6. Magnetic measurements

Magnetic hysteresis measurements for Ce doped hematite α-$Fe_{2-x}Ce_xO_3$ (x = 0.00, 0.02, 0.05, 0.08 and 0.10) samples annealed at 600 °C were carried out by a vibrating sample magnetometer (VSM) with a varying magnetic field ranging from −10KOe to +10 KOe at room temperature (300 K). By the analysis of hysteresis loops from Fig. 6, it is observed that Ce doped hematite α-$Fe_{2-x}Ce_xO_3$ (x = 0.00, 0.02, 0.05, 0.08 and 0.10) exhibit hysteretic features with coercivity values determined as2318.6Oe, 2885.4Oe, 2582.2Oe, 2774.3Oe and 3379.8Oe respectively.

Coercivity is an extrinsic property of matter, depending on the spin carrier as well as shape and size of the domains inside a magnetic material [87,88].The pure α-$Fe_{2-x}Ce_xO_3$ (x = 0.00) shows weak ferromagnetic behaviour with the remnant magnetization (M_R) 0.128 emu/g and coercivity (H_C) 2318.6 Oe due to non-availability of magnetic moment of Ce ions in the host lattice. By increasing the Ce ions doping concentration (x) in the α-$Fe_{2-x}Ce_xO_3$, the coercivity and remanence increased showing ferromagnetic nature up to a limited concentration until the solubility limit is reached, after that a random variation is observed.

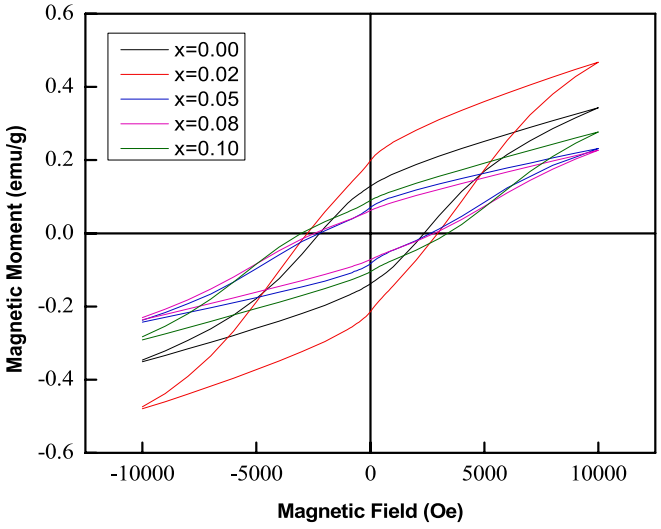

Fig. 6. Magnetic hysteresis loops of $Fe_{2-2x}Ce_{2x}O_3$ (x = 0.00, 0.02, 0.05, 0.08, 0.10) nanoparticles. All doping concentrations show characteristic ferromagnetic hysteresis loops.

Results of some important magnetic parameters are summarized in the Table 2, as can be seen for high concentration of Ce doping in the hematite leads to high value of coercivity (H_C), 3379.8Oe that depicts ferromagnetic nature. The high value of coercivity (H_C) is due to the high magnetic moment of Ce ions incorporated as dopants in the hematite material.

4. Conclusions

Ce-doped hematite samples (nanoparticles) of different compositions i.e. $Fe_{2-2x}Ce_{2x}O_3$ (x = 0.00, 0.02, 0.05, 0.08, 0.10) were prepared successfully by sol–gel method. Analysis of XRD and Raman measurements confirm the hematite phase up to 5% doping concentration of Ce and by the further increase of Ce doping (x = 0.08 and x = 0.10) in the host lattice, secondary phase starts arising due to solubility limit attained at 5% Ce-doping. The conditions of solubility limit of Ce with different compositions were analysed with the help of XRD and Raman spectroscopy results. The structural parameter such as crystallite size was found to decrease with Ce doping upto 5% due to larger ionic radii of Ce as compared to Fe. From FE-SEM, variation in grain size as well as the grain growth may be attributed to difference in ionic radii of dopant Ce ions than the host Fe ions. It has also been observed that there is a decrease in electrical resistivity up to 5% concentration of Ce and after that random variations were observed. Our results reveal an enhancement in DC electrical conductivity, coercivity, and remanence of Ce-doped hematite samples than the pure hematite sample, which can be attributed to their enhanced shape and magnetic-crystalline anisotropy. It is concluded that the modifications of electric and magnetic parameters by Ce doping are in full agreement with the variation of XRD, FE-SEM, FTIR and Raman spectroscopy results and these modifications are suitable for various technological applications.

Table 2
Magnetic parameters for $Fe_{2-2x}Ce_{2x}O_3$ (x = 0.00, 0.02, 0.05, 0.08, 0.10) obtained from VSM measurement carried at room temperature, showing the variation in parameters caused due to varying doping concentration of Ce.

Composition (x)	M_S (emu/g)	M_R (emu/g)	H_C (Oe)	Squareness Ratio (M_R/M_S)
x = 0.00	0.341	0.128	2318.6	0.375
x = 0.02	0.471	0.201	2885.4	0.375
x = 0.05	0.231	0.071	2582.2	0.309
x = 0.08	0.228	0.062	2774.3	0.273
x = 0.10	0.276	0.093	3379.8	0.337

Declaration of Competing Interest

The authors declare that they have no known competing financial interests or personal relationships that could have appeared to influence the work reported in this paper.

Acknowledgements

The author (Vijay Kumar) is thankful to UGC (India), New Delhi for providing the junior research fellowship (JRF) and is also thankful to IUAC, New Delhi for providing characterisation facilities.

References

[1] N.C. Pramanik, T.I. Bhuiyan, M. Nakanishi, T. Fujii, J. Takada, S. Seok, Synthesis and characterization of cerium substituted hematite by sol–gel method, Mater. Lett. 59 (2005) 3783–3787.
[2] C. Burda, X. Chen, R. Narayanan, M.A. El-Sayed, Chemistry and properties of nanocrystals of different shapes, Chem. Rev. 105 (2005) 1025–1102.
[3] W.U. Huynn, J.J. Dittmer, A.P. Alivisatos, Hybrid nanorod-polymer solar cells, Science 295 (2002) 2425–2427.
[4] H. Mattoussi, L.H. Radzilowski, B.O. Dabbousi, E.L. Thomas, M.G. Bawendi, M. F. Rubner, Electroluminenscence from hetrostructures of poly (phenylenevinylene) and inorganic CdSenanocrystals, J. Appl. Phys. 83 (1998) 7965.
[5] T.S. Ahmadi, Z.L. Wang, T.C. Green, A. Henglein, M.A. Elsayed, Shape controlled synthesis of colloidal platinum nanoparticles, Science 272 (1996) 1924–1930.
[6] S. Mitra, S. Das, K. Mandal, S. Chaudhuri, Synthesis ofα-Fe_2O_3 Nanocrystalline its different morphological attributes: Growth, mechanics, optical and magnetic properties, Nanotechnology 18 (2007), 275608.
[7] J. Jacob, M.A. Khadar, VSM and Mossbauer study of nanostructured hematiteJ. Magn. Magn. Mater.322(2010)614-621.
[8] R. Yao, C. Cao, Self-assembly of α-Fe_2O_3 mesocrystals with high coercivity, RSC Adv. 2 (2012) 1979–1985.
[9] V. Malik, S. Sen, D.R. Gelting, M.G. Josifovska, M. Schmidtand, P. Guptasarma, Field-enchanced magnetic moment in ellipsoidal nano-hematite, Mater. Res. Express 1 (2014) 026114–026123.
[10] A.K. Gupta, M. Gupta, Synthesis and surface engineering of iron oxide nanoparticles for biomedical applications, Biomaterials 26 (2005) 3995–4021.
[11] J. Murbe, A. Rechtenback, J. Topfer, Synthesis and physical characterization of magnetite nanoparticles for biomedical applications, Mater. Chem. Phys. 110 (2008) 426–433.
[12] P. Tartaj, M. Del Puerto Morales, S. Veintemillas-Verdaguer, T. González-Careno, C.J. Serna, The preparation of magnetic nanoparticles for applications in biomedicine, J. Phys. D: Appl. Phys. 36 (2003) R182–R197.
[13] A.S. Teja, P.Y. Koh, Synthesis, properties, and applications of magnetic iron oxide nanoparticles, Prog. Cryst. Growth Charact. Mater. 55 (2009) 22–45.
[14] P. Liao, J.A. Keith, E.A. Carter, Water oxidation on pure and doped hematite (0001) surfaces: prediction of Co and Ni as effective dopants for electrocatalysis, J. Am. Chem. Soc. 134 (2012) 13296–13309.
[15] A.K. Shwarsctein, Y.S. Hu, A.J. Forman, G.D. Stucky, E.W. McFarland, Electrodeposition of α-Fe_2O_3 doped with Mo or Cr as photoanodes for photocatalytic water splitting, J. Phys. Chem. C 112 (2008) 15900–15907.
[16] Y. Lin, Y. Xu, M.T. Mayer, Z.I. Simpson, G. McMahon, S. Zhou, D. Wang, Growth of p-type hematite by atomic layer deposition and utilization for improved solar water splitting, J. Am. Chem. Soc. 134 (2012) 5508–5511.
[17] W.B. Ingler, J.P. Baltrus, S.U.M. Khan, Photoresponse of p-Type Zinc-Doped Iron (III) Oxide Thin Films, J. Am. Chem. Soc. 126 (2004) 10238–10239.
[18] V.R. Satsangi, S. Kumari, A.P. Singh, R. Shrivastav, S. Dass, Nanostructure hematite for photoelectrochemical generation of hydrogen, Int. J. Hydrogen Energ. 33 (2008) 312–318.
[19] H. Kockar, M. Bayirli, M. Alper, A new example of the diffusion-limited aggregation: Ni–Cu film patterns, Appl. Surf. Sci. 256 (2010) 2995–2999.
[20] Y. Koseoglu, F. Kurtulus, H. Kockar, H. Guler, O. Karaagac, S. Kazan, B. Aktas, Magnetic characterizations of cobalt oxide nanoparticles, J Supercond Nov Magn 25 (2012) 2783–2787.
[21] F. Ozel, H. Kockar, S. Beyaz, O. Karaagac, T. Tanrisever, Superparamagnetic iron oxide nanoparticles: effect of iron oleate precursors obtained with a simple way, J. Mater. Sci.: Mater. Electron. 24 (2013) 3073–3080.
[22] O. Karaagac, B. Bilir, H. Kockar, Superparamagnetic Cobalt Ferrite nanoparticles: effect of temperature and base concentration, J Supercond Nov Magn 28 (2015) 1021–1027.
[23] C.R. De Silva, S. Simth, I. Shim, J. Pyun, T. Guta, J. Jiao, Z. Zheng, Lanthanide(III)-doped magnetite nanoparticles, J. Am. Chem. Soc. 131 (2009) 6336–6337.
[24] L.E. Mathevula, L.L. Noto, B.K. Mothudi, M.S. Dhlamini, Structural and optical properties of α-Fe_2O_3nanoparticles, influence by holmium ions, Physica B 535 (2018) 258–261.
[25] C. Frandsen, C.R.H. Bahl, B. Lebech, K. Lefmann, L.T. Kuhn, L. Keller, N. H. Andersen, M.V. Zimmermann, E. Johnson, S.N. Klausen, S. Morup, Oriented attachment and exchange coupling of α-Fe_2O_3 nanoparticles, Phys. Rev. B 72 (2005) 214406–214413.
[26] F. Bodker, M.F. Hansen, C.B. Koch, K. Lefmann, S. Morup, Magnetic properties of hematite nanoparticles, Phys. Rev. B 61 (2000) 6826–6838.
[27] M.F. Hansen, C.B. Koch, S. Morup, Magnetic dynamics of weakly and strongly interacting hematite nanoparticles, Phys. Rev. B 62 (2000) 1124–1135.
[28] R. Bhat, B. Want, A. Firdous, G.N. Dar, Probing of electric and magnetic properties of holmium doped iron oxide nanoparticles, J. Mater. Sci.: Mater. Electron. 29 (2018) 19472–19483.
[29] F.S. Freyria, G. Barrera, P. Tiberto, E. Belluso, D. Levy, G. Saracco, P. Allia, E. Garrone, B. Bonelli, Eu-doped α-Fe_2O_3 nanoparticles with modified magnetic properties, J. Solid State Chem. 201 (2013) 302–311.
[30] G. Goyal, A. Dograb, S. Rayaprol, S.D. Kaushik, V. Siruguri, H. Kishan, Structural and magnetization studies on nanoparticles of Nd doped α-Fe_2O_3, Mater. Chem. Phys. 134 (2012) 133–138.
[31] H. Wan, P. Rong, X. Liu, L. Yang, Y. Jiang, N. Zhang, R. Ma, S. Liang, H. Wang, G. Qiu, Morphological evolution and magnetic property of rare-earth-doped hematite nanoparticles: promising contrast agents for T1-weighted magnetic resonance imaging, Adv. Funct. Mater. 27 (2017) 1606821–1606832.
[32] I. Cesar, A. Kay, J.A.G. Martinez, M. Gratzel, Translucent thin film Fe_2O_3 photoanodes for efficient water splitting by sunlight: nanostructure-directing effect of Si-doping, J. Am. Chem. Soc. 128 (2006) 4582–4583.
[33] X. Wang, K.Q. Peng, Y. Hu, F.Q. Zhang, B. Hu, L. Li, M. Wang, X.M. Meng, S.T. Lee, Silicon/hematite core/shell nanowire array decorated with gold nanoparticles for unbiased solar water oxidation, Nano Lett. 14 (2014) 18–23.
[34] A. Kay, I. Cesar, M. Gratzel, New benchmark for water photo-oxidation by nanostructured α-Fe_2O_3 Films, J. Am. Chem. Soc. 128 (2006) 15714–15721.
[35] M. Rahman, N. Wadnerkar, N.J. English, J.M.D. MacElroy, The influence of Ti and Si doping on the structure, morphology and photo-response properties of α-Fe_2O_3 for efficient water splitting: experiment and first-principle calculations, Chem. Phys. Lett. 592 (2014) 242–246.
[36] Y. Hu, D.K. Bora, F. Boudoire, F. Haussler, M. Gratzel, E.C. Constable, A. Braun, A dip coating process for large silicon-doped high performance hematite photoanodes, J. Renew. Sustain. Energy 5 (2013) 043109–043118.
[37] S. Park, H.J. Kim, C.W. Lee, H.J. Song, S.S. Shin, S.W. Seo, H.K. Park, S. Lee, D. W. Kimb, K.S. Hong, Sn self-doped α-Fe_2O_3 nanobranch arrays supported on a transparent, conductive SnO_2 trunk to improve photoelectrochemical water oxidation, Int. J. Hydrog. Energy 39 (2014) 16459–16467.
[38] J.S. Jang, J. Lee, H. Ye, F.R.F. Fan, A.J. Bard, Rapid screening of effective dopants for Fe_2O_3 photocatalysts with scanning electrochemical microscopy and investigation of their photoelectrochemical properties, J. Phys. Chem. C 113 (2009) 6719–6724.
[39] L. Xi, S.Y. Chiam, W.F. Mak, P.D. Tran, J. Barber, S.C.J. Loo, L.H. Wong, A novel strategy for surface treatment on hematite photoanode for efficient water oxidation, Chem. Sci. 4 (2013) 164–169.
[40] J. Frydrych, L. Machala, J. Tucek, K. Siskova, J. Filip, J. Pechousek, K. Safarova, M. Vondracek, J.H. Seo, O. Schneeweiss, M. Gratzel, K. Sivula, R. Zboril, Facile fabrication of tin-doped hematite photoelectrodes–effect of doping on magnetic properties and performance for light-induced water splitting, J. Mater. Chem. 22 (2012) 23232–23239.
[41] J.S. Jang, K.Y. Yoon, X. Xiao, F.R.F. Fan, A.J. Bard, Development of a potential Fe_2O_3-based photocatalyst thin film for water oxidation by scanning electrochemical microscopy: effects of Ag−Fe_2O_3 nanocomposite and Sn doping, Chem. Mater. 21 (2009) 4803–4810.
[42] Y.S. Hu, A. Kleiman-Shwarsctein, A.J. Forman, D. Hazen, J.N. Park, E. W. McFarland, Pt-doped α-Fe_2O_3 thin films active for photoelectrochemical water splitting, Chem. Mater. 20 (2008) 3803–3805.
[43] H.G. Cha, J. Song, H.S. Kim, W. Shin, K.B. Yoon, Y.S. Kang, Facile preparation of Fe_2O_3 thin film with photoelectrochemical properties, Chem. Comm. 47 (2011) 2441–2443.
[44] V.M. Aroutiounian, V.M. Arakelyan, G.E. Shahnazaryan, G.M. Stepanyan, E. A. Khachaturyan, H. Wang, J.A. Turner, Photoelectrochemistry of semiconductorelectrodes made of solid solutions in the system Fe_2O_3–Nb_2O_5, Sol. Energy 80 (2006) 1098–1111.
[45] C. Sanchez, K.D. Sieber, G.A. Somorjai, Photoelectrochemistry of niobium doped α-Fe_2O_3, J. Electroanal. Chem. 252 (1988) 269–290.
[46] Y. Liu, Y.X. Yu, W.D. Zhang, MoS_2/CdS heterojunction with high photoelectrochemical activity for H_2 evolution under visible light: the role of MoS_2, Electrochim. Acta 59 (2012) 121–127.
[47] C.J. Sartoretti, B.D. Alexander, R. Solarska, I.A. Rutkowska, J. Augustynski, Photoelectrochemical oxidation of water at transparent ferric oxide film electrodes, J. Phys. Chem. B 109 (2005) 13685–13692.
[48] J. Engel, H.L. Tuller, The electrical conductivity of thin film donor doped hematite : from insulator to semiconductor by defect modulation, Phys. Chem. Chem. Phys. 16 (2014) 11374–11380.
[49] H. Magnan, D. Stanescu, M. Rioult, E. Fonda, A. Barbier, Enhanced photoanode properties of epitaxial Ti doped α-Fe_2O_3(0001) thin films, Appl. Phys. Lett. 101 (2012) 133908–133912.
[50] A. Boudjemaa, M. Trari, Photo-catalytic hydrogen production over Fe_2O_3based catalysts, Int. J. Hydrog. Energy 35 (2010) 7684–7689.
[51] A. Kleiman-Shwarsctein, Y.S. Hu, A.J. Forman, G.D. Stucky, E.W. McFarland, Pt-doped α-Fe_2O_3thin films active for photoelectrochemical water splitting, J. Phys. Chem. C 112 (2008) 15900–15907.
[52] V. Kumar, S. Chahal, D. Singh, A. Kumar, P. Kumar, K. Asokan, Annealing effect on the structural and dielectric properties of hematite nanoparticles, AIP Conference Proceeding 2018 (1953) 030245–030249.
[53] Y. Han, Y. Wu, X. Zhao, Photocatalytic activity of Ce-doped hematite for hydrogen production, Mater. Sci. Forum 787 (2014) 46–51.

[54] X. Wang, T. Wang, G. Si, Y. Li, S. Zhang, X. Deng, X. Xu, Oxygen vacancy defects engineering on Ce-doped α-Fe_2O_3 gas sensor for reducing gases, Sens. Actuators, B 302 (2020) 127165–127173.

[55] D. Wang, L. Jin, Y. Li, D. Yao, J. Wang, H. Hu, Upgrading of vacuum residue with chemical looping partial oxidation over Ce doped Fe_2O_3, Energy 162 (2018) 542–553.

[56] E. Van San, E. De Grave, R. Vandenberghe, Study of Al-substituted hematites, prepared from thermal treatment of lepidocrocite, Physics Chemistry Miner 28 (2001) 488–497.

[57] H. Kanai, H. Mizutani, T. Tanaka, X-ray absorption study on the local structures of fine α-Fe_2O_3–SnO_2 gas sensors, J. Mater. Particles Chem. 2 (1992) 703–707.

[58] D. Owoc, J. Przewoznik, A. Kozlowsk, X-ray xMe_xO_4, Me = Zn, Ti and Al; the−studies of Fe_3 impact of doping on the verwey transition, Phys. B 359 (2005) 1339–1341.

[59] G. Busca, G. Ramis, M.C. Prieto, Preparation and characterization of $Fe_{2-x}Cr_xO_3$mixed oxide powders, J. Mater. Chem. 3 (1993) 665–673.

[60] S. Music, M. Lenglet, S. Popovic, Formation and characterization of the solid solutions $(Cr_xFe_{1-x})_2O_3$, 0≤ x≤ 1, J. Mater. Sci. 31 (1996) 4067–4076.

[61] R.D. Zysler, D. Fiorani, A.M. Testa, Size dependence of the spin-flop transition in hematite nanoparticles, Phys. Rev. B 68 (2003) 212408–212412.

[62] J.L. Lopez, H.D. Pfannes, R. Paniago, Investigation of the static and dynamic magnetic properties of $CoFe_2O_4$ nanoparticles, J. Magn. Magn. Mater. 320 (2008) 327–330.

[63] M.Z. Dang, D.G. Rancourt, J.E. Dutrizac, G. Lamarche, R. Provencher, Interplay of surface conditions, particle size, stoichiometry, cell parameters, and magnetism in synthetic hematite-like materials, Hyperfine Interact. 117 (1998) 271–319.

[64] P. Kumar, P. Kumar, A. Kumar, R.C. Meena, F. Chand, K. Asokan, R. Tomar, Structural, morphological, electrical and dielectric properties of Mn doped CeO_2, J. Alloy. Compd. 672 (2016) 543–548.

[65] G. Neri, A. Bonavita, G. Rizzo, S. Galvango, P. Siciliano, Methanol gas sensing properties of CeO_2-Fe_2O_3 thin films, Sens. Actuators B Chem. 114 (2006) 687–695.

[66] Y. Liu, D. Sun, Effect of CeO_2 doping on catalytic of Fe_2O_3 /γ-Al2O3 catalyst for catalytic wet peroxide oxidation of azo dyes, J. Hazard. Mater. 143 (2007) 448–454.

[67] A. Burton, K. Ong, T. Rea, I.Y. Chan, On the estimation of average crystallite size of zeolites from the Scherrer equation: a critical evaluation of its application to zeolites with one-dimensional pore systemsMicropor, Mesopor. Mater. 117 (2009) 75–90.

[68] P. Kumar, V. Singh, V. Sharma, G. Rana, H.K. Malik, K. Asokan, Investigation of phase segregation in yttrium doped zinc oxide Ceram, Intern. 41 (2015) 6734–6739.

[69] G. Rana, U.C. Jhori, A study on structural and magnetic properties of Ni-substituted magnetite nanoparticles, J. Alloy. Compd. 577 (2013) 376–381.

[70] M. Mohapatra, S.K. Sahoo, C.K. Mohanty, R.P. Das, S. Anand, Effect of Ce (IV) doping on formation of goethite and its transformation to hematite, Mater. Chem. Phys. 94 (2005) 417–422.

[71] J. Ning, P. Shi, M. Jiang, C. Liu, X. Li, Effect of Ce doping on the structure and chemical stability stability of Nano- α-Fe_2O_3, Nanomaterials 9 (7) (2019) 1039–1051, https://doi.org/10.3390/nano9071039.

[72] D. Cardillo, K. Konstantinov, T. Devers, The effects of cerium doping on the size, morphology, and optical properties of α-hematite nanoparticles for ultraviolet filtration, Mater. Res. Bull. 48 (2013) 4521–4525.

[73] T.I. Bhuiyan, M. Nakanishi, Y. Kusano, T. Fujii, J. Takada, Y. Ikeda, Synthesis, structures and properties of the cerium doped hematite co-existing with CeO_2, J. Jpn. Soc. Powder Metallurgy 54 (2007) 112–118.

[74] S. Liu, K. Yao, L. Fu, M. Ma, Selective synthesis of Fe3O4, γ-Fe2O3, and α -Fe2O3 using cellulose-based composites as precursors, RSC Adv. 6 (2016) 2135-2140.

[75] P.I.P. Soares, A.M.R. Alves, L.C.J. Pereira, J.T. Coutinho, I.M.M. Ferreira, C.M. M. Novo, J.P.M.R. Borges, Effects of surfactants on the magnetic properties of iron oxide colloids, J. Colloid Interface Sci. 419 (2014) 46–51.

[76] Y.P. Fu, C.H. Lin, C.S. Hsu, Preparation of ultrafine CeO_2, powders by microwave-induced combustion and precipitation, J. Alloys Compd. 391 (2005) 110–114.

[77] J.S. Justus, S.D. Dharma. Roy, A.M. Ezhil Raj, Influence of Lanthanum doping on the structural and optical properties of hematite nanopowders, J. Appl. Sci. Eng. Methodol. 2 (2016) 272-277.

[78] R. Kant, D. Kumar, V. Dutta, High coercivity α-Fe_2O_3 nanoparticles prepared by continuous spray pyrolysis, RSC Adv. 5 (2015) 52945–52951.

[79] I.V. Chernyshova, M.F. HochellaJrb, A.S. Maddenc, Size-dependent structural transformations of hematite nanoparticles. 1. Phase transition, Phys. Chem. Chem. Phys. 9 (2007) 1736–1750.

[80] K. Suzuki, E. Oho, Special raster scanning for reduction of charging effects in scanning electron microscopy, J. Scanning Microscopies 36 (2014) 327–333.

[81] S.A. Ul Islam, F.A. Andrabi, F. Mohmed, K. Sultan, M. Ikram, K. Asokan, Ba doping induced modifications in the structural, morphological and dielectric properties of double perovskite La_2NiMnO_6 ceramics, J. Solid State Chem. 290 (2020) 121597–121607.

[82] T.I. Bhuiyan, M. Nakanishi, Y. Kusano, T. Fujii, Synthesis, morphology and color tone properties of the lanthanum substituted hematite, Mater. Lett. 61 (2007) 3774–3777.

[83] T. Ivetic, M.V. Nikolic, M. Slankamenac, M. Zivanov, D. Minic, P.M. Nikolic, M. M. Ristic, Influence of Bi_2O_3 on microstructure and electrical properties of ZnO-SnO_2ceramic, Sci. Sintering 39 (2007) 229–240.

[84] S.S. Shinde, R.A. Bansode, C.H. Bhosale, K.Y. Rajpure, Physical properties of hematite α -Fe2O3 thin films: application to photoelectrochemical solar cells, J. Semiconductors, 32(1)(2011)013001-8.

[85] M. Slankamenac, T. Ivetic, M.V. Nikolic, N. Ivetic, M. Zivanov, V.B. Pavlovic, Impedance response and dielectric relaxation in liquid-phase sintered Zn_2SnO_4-SnO_2 ceramics, J. Electron. Mater. 39 (2010) 447–455.

[86] M.V. Nikolic, D.L. Sekulic, N. Nikolic, M.P. Slankamenac, O.S. Aleksic, H. Danninger, E. Halwax, V.B. Pavlovic, P.M. Nikolic, Structural and electrical properties of Ti doped α-Fe_2O_3, Sci. Sinter. 45 (2013) 281–292.

[87] Lili Li, Ying Chu and Yang Liu, Synthesis and characterization of ring-like α-Fe2O3, Nanotechnology 18 (2007) 105603-105609.

[88] J. Jacob, M. Abdul Khadar, VSM and Mossbauer study of nanostructured hematite, J. Magn. Magn. Mater. 322 (2010) 614–621.

IJNRD.ORG ISSN : 2456-4184
INTERNATIONAL JOURNAL OF NOVEL RESEARCH AND DEVELOPMENT (IJNRD) | IJNRD.ORG
An International Open Access, Peer-reviewed, Refereed Journal

"Initiatives taken by State Government in promoting startups in Haryana"

Dr Raman Deep Singh
Assistant Professor
Department of Commerce
Government College
Ding Mandi, Sirsa (Haryana)

Vikrant Mohan
Assistant Professor
Department of Commerce
Government College
Bhattu Kalan, Fatehabad (Haryana)

Abstract

India ranks 3rd in the global startup ecosystem and also in terms of the number of Unicorns. Several Indian companies which started their initial journey as humble Startups have now been able to make a significant mark in the global business fraternity. The Government of Haryana firmly believes that innovation is the backbone of the economy and for that purpose it has developed an inclusive Blueprint of the growth of the Startups in the State. Government of Haryana has been instrumental in providing institutional support to the startups. The present study discusses the initiatives taken and benefits provided by Government for the Startups in the Haryana. Moreover, this study also assesses the various challenges which are faced by Government in the setting up and promoting the startups.

Introduction

Haryana is the home land of various new age entrepreneurs and is birth place of the many successful business magnets and large industrial houses of India. Gurugram, the IT city of Haryana has evolved as a technology startup hub of India and has nurtured many successful startups, which now have become big brands. The Government of Haryana is determined to use the potential of young entrepreneurs by offering them the necessary vital policies and maximum convergence by linking the broader Government of India initiatives including Digital India, Make in India, Skill India and Startup India.

With easy access to markets, an educated workforce along with excellent infrastructure, the State of Haryana has all the right ingredients to develop a strong ecosystem for both social betterment & sustained growth. At this point, when Government of India is brutally chasing the goal of creating an enterprising

India, it is very important for the State Governments to place startups at the core of policy making and launch a committed policy for foster growth of entrepreneurship. Historically an agrarian state, Haryana today is a well-developed industrial state. Out of 101 Unicorn Startups in India, 14 Unicorn Startups are based out in Haryana like Zomato, Urban Company, Policy bazaar, Delhivery, Cars24, Spinny, OfBusiness etc.

Presently, 3910 Haryana based startups are recognized by the Department for Promotion of Industry and Internal Trade (DPIIT) under the ministry of Commerce and Industry, Government of India as of 15th June 2022. Through this policy, the state government aims to promote and nurture the vibrant startup ecosystem in Haryana. The state has taken a multitude of initiatives to prioritize startup businesses and position them on an equal platformas established companies, by easing public procurement. The objective of the present study isto discuss the distinct levels of initiatives taken by government at every stage of startups in Haryana.

Definition of Startup

An entity shall be considered as a Startup:

a) Up to a period of ten years from the date of incorporation/registration, if it is incorporated as a private limited company or listed as partnership form or a limited liability partnership in India.
b) Turnover of the entity for any of the financial years since incorporation/ registration has not exceeded Rs 100 crores.
c) Entity is working towards innovation, development or improvement of products or processes or services.
d) Provided that an entity formed by splitting up or reconstruction of an existing business shall not be considered a 'Startup'.

Initiatives taken by Government of Haryana for the startups

The State Government on June 27, 2022 approved a new Haryana State Startup Policy, 2022 prepared by the Department of Information Technology, Electronics and Communications, Haryana. Through this policy, the state government aims to promote and nurture the vibrant startup ecosystem in Haryana. The following initiatives have been taken by the government to boost up the startups in Haryana:

1. Infrastructure augmentation

Infrastructure will be the key to the growth of the startups in the State. For this purpose, the Haryana Government aims to develop the world-class physical infrastructure in the state that provides an encouraging environment for ideas to originate, scale-up and see business fruition.

1.1 Developing Infrastructure

The State Government has set up an innovation hub in Gurugram covering an area of 30,000 square feet comprising of Startup Warehouse, Mobile Application Centre, United Nation Technology & Innovation lab and IoT (Internet of Things) Centre to enhance the start-up ecosystem in Haryana.

a. Start-up Warehouse in Gurugram:

Haryana State Electronic Development Corporation Limited (HARTRON) introduced a start-up

warehouse on 10,000 Sq. ft. of land in Gurugram in association with NASSCOM in the year 2018. The Startup warehouse shall offer shared office space to startups and entrepreneurs.

b. IoT Centre

An IoT center has been setup in Gurugram collaboration with NASSCOM and ERNET in the year 2018 with the aim to provide platform for Design, prototype to realizing product by harnessing creative capability of Academia, Industry, start-ups and entrepreneur.

c. Entrepreneurs Centre

New Entrepreneurs Centre would be developed in the state in addition to already established centre in Gurugram. The purpose of these centers would be to provide holistic infrastructure support to startups. These centers would be attracting the best startups and entrepreneur organization from across the world to various districts in the state.

d. New Incubation Centers in Government Universities and other Institutions Financial assistance for creating incubation center at government universities and other government institutions up to the extent of Rs 50 Lakhs per incubator and Rs 20 Lakhfor recurring expenditure for 5 years.

Financial assistance up to Rs 10 Lakh per incubator for existing incubation center atgovernment universities and other government institutions for upgrading the facilities.

e. New Mobile Application Centre:

Financial support of Rs 4 crore for capital expenditure to any Government Department for creating Mobile Apps Development Center in collaboration with Internet & Mobile Association of India/Central/State Government Universities and yearly support of Rs 1 crore for three years at Panchkula, Hisar and other locations in Block ‘C’ and ‘D’.

f. Incubation Center

The incubation centers would be created in every district in phased manner based on the resources which are available in that region. The Government will give space to the startup in their Incubation centre for one year in the first instance. The period may be extended to a maximum of 3 years. The Incubation centers would assist the following activities.

1. Play and Plug Infrastructure
2. Mentoring support in business plans, networking of business resources, and entrepreneurial development through Haryana Startup Ecosystem.
3. Facilitate in project and product selection
4. Credit facilitation such as seep capital assistance, marketing assistance,professional assistance.

g) Incubation Network in Haryana

a) State Owned Incubation Network

The Government would develop its own incubation network by utilizing the existing infrastructure in the State. All the Government/Private incubators operating from Haryana have to mandatorily register with the Startup Haryana, DITECH.

b) Accelerator

The Government will establish at least one world class Accelerator by inviting Global

Accelerators to set up their program in State.

2. Fiscal Support

The State Government has proposed many incentives for Incubators, startups and other stakeholders.

2.1 Incentives to Startups/Entrepreneurs

a) Lease rental subsidy:

Reimbursement of 30% of lease rental for general Startups and 45% for startups with only women founders, operating from incubators/IT parks/Industrial Clusters shall be eligible for a period of 1 year subject to minimum of Rs 5 Lakh.

b) Patent Cost

Reimbursement of 100% of the actual expenses with a maximum of Rs 25 Lakh for domestic and international registration.

c) Net SGST Reimbursement

50% Net SGST Reimbursement for 7 years with a cap of 100 FCI.

d) Assistance in Acceleration Program

Support Startups up to Rs 2.5 Lakh to attend national acceleration programs and Rs 5Lakh for international acceleration programs.

3. Regulatory Easing

3.1 Optimizing Regulatory Framework

In its endeavor to create a encouraging environment for companies, the Government of Haryana shall be implementing some landmark reforms for regulatory simplification. All the regulatory clearances shall be approved under the Single Roof Clearance System of Haryana Enterprise Promotion Center in a time bound manner by implementing an online state startup portal.

3.2. Preferential Procurement

The Government shall encourage the participation of startups in the Government procurements by the exemption of Tender Fee, Earnest Money Deposit, and concession in security etc.

3.3. CSR Fund Utilization for Development of Startup Ecosystem

The CSR Funds of PSUs/Corporate will be utilized to strengthen the incubators & other infrastructure.

4. Entrepreneurial Development

The Government would work with universities, educational institutions and the industry to inculcate the habit of innovation and entrepreneurship in the minds of citizens.

4.1. Academic Intervention

A special training program will be designed organized by faculty development to be equipped with the know-how of startups in order to cultivate entrepreneurship intellect.

4.2 Distribution of Technology Kit

Distribution of microcontroller or microprocessor-based startup boxes to students to promote the learning of basic computer science and electronics in schools and ignite the imagination of students

through Do-it-yourself projects.

4.3 Scientific Conferences for industry-institute collaboration

Scientific Conference would be conducted annually by DITECH along with Department of Science and Technology by inviting scientists and researchers from around the world in association with Research Institutions with the aim to create collaborations among colleges.

5. Awareness and Outreach

Entrepreneurship Development Programs across 22 districts of Haryana will be organized every six months for sensitization and awareness among the aspiring innovators/entrepreneurs and school/college students about their growth opportunities and potential in the Startup Ecosystem. The incubator will be given assistance of up to Rs 20 Lakh per event for organizing startup competition festival in institutes of national importance.

6. Way Forward

There are additional steps that the state could take in order to build upon the already engaged initiatives.

1. Increase number of registered startups
2. Prioritize market outreach to boost Women Entrepreneurship
3. Additional amendments in rules and regulations to support startups
4. Real-time query resolution support integration
5. Setting up additional incubators

7. Conclusion

At present day, startups are growing like a grapevine. Haryana's financial development has been praiseworthy and regardless of being little in size, its contribution to public money is almost 3.5 percent of the GDP. The State firmly believes that innovation is the backbone of the economy and hence developed an inclusive blueprint for the development of a Startup Ecosystem in the State. While the State economy is having a strong manufacturing base, the Startup Sector is moving at a very pace. The Government of Haryana needs to provide the youngsters and new entrepreneurs with the necessary policy push, robust infrastructure and liberalized regulatory compliances. The state has also developed a well-equipped online implementation system along with a mentor network to support the startups. A call center has been setup by the state to respond to the queries raised by startups. Additionally, the state is also taking support from various other departments in order to boost the startup ecosystem. The economy of the state is developing at a high speed especially in the area of Services and IT making Haryana ready for the startups. At this stage when The Government of India is very much committed towards making India an Enterprising economy, the Government of Haryana is quick to taking major initiatives for creating a good environment for the Startups. The government needs to reduce the procedural and bureaucratic hurdles which hinder the functioning of Startups.

References

https://fcd.haryana.gov.in/images/FileUploaded/HaryanaStartupPolicy2022pdf71820222 1514PM.pdf https://www.startupindia.gov.in/srf/reports/Haryana_State_Report_26072020.pdf

https://www.drishtiias.com/state-pcs-current-affairs/haryana-state-startup-policy-2022
https://www.newindianexpress.com/nation/2022/jul/05/gujarat-on-top-of-list-of-states-in- startup-ranking-meghalaya-best-among-smaller-states-2473079.html https://www.india.com/business/india-ranks-3rd-in-global-startup-ecosystem-number-of- unicorns-says-minister-5568608/
https://manavrachna.edu.in/wp-content/uploads/2021/01/Haryana-startup- policy_final_28th-sep-2017.pdf https://www.startupindia.gov.in/content/dam/investindia/Templates/public/Dpiit_new%20V3.pdf

IJNRD.ORG ISSN : 2456-4184
INTERNATIONAL JOURNAL OF NOVEL RESEARCH AND DEVELOPMENT (IJNRD) | IJNRD.ORG
An International Open Access, Peer-reviewed, Refereed Journal

ई -क्रांति की ओर बढ़ते कदम - डिजिटल इंडिया

Rajesh Kumar, Assistant Professor Govt. College Bhattu Kalan (Fatehabad)

Vikrant Mohan, Assistant Professor Govt. College Bhattu Kalan (Fatehabad)

परिचय-

भारत में प्रौद्योगिकी के उपयोग को बढ़ाने के लिए भारत सरकार द्वारा "डिजिटल इंडिया" अभियान शुरू किया गया था। इसका उद्देश्य पूरे देश में अपने ऑनलाइन बुनियादी ढांचे में सुधार करके नागरिकों को इलेक्ट्रॉनिक रूप से सरकारी सेवाएं आसानी से उपलब्ध कराना था। इंटरनेट कनेक्टिविटी में वृद्धि के द्वारा देश को डिजिटल रूप से सशक्त बनाने के लिए इस प्रक्रिया को अपनाया गया है । यह आम जनता तक पहुंचने का आसन तरीका है और उन्हें अपने दैनिक जीवन में प्रौद्योगिकी का उपयोग करने के लिए प्रोत्साहित करता है। प्रधान मंत्री श्री नरेंद्र मोदी द्वारा 1 जुलाई, 2015 को इस अभियान को शुरू किया गया । इस अभियान की सहायता से ग्रामीण भारत को हाई-स्पीड इंटरनेट कनेक्टिविटी से जोड़ना है।

“डिजिटल इंडिया” अभियान के मुख्य घटक –

डिजिटल इंफ्रास्ट्रक्चर का निर्माण

देश भर में विभिन्न डिजिटल सेवाओं को लागू करने में , विशेष रूप से देश के ग्रामीण क्षेत्रों में एक मजबूत डिजिटल बुनियादी ढांचा तैयार करना आवश्यक है। देश के आंतरिक क्षेत्रों में इलेक्ट्रॉनिक नेटवर्क या तो बहुत कम है या बिल्कुल भी नहीं है। पूरे देश में डिजिटल नेटवर्क स्थापित करने के पीछे यही कारण है। भारत ब्रॉडबैंड नेटवर्क लिमिटेड, एक सरकारी निकाय जो राष्ट्रीय ऑप्टिकल फाइबर नेटवर्क परियोजना को लागु करने के लिए कार्य कर रही है , डिजिटल इंडिया परियोजना के लिए भी जिम्मेदार है। भारत ब्रॉडबैंड नेटवर्क का लक्ष्य देश भर में 2,50,500 ग्राम पंचायतों को ऑप्टिकल फाइबर नेटवर्क के माध्यम से एक हाई-स्पीड इंटरनेट नेटवर्क से जोड़ना है। कार्यक्रम के हिस्से के रूप में पूरे देश में 4,00,000 इंटरनेट बिंदु स्थापित किए जाएंगे, जहां से हर कोई इंटरनेट सेवा का उपयोग कर सकेगा।

डिजिटल सेवा की डिलीवरी

डिजिटल इंडिया अभियान का एक प्रमुख घटक सरकारी सेवाओं और अन्य आवश्यक सेवाओं को डिजिटल रूप से वितरित करना है।डिजिटल इंडिया अभियान के तहत भारत सरकार की कई सेवाओं को डिजिटल किया गया।

इस योजना के तहत सभी मंत्रालयों को जोड़ा जाएगा, और सभी विभाग मूलभूत सेवाओं जैसे स्वास्थ्य देखभाल, बैंकिंग, शिक्षा, छात्रवृत्ति, गैस सिलेंडर, पानी और बिजली के बिल और न्यायिक सेवाओं के साथ लोगों से जुड़ सकेंगे। लोगों के दैनिक वितीय लेन-देन को भी डिजिटल मोड में बदल दिया गया। लेन-देन में पारदर्शिता सुनिश्चित करने और भ्रष्टाचार पर रोक लगाने के लिए सभी वितीय लेन-देन ऑनलाइन और वन टाइम पासवर्ड द्वारा सुरक्षित किए जा रहे हैं।

डिजिटल साक्षरता

डिजिटल इंडिया अभियान में भारत के सभी लोगों की पूर्ण भागीदारी के लिए जो योग्यता होनी चाहिए, उसे डिजिटल साक्षरता कहते हैं। डिजिटल उपकरणों का प्रभावी ढंग से उपयोग करने के लिए आवश्यक बुनियादी ढांचा , ज्ञान और कौशल अनिवार्य हैं। डेस्कटॉप पीसी, लैपटॉप, टैबलेट और स्मार्टफोन डिजिटल उपकरण हैं जिनका उपयोग संचार, अभिव्यक्ति, मिल कर काम करने और नेटवर्किंग करने के उद्देश्य से किया जाता है। डिजिटल साक्षरता का मिशन छह करोड़ से अधिक ग्रामीण परिवारों को कवर करेगा।

डिजिटल इंडिया का लक्ष्य विकास क्षेत्रों के नौ स्तंभों पर अत्यधिक आवश्यक बल प्रदान करना है। इनमें से प्रत्येक क्षेत्र अपने आप में एक जटिल कार्यक्रम है और कई मंत्रालयों और विभागों से जुड़ा हुआ है। डिजिटल इंडिया के नौ स्तंभ नीचे दिए गए हैं:

- **ब्रॉडबैंड हाईवे** - इसमें तीन उप घटक शामिल हैं, अर्थात् सभी के लिए ब्रॉडबैंड –ग्रामीण , शहरी और राष्ट्रीय सूचना अवसंरचना ।

- **मोबाइल कनेक्टिविटी के लिए यूनिवर्सल एक्सेस**- यह अभियान देश में नेटवर्क पहुंच और कनेक्टिविटी में अंतराल को कम करने पर पर केंद्रित है।
- **सार्वजनिक इंटरनेट एक्सेस कार्यक्रम**-सार्वजनिक इंटरनेट एक्सेस प्रोग्राम के दो उप घटक-
  1- सामान्य सेवा केंद्र (सीएससी) 2 – डाकघर- बहु-सेवा केंद्रों के रूप में।
- **ई-गवर्नेंस:** प्रौद्योगिकी के माध्यम से सरकार में सुधार- सरकारी प्रक्रियाओं को सरल और अधिक कुशल बनाने के लिए आईटी का उपयोग करके सरकारी प्रक्रिया की री-इंजीनियरिंग विभिन्न सरकारी डोमेन में सरकारी सेवाओं के वितरण को अधिक प्रभावी बनाने के लिए यह परिवर्तन महत्वपूर्ण है। इसलिए सभी मंत्रालयों/विभागों द्वारा इसे लागू करने की आवश्यकता है।
- **ई-क्रांति**- सेवाओं की इलेक्ट्रॉनिक डिलीवरी- सार्वजनिक सेवाओं की डिलीवरी में सुधार करना और उन तक पहुंचने की प्रक्रिया को सरल बनाना। इस संबंध में, विभिन्न राज्य सरकारों और केंद्रीय मंत्रालयों द्वारा ई-गवर्नेंस के युग में प्रवेश करने के लिए ई-गवर्नेंस से सम्बंधित कई कदम उठाये गये हैं। भारत में ई-गवर्नेंस सरकारी विभागों के कम्प्यूटरीकरण से लेकर उन पहलों तक जो शासन के सूक्ष्म बिंदुओं को समाहित करती हैं, तेजी से विकसित हुआ है-जैसे कि नागरिक केंद्रितता, सेवा उन्मुखीकरण और पारदर्शिता।
- **सभी के लिए सूचना**- इस स्तंभ का उद्देश्य देश के लोगों के उपयोग, पुन: उपयोग और पुनर्वितरण के लिए विभिन्न मंत्रालयों द्वारा उत्पन्न विश्वसनीय डेटा की पारदर्शिता और उपलब्धता सुनिश्चित करना है।
- **इलेक्ट्रॉनिक्स विनिर्माण**- यह स्तंभ देश में इलेक्ट्रॉनिक्स मैन्युफैक्चरिंग को बढ़ावा देने पर फोकस करता है।
- **नौकरियों के लिए आई.टी**- यह स्तंभ आईटी/आईटीईएस क्षेत्र में रोजगार के अवसरों का लाभ उठाने के लिए आवश्यक कौशल हेतु युवाओं को प्रशिक्षण प्रदान करने पर केंद्रित है।
- **Early Harvest Programmes** - इस स्तंभ में विभिन्न अल्पकालिक परियोजनाओं का एक समूह जैसे कि बड़े पैमाने पर संदेश भेजने के लिए आईटी प्लेटफॉर्म, ई-ग्रीटिंग्स की क्राउड सोर्सिंग, सरकारी कार्यालयों में बायोमेट्रिक उपस्थिति, सभी विश्वविद्यालयों में वाई-फाई आदि शामिल है, जो भारतीय डिजिटल सिस्टम पर तत्काल प्रभाव डालते हैं ।

डिजिटल इंडिया पहल

डिजिटल इंडिया अभियान के तहत सरकार ने कई कदम उठाये हैं।ऐसी ही कुछ महत्वपूर्ण स्कीम निम्नलिखित हैं -

- **सुलभ भारत अभियान और मोबाइल ऐप**- इसे सुगम्य भारत अभियान के नाम से भी जाना जाता है। इसका मुख्य लक्ष्य सभी प्रकार की सेवाओं को दिव्यांग व्यक्तियों के लिए उपलब्ध करवाना है।

- **Mygov.in**- यह मंच उपयोगकर्ताओं को सरकार की प्रशासन रणनीति पर अपने विचार व्यक्त करने की अनुमति देता है। इसे इसलिए लागू किया गया है ताकि स्थानीय लोग सक्रिय रूप से भाग ले सकें।

- **नए युग के शासन के लिए एकीकृत मोबाइल एप्लिकेशन (UMANG)**- इस मोबाइल प्लेटफॉर्म का इस्तेमाल किसी भी डिवाइस पर किया जा सकता है। यह सॉफ्टवेयर विभिन्न भारतीय भाषाओं में उपलब्ध है। यह सॉफ़्टवेयर उपयोगकर्ताओं को विभिन्न प्रकार की सेवाओं तक पहुँचने की अनुमति देता है। उमंग एप्प पर उपलब्ध सेवाओं में शिक्षा पोर्टल, डिजिटल लॉकर,पासपोर्ट सेवा,भारत बिल भुगतान सेवा, गैस सेवा,फसल बीमा, आधार, टैक्स और ट्रेन टिकट खरीदारी शामिल हैं।

- **कृषि बाजार ऐप**- इसे किसानों को कृषि कीमतों से अवगत कराने और उन्हें फसल बेचते समाय जल्दबाजी न करने के उद्देश्य के लिए बनाया गया था।

- **बेटी बचाओ बेटी पढ़ाओ**- एक बालिका के कल्याण और पोषण को सुनिश्चित करना और यह भी सुनिश्चित करना कि हर लड़की स्कूल जाती है ।

- **भारत इंटरफेस फॉर मनी (भीम)**- यह यूनिफाइड पेमेंट इंटरफेस (UPI) जल्दी, आसानी से और सरलता से भुगतान करता है। यह बैंक को मोबाइल फोन नंबरों का उपयोग करके तत्काल भुगतान और धन संग्रह स्वीकार करने की भी अनुमति देता है

- **फसल बीमा मोबाइल ऐप**- यदि कोई ऋण लिया जाता है, तो क्षेत्र या ऋण राशि जैसी कई विशेषताओं के आधार पर फसल बीमा प्रीमियम की गणना करने के लिए **ऐप** उपयोग किया जाता है।

- **ई-अस्पताल**- यह अस्पतालों के आंतरिक कार्यप्रणाली और संचालन के लिए एक HMIS (अस्पताल प्रबंधन सूचना प्रणाली) है।

- **E-Pathshala**- नेशनल काउंसिल ऑफ एजुकेशनल रिसर्च एंड ट्रेनिंग (एनसीईआरटी) ने विद्यार्थिओं से सम्बंधित सभी प्रकार की पुस्तकों , टेक्स्ट बुक्स,ऑडियो **,** विडियो के अतिरिक्त अन्य डिजिटल संसाधनों को ऑनलाइन उपलब्ध कराए जाने के लिए बनाया है।

- **ईपीएफओ वेब पोर्टल और मोबाइल ऐप**- यह ऐप कर्मचारियों को ई-पासबुक का उपयोग करके अपने भविष्य निधि की राशि की जांच करने की अनुमति प्रदान करती है , जो वास्तविक पासबुक के जैसी होती है।

- **स्टार्ट-अप इंडिया पोर्टल और मोबाइल ऐप**- यह भारत सरकार का एक कार्यक्रम है जो उद्यमियों को देश में नये व्यवसायों (स्टार्ट-अप) को विकसित करने और स्थायी रूप से विस्तार करने के लिए प्रोत्साहित करता है।

डिजिटल इंडिया के उद्देश्य

- यह अभियान स्वास्थ्य देखभाल और साक्षरता को और अधिक सुलभ बनाता है। परम्परागत तरीके की अपेक्षा डॉक्टर की नियुक्ति, शुल्क का भुगतान, डायग्नोस्टिक परीक्षण और रक्त परीक्षण हेतु ऑनलाइन पंजीकरण आसानी से और घर बैठे ही किया जा सकता है है।

- यह उपभोक्ताओं को परम्परागत थकान भरे भौतिक कार्य को कम करते हुए कहीं से भी अपने कागजी कार्रवाई और प्रमाणपत्र ऑनलाइन जमा करने की अनुमति देता है।

- नागरिक डिजिटल रूप से अपने रिकॉर्ड पर ऑनलाइन हस्ताक्षर कर सकते हैं।

- यह राष्ट्रीय छात्रवृत्ति पोर्टल के लाभार्थियों को आवेदन ऑनलाइन जमा करने, उन्हें सत्यापित करने और भुगतान करने की अनुमति देकर लाभान्वित करता है।

- बीएसएनएल मोबाइल उपकरणों पर वॉयस, डेटा, मल्टीमीडिया आदि जैसे ऑनलाइन सेवाओं के बेहतर प्रशासन के लिए 30 साल पुराने टेलीफोन एक्सचेंजों की जगह लेगा।

- सभी प्रकार के वितीय लेन-देन डिजिटल तरीके से पूरे किए जाते हैं, इस प्रकार यह कालाबाजारी को कम करने में भी सहायक होता है।

डिजिटल इंडिया मिशन के लाभ

डिजिटल इंडिया मिशन एक ऐसा कदम है जिसमें देश के ग्रामीण क्षेत्रों को हाई-स्पीड इंटरनेट नेटवर्क से जोड़ने की योजना शामिल है। पब्लिक इंटरनेट एक्सेस प्रोग्राम डिजिटल इंडिया के नौ स्तंभों में से एक है। डिजिटल सिस्टम अपनाने के मंच पर, भारत विश्व में शीर्ष 2 देशों में शामिल है और भारत की डिजिटल अर्थव्यवस्था वर्ष 2023 तक $1 ट्रिलियन को पार करने की संभावना है।

डिजिटल इंडिया के कुछ लाभ हैं:

- ई-गवर्नेंस से संबंधित इलेक्ट्रॉनिक लेनदेन में वृद्धि हुई है। विश्व बैंक द्वारा जारी वैश्विक फाइंडेक्स रिपोर्ट में कहा गया कि भारत में वित्तीय समावेशन में तेजी से बढ़ोतरी हो रही और खाताधारकों की संख्या जो 2011 में 35 फीसदी थी और 2014 में 53 फीसदी थी। वह 2017 में बढ़कर 80 फीसदी हो गई है।
- भारत नेट कार्यक्रम के तहत 2,74,246 किलोमीटर के ऑप्टिकल फाइबर नेटवर्क ने 1.15 लाख से अधिक ग्राम पंचायतों को जोड़ा है।
- भारत सरकार की राष्ट्रीय ई-गवर्नेंस परियोजना के तहत एक सामान्य सेवा केंद्र (सीएससी) बनाया गया है जो सूचना और संचार प्रौद्योगिकी (आईसीटी) तक पहुंच प्रदान करता है। कंप्यूटर और इंटरनेट एक्सेस के माध्यम से, सीएससी ई-गवर्नेंस, शिक्षा, स्वास्थ्य, टेलीमेडिसिन, मनोरंजन और अन्य सरकारी और निजी सेवाओं से संबंधित मल्टीमीडिया सामग्री प्रदान करते हैं।
- सोलर लाइटिंग, एलईडी असेंबली यूनिट, सैनिटरी नैपकिन प्रोडक्शन यूनिट और वाई-फाई चौपाल जैसी सर्वसुविधायुक्त सुविधाओं के साथ डिजिटल गांवों की स्थापना।
- इंटरनेट डेटा का उपयोग सेवाओं के वितरण के लिए एक प्रमुख उपकरण के रूप में किया जाता है और शहरी इंटरनेट की पहुंच 64% तक पहुंच गई है।

- देश के लगभग 80 प्रतिशत लोग बैंक में अपना खता खुलवा चुके है । ग्रामीण स्तर पर भी लोगो द्वारा बैंकिग माध्यम से वितीय लेनदेन किये जाने लगे हैं ।

डिजिटल इंडिया की चुनौतियाँ

भारत सरकार ने देश के ग्रामीण क्षेत्रों को हाई-स्पीड इंटरनेट नेटवर्क से जोड़ने के लिए डिजिटल इंडिया मिशन के माध्यम से एक महत्वपूर्ण पहल की है। डिजिटल इंडिया अभियान में सरकार द्वारा उठाये गये विभिन्न कदमों के अतिरिक्त इसमें कई चुनौतियों का सामना भी करना पड़ता है।

डिजिटल मिशन की कुछ चुनौतियाँ और कमियाँ नीचे दी गई हैं:

- भारत में अन्य विकसित देशों की तुलना में दैनिक इंटरनेट गति और वाई-फाई हॉटस्पॉट की गति धीमी हैं।
- अधिकांश छोटे और मध्यम उद्योग को नई आधुनिक तकनीक को अपनाने के लिए बहुत संघर्ष करना पड़ता है।
- सुगम इंटरनेट एक्सेस के लिए शुरुआती स्तर के स्मार्टफोन की सीमित क्षमता।
- डिजिटल प्रौद्योगिकी के क्षेत्र में कुशल मानवीय संशाधन की कमी।
- डिजिटल अपराध के बढ़ते खतरे की जांच और निगरानी के लिए साइबर सुरक्षा विशेषज्ञों की नियुक्ति भी एक चुनौती है ।
- डिजिटल शिक्षा का अभाव।

- संस्कृति की दृष्टि से भारत एक विविधतापूर्ण देश है। प्रत्येक राज्य की अपनी विशिष्ट भाषा, रीति-रिवाज, खान-पान, कानून और परंपराएँ होती हैं। डिजिटल इंडिया प्रोग्राम का उद्देश्य पूरे देश को डिजिटल रूप से एकीकृत करना है। पूर्ण एकीकरण जो प्रौद्योगिकी और भाषा का एकीकरण है, मिशन को इसके कार्यान्वयन में सामना करने वाली मुख्य चुनौतियों में से एक है।

निष्कर्ष

डिजिटल रूप से जुड़े भारत का उद्देश्य देश में जनता की सामाजिक और आर्थिक स्थिति का विकास करना है। गैर-कृषि आर्थिक गतिविधियों का विकास वित्तीय सेवाओं, स्वास्थ्य और शिक्षा तक पहुंच प्रदान करने के लिए ऐसी उपलब्धि का मार्ग प्रशस्त कर सकता है। सूचना और संचार प्रौद्योगिकी अकेले किसी देश के समग्र विकास को प्रत्यक्ष रूप से प्रभावित नहीं कर सकती है। बुनियादी डिजिटल ढांचा समग्र विकास हासिल करने में मदद कर सकता है।

साक्षरता और विनियामक व्यावसायिक वातावरण भी इसे प्राप्त करने में मदद कर सकते हैं। यह एक बहुत ही लाभदायक दृष्टिकोण होगा क्योंकि यह कागजी कार्रवाई पर समय खर्च करने के बोझ से राहत देता है और लोगों को अपना समय सरकार के अन्य पहलुओं को समर्पित करने की अनुमति देता है। यह बड़े पैमाने पर काम करने वाले सरकारी कर्मचारियों के लिए बेहद कुशल और फायदेमंद है।

REFERENCES:

https://yojana.divyabihar.com/umang-app/

https://knowledgemaps.org/e-pathshala-app-in-hindi/

Himakshi Goswami (2016)"OPPORTUNITIES AND CHALLENGES OF DIGITAL INDIA PROGRAMME E" ISSN No : 2454-9916 | Volume - 2 |

ErHarjotKaur and MrsDaljitKaur (2015)," E-commerce in India – challenges and prospects" International Journal of Engineering and Techniques, Vol-1, issue 2, pg No- 36- 40.

Digital India, a programme to transform India into a digitally empowered society and knowledge economy, Department of Electronics and Information Technology, Government of India, available at www.slideshare.net.

3. Recommendation of the council on digital Government strategies, adopted by the th OECD council on 15 July 2014, OECD.

4. M.M.K Sardana(2012)," Vision of Digital india challenges ahead for political establishment DN2012/09,ISID.

5. Usha Rani Das, challenges of Digital India some heads –up of NarendraModi, Business insider India.

6. Digital India power to empower, available at www.nextgenias.com/2015/09/eassydigital-india-programme-upsc-ias

7. Kaur,P.and Joshi, M.M., "E-Commerce in India: A Review", IJCST,Vol.3, Issue 1,JanMarch 2012,pp-802-804

8. Kaur,Ranmeet, E-Commerce in India, Asian journal of research in business economics and management, vol.2, issue 6,2012

9. ERNET: Education and Research Network, an autonomous scientific society of Ministry of Communications and Information Technology (Govt. of India).

10. Balasubramanian, D. (2013), 'Sixty years of IT in India,' The Hindu, February 20.

11. e-governance: Reforming government through technology.

12. e-kranti: Electronic delivery of services.

https://www.vedantu.com/english/digital-india

https://www.livehindustan.com/national/story-as-per-world-bank-report-number-of-bank-accounts-in-india-increased-27-percent-in-last-four-year-tenure-of-narendra-modi-government-1914063.html

RNI Regd. No. UTTBIL/2011/40666 **ISSN: 2230-8938**

UGC Journal No: 41391 **Impact Factor: 5.527**

ANUSANDHAN VATIKA

(An International Multidisciplinary Quarterly Bilingual
Peer Reviewed Refereed Research Journal)

✸ Vol 13 ✸ Issue 1 ✸ January-March 2023

PUBLISHED BY
Sahitya Kala Vigyan Tatha Sanskriti Anusandhan Samiti
Uttarkashi, Uttarakhand –249193 (INDIA)

EDITOR'S NOTE

With the progress of science in the modern era, research has special importance in our life because research is now being used for the in-depth study of each and every branch of knowledge. Through research efforts are made to answer those fundamental questions whose answers have not yet been available. But the answer to each question depends on the efforts of man. This concept can be clarified with this example, until a few years ago man did not reach the moon, in fact he did not know what the moon actually was? It was a problem that had no solution. Man had only assumptions about the moon, did not have pure knowledge. But with his efforts, he reached the moon, brought the soil from there, and from its analysis, it was possible to know what the moon is? Through research works, an attempt is made to find answers to those questions whose answer is not available in the literature or in the knowledge of man. In fact, the word 'research' is a process in which the activities of 'research' and 'investigation' are also included, in which a reliable solution to a problem is found on the basis of gathering and analyzing many types of facts. According to the nature of the word 'research', the process of enquiry, investigation, intensive inspection, extensive testing, planned study, purposeful and prompt general determination, etc. are important, that is, 'research' is a systematic and well-planned process by which human knowledge is increased. Human tensions are also reduced by research work. It is an effective method of solving scientific problems because research involves scientific investigation of a problem. The action of investigation is indicative of the fact that the problem should be looked at very closely. He should be investigated and his knowledge should be obtained.

As part of this process, the journal Anusandhan Vatika is presented to you as a medium of cognitive dialogue between Scholars, teachers and the academicians. Conceptual and experiential interpretation and analysis have been presented in this issue along with new factual information on multidisciplinary research related questions. Some of the research papers included in the research journal does not appear to be fully following the theoretical criteria of the research methodology. Nevertheless, due to the originality and novelty of the ideas, they have been given a place in the journal so that they can be combined in the integrated curriculum of the journal. Hope this issue of Anusandhan Vatika will be helpful in communication of research stream.

— Editor

TABLE OF CONTENT

RNI Regd. No. UTTBIL/2011/40666 ISSN: 2230-8938

ANUSANDHAN VATIKA

(An International Multidisciplinary Quarterly Bilingual Peer Reviewed Refereed Research Journal)

Vol 13 **Issue 1** **January-March 2023**

लघु उद्योग और भारत का ग्रामीण विकास

विक्रांत मोहन

सहायक प्राध्यापक वाणिज्य संकाय, राजकीय महाविद्यालय भट्टू कलां फतेहाबाद, हरियाणा

डॉ0 रमन दीप सिंह

सहायक प्राध्यापक वाणिज्य संकाय, राजकीय महिला महाविद्यालय सिरसा, हरियाणा

परिचय (Introduction)

एक उद्यमी वह इकाई है जो एक उद्यम के विचार की अवधारणा करता है और उत्पादन के सभी आवश्यक कारकों के संयोजन की पहल करके और उद्यम को पूरा करने और बनाए रखने के लिए जोखिम उठाने की पहल करके विचारों को वास्तविकता में परिवर्तित करता है। यह आर्थिक विकास की प्रक्रिया में योगदान देकर अर्थव्यवस्था में महत्वपूर्ण भूमिका निभाता है। एक अवधारणा के रूप में उद्यमिता उस सार को संदर्भित करती है जिसमें एक उद्यमी से जुड़े सभी लक्षण, कौशल, प्रक्रिया, पहल, गतिविधियाँ शामिल होते हैं। राष्ट्रपिता महात्मा गांधी ने ठीक ही कहा है कि भारत गांवों में वास करता है। गांव भारतीय समाज के मूल में शामिल हैं और वास्तविक भारत का प्रतिनिधित्व करते हैं। ग्रामीण उद्यमी वे हैं जो अर्थव्यवस्था के ग्रामीण क्षेत्र में औद्योगिक और व्यावसायिक इकाइयों की स्थापना करके उद्यमशीलता की गतिविधियों को अंजाम देते हैं। दूसरे शब्दों में, ग्रामीण क्षेत्रों में औद्योगिक और व्यावसायिक इकाइयों की स्थापना का तात्पर्य ग्रामीण उद्यमिता से है। उद्यमिता राष्ट्रीय अर्थव्यवस्था में ग्रामीण विकास की गति को बढ़ाकर महत्वपूर्ण योगदान दे सकती है। कृषि आज भी ग्रामीण समाज की रीढ़ है। 2011 की जनगणना के अनुसार भारत के ग्रामीण क्षेत्रों में 68.84 प्रतिशत लोग रहते हैं। 70 प्रतिशत भूमि छोटे और सीमांत किसानों के पास है जिसके परिणामस्वरूप कृषि भूमि पर निर्भरता का अनुपात बहुत अधिक है। इसके विपरीत कृषि उपज बहुत कम है। परिणामस्वरूप बड़ी संख्या में कृषि श्रमिकों का शहरी क्षेत्रों की ओर पलायन होता जा रहा है। सीमित भूमि और कृषि द्वारा श्रम शक्ति को पूर्ण रोजगार प्रदान करने में असमर्थता के कारण ग्रामीण बेरोजगारी और शहरी क्षेत्रों की ओर ग्रामीण पलायन को रोकने के लिए ग्रामीण उद्योगों को विकसित करने की आवश्यकता है। ग्रामीण अर्थव्यवस्था का विकास देश के समग्र विकास के लिए एक आवश्यक पूर्व शर्त है। ग्रामीण व शहरी असमानताओं के बीच की खाई को कम किया जाना चाहिए। ग्रामीण लोगों के जीवन स्तर में वृद्धि की जानी चाहिए। ग्रामीण क्षेत्र में उद्यमिता उपरोक्त समस्याओं का उत्तर प्रदान करती है।

ग्रामीण विकास के लिए आवश्यक सिद्धांत हैं–

1. ग्रामीण लोगों द्वारा उद्यम में प्रयुक्त ग्रामीण संसाधनों का इष्टतम उपयोग।
2. कृषि उपज के बेहतर वितरण द्वारा ग्रामीण समृद्धि में वृद्धि करना।
3. ग्रामीण उद्यमिता का ग्रामीण और शहरी आबादी के भेदभाव को कम करने और ग्रामीण पलायन को रोकने के वैकल्पिक साधन के रूप में प्रयोग ।
4. ऐसी प्रणाली को सक्रिय करना जो ग्रामीण विकास के लिए मानव संशाधन , धन , सामग्री, मशीनरी, प्रबंधन और बाजार उपलब्ध कराने में सहायक हो सके ।

ग्रामीण उद्यमिता के प्रकार

भारत में ग्रामीण उद्यमियों को निम्नलिखित प्रकार से वर्गीकृत किया जा सकता है –

कृषि आधारित उद्योग

इस प्रकार के ग्रामीण उद्योग कृषि पर आधारित होते हैं। कृषि उद्योग जिसमें अचार, फलों का जूस, जैम, डेयरी उत्पाद, चावल से बने उत्पाद, चीनी उद्योग, गुड़, तिलहन से तेल, मसाले जैसे कृषि उत्पादों का प्रसंस्करण और बिक्री शामिल है ।

वन आधारित उद्योग

वन उत्पादों पर आधारित ग्रामीण उद्योग इस श्रेणी के अंतर्गत आते हैं। वन आधारित उद्योग जिनमें शहद बनाना, लकड़ी के उत्पाद, बांस और गन्ना उत्पाद, बीड़ी बनाना, पत्तों से खाने की थाली बनाना आदि शामिल है ।

खनिज आधारित उद्योग

यह खनन और खनिज पदार्थो पर आधारित एक प्रकार की ग्रामीण उद्यमिता है । इनमें से कुछ उद्यम स्टोन क्रशिंग, सीमेंट उत्पाद, दीवार कोटिंग पाउडर, संगमरमर और ग्रेनाइट से बने सजावटी सामान हैं। इस प्रकार के उद्योग हमारे देश के अधिकतर ग्रामीण क्षेत्रों में चलाये जाते है।

वस्त्र उद्योग

यह कैटेगरी टेक्सटाइल और कॉटन प्रोडक्ट्स पर आधारित है। इसमें कपड़े की बुनाई, कताई और रंगाई शामिल है।

इंजीनियरिंग और सेवाएं

इंजीनियरिंग उद्योगों में कृषि उपकरणों के पुर्जों, औजारों , मशीनरी के पुर्जों आदि का निर्माण और मरम्मत शामिल है।

हस्तशिल्प उद्योग

इनमें लकड़ी या बांस से हस्तशिल्प बनाना, पारंपरिक सजावटी उत्पाद, खिलौने और गुड़िया बनाना, क्षेत्र विशेष के प्रशिद्ध विशिष्ट हस्तशिल्प के अन्य सभी रूप शामिल हैं।

उपर्युक्त सभी ग्रामीण उद्यम ग्रामीण विकास में एक प्रमुख भूमिका निभाते हैं जो इन पारंपरिक ग्रामीण उद्यमियों के विकास पर आधारित है। अतः स्पष्ट है कि भारत में ग्रामीण विकास का सीधा संबंध हमारे देश के ग्रामीण उद्यमियों की विभिन्न श्रेणियों के विकास से है।

ग्रामीण उद्योगों का निवेश अनुसार वर्गीकरण

(एमएसएमई) 2006 में एमएसएमई विकास अधिनियम, 2006 के अधिनियमन के साथ एक बड़ा परिवर्तन हुआ। सूक्ष्म, लघु और मध्यम उद्यम, (एमएसएमई) विकास मंत्रालय अधिनियम, 2006 के अनुसार संयंत्र और मशीनरी में निवेश या उपकरण में निवेश के अनुसार विनिर्माण और सेवा उद्यमों पर परिभाषित किया गया है। एमएसएमई मंत्रालय के अनुसार, सूक्ष्म, लघु और मध्यम उद्यमों के रूप में वर्गीकृत किए जाने वाले उद्यमों के लिए निवेश पर हाल की सीमाएं इस प्रकार हैं

सूक्ष्म, लघु और मध्यम उद्यम की परिभाषा, 2018

नई परिभाषा 7 अप्रैल,2018 से लागू है जिसे प्रधानमंत्री की अध्यक्षता वाली कैबिनेट कमेटी की बैठक में अंतिम रूप दिया गया था. इस परिवर्तन के बाद अब "प्लांट और मशीनरी" में निवेश की जगह "टर्नओवर" के आधार पर MSMEs वर्गीकरण किया जायेगा.

सूक्ष्म, लघु और मध्यम उद्यम की परिभाषा, 2018

विनिर्माण क्षेत्र

सूक्ष्म उद्योग	सालाना टर्न ओवर रु. 5 करोड़ से कम
लघु उद्योग	सालाना टर्न ओवर रु. 5 करोड़ से 75 करोड़ के बीच
मध्यम उद्योग	सालाना टर्न ओवर रु. 75 करोड़ से 250 करोड़ के बीच

सेवा क्षेत्र

सूक्ष्म उद्योग	सालाना टर्न ओवर रु. 5 करोड़ से कम
लघु उद्योग	सालाना टर्न ओवर रु. 5 करोड़ से 75 करोड़ के बीच
मध्यम उद्योग	सालाना टर्न ओवर रु. 75 करोड़ से 250 करोड़ के बीच

सूक्ष्म, लघु और मध्यम उद्यम की परिभाषा, 2020. सरकार द्वारा इसकी नई परिभाषा इस प्रकार दी गयी है–

वर्गीकरण	**सूक्ष्म उद्योग उद्योग**	**लघु उद्योग**	**माध्यम**
विनिर्माण एवं सेवा क्षेत्र	निवेश 1 करोड़ से कम & टर्नओवर 5 करोड़ से कम	निवेश 10 करोड़ से कम & टर्नओवर 50 करोड़ से कम	निवेश 20 करोड़ से कम & टर्नओवर 100 करोड़ से कम

ग्रामीण उद्यमिता की भूमिका और महत्व निम्न प्रकार से प्रकट होता है–

गरीबी और बेरोजगारी में कमी

ग्रामीण उद्यमिता मूलरूप से श्रम प्रधान है और ग्रामीण लोगों के लिए बड़े पैमाने पर रोजगार के अवसर पैदा करती है। ग्रामीण उद्यमिता में ग्रामीण क्षेत्रों में प्रचलित बेरोजगारी और अल्परोजगार की समस्या को कम करने की क्षमता है।

विकेंद्रीकृत औद्योगिक विकास एवं धन का एवं समान वितरण–

ग्रामीण उद्यमिता देश के आर्थिक विस्तार में महत्वपूर्ण भूमिका निभाती है और इसके परिणामस्वरूप विकेंद्रीकृत औद्योगिक विकास, लोगों के बीच आय और धन का समान वितरण होता है।

स्थानीय संसाधनों का उचित उपयोग–

ग्रामीण उद्योग स्थानीय संसाधनों जैसे कच्चे माल और श्रम के उत्पादक उद्देश्यों के लिए अधिकतम उपयोग में सहयोग करते हैं और इस प्रकार उत्पादकता बढ़ाते हैं। उद्यमियों द्वारा सीमित स्थानीय संसाधनों के कुशल और प्रभावी उपयोग से ग्रामीण क्षेत्र का समग्र आर्थिक विकास होता है।

ग्रामीण आबादी के पलायन पर रोक–

श्रमिकों सहित ग्रामीण आबादी आय सृजन, अच्छी नौकरी, विभिन्न सुविधाओं की खोज और कमजोर आर्थिक स्थिति जैसे विभिन्न कारणों से शहरी क्षेत्रों की ओर बढ़ती है। ग्रामीण उद्यमिता शहरी और ग्रामीण क्षेत्रों के बीच विद्यमान अंतर को कम करने की क्षमता रखती है। ग्रामीण उद्यमशीलता रोजगार के अवसर पैदा कर सकती है और ग्रामीण भारत में बुनियादी ढांचे और अन्य सुविधाओं के विकास में योगदान दे सकती है।

संतुलित क्षेत्रीय विकास–

ग्रामीण उद्यमिता दूरस्थ क्षेत्रों में लघु इकाइयों की स्थापना कर शहरी क्षेत्रों में उद्योगों के केन्द्रीयकरण पर रोक लगाती है।उद्यमिता विकास कार्यक्रम संतुलित क्षेत्रीय विकास के उद्देश्य को प्राप्त करने में सहायक होते है ।

कलात्मक गतिविधियों को बढ़ावा देना–

ग्रामीण उद्यमिता के माध्यम से कला और शिल्प का संरक्षण और प्रचार करना ग्रामीण भारत की सदियों पुरानी समृद्ध विरासत को संरक्षित किया जा सकता है।

सामाजिक बुराइयों पर रोक–

उद्यमिता की वृद्धि सामाजिक बुराइयों जैसे चोरी, डकैती, नशाखोरी, गरीबी, सामाजिक तनाव, वायुमंडलीय प्रदूषण आदि को कम करती है ।

जीवन स्तर में सुधार–

ग्रामीण उद्यमशीलता ग्रामीण क्षेत्रों में जीवन स्तर में सुधार कर सकती है। विकास और समृद्धि के बढ़ते अवसर ग्रामीण समुदायों का उत्थान कर सकते हैं।

प्रति व्यक्ति आय में सुधार–

ग्रामीण उद्यमशीलता नए अवसरों का लाभ उठाकर अधिक उत्पादन, रोजगार और धन उत्पन्न करती है, जिससे ग्रामीण लोगों की प्रति व्यक्ति आय में वृद्धि और जीवन स्तर में सुधार में मदद मिलती है।

विदेशी मुद्रा भंडार में वृद्धि–

यदि ग्रामीण उद्योगों के उत्पादों को मान्यता दी जाती है और विदेशी मांग में वृद्धि की जाती है तो ग्रामीण उद्यमिता देश की विदेशी मुद्रा भंडार को बढ़ाने में महत्वपूर्ण भूमिका निभा सकती है।

ग्रामीण उद्यमियों के सामने आने वाली समस्याएं–

एक अर्थव्यवस्था के ग्रामीण विकास में उद्यमी बहुत महत्वपूर्ण भूमिका निभा रहे हैं। ग्रामीण भारत के उद्यमियों को अनेक बाधाओं और समस्यायों का सामना करना पड़ता है। ग्रामीण उद्यमियों द्वारा सामना की जाने वाली कुछ प्रमुख समस्याओं को निम्नानुसार वर्गीकृत किया गया है रू.

1. निरक्षरता

साक्षरता का स्तर इच्छुक ग्रामीण उद्यमियों के लिए एक गंभीर बाधा है। उनके लिए व्यावसायिक गतिविधियों की तकनीक, तकनीकी वातावरण में बदलाव और व्यापार के विभिन्न क्षेत्रों की संभावनाओं को समझना बहुत मुश्किल है। इसके अलावा, ग्रामीण क्षेत्रों में, ग्रामीण उद्यमियों को उपलब्ध श्रम शक्ति के बीच निरक्षरता की समस्या से भी निपटना पड़ता है। श्रमिकों की साक्षरता का स्तर ग्रामीण उद्यमियों की व्यावसायिक संभावनाओं को प्रभावित करता है और इस तरह यह एक गंभीर चुनौती है। साक्षरता के निम्न स्तर के कारण ग्रामीण उद्यमी कानूनी औपचारिकताओं को समझने और उनका पालन करने में बहुत बोझिल हो जाते हैं।

2. अनुभव की कमी–

ग्रामीण उद्यमी ज्यादातर पहली पीढ़ी के उद्यमी हैं। वे उद्यमिता के गहन अनुभव के साथ शायद ही कभी संपन्न होते हैं। यह स्पष्ट है कि उन्हें गहन अनुभव वाले लोगों के साथ प्रतिस्पर्धा करनी होती हैं ।

3. क्रय शक्ति सीमित है–

क्रय शक्ति का अभाव ग्रामीण उद्यमियों के लिए एक गंभीर बाधा है। कुछ अपवादों को छोड़ दें, तो ग्रामीण उद्यमी संसाधन और मशीनरी खरीदने की क्षमता के अभाव के संकट का सामना करते हैं।

4. मौजूदा शहरी उद्यमियों से खतरा–

शहरी उद्यमी लाभकारी और बाजार में एकाधिकारी स्थिति में हैं। उनके पास सूचना प्रौद्योगिकी, व्यावसायिक संभावनाएं, ऋण सुविधा आदि की

बेहतर पहुंच है। ग्रामीण उद्यमियों को अंततः शहरी समकक्षों के साथ प्रतिस्पर्धा करनी पड़ती है । इस प्रकार ग्रामीण उद्यमियों के विकास की संभावनाए कमजोर हो जाती है ।

5. धन की कमी

ग्रामीण क्षेत्रों के उद्यमी वित्तीय सुरक्षा के अभाव में वितीय संस्थाओ से फंड प्राप्त नही कर पाते हैं। इसके अलावा, ऋण सुविधाओं की कमी भी उनकी दुर्दशा को बढाती है । वे अक्सर असंगठित वित्तीय क्षेत्र से उधार लेते हैं और हानि उठाते है

6. बिचौलियों का अस्तित्व

बिचौलियों के विभिन्न स्तरों का अस्तित्व ग्रामीण क्षेत्रों के उद्यमियों के लिए एक गंभीर समस्या है। ग्रामीण उद्यमी अक्सर बिचौलियों पर निर्भर होते हैं और इस प्रक्रिया में उनका शोषण होता है।

7. कच्चे माल की खरीद

क्योंकि प्रारंभ में ग्रामीण उद्यमियो की आर्थिक स्थिति सुदृढ़ नही होती है इसलिए कच्चे माल की खरीद में ग्रामीण उद्यमियों को गंभीर बाधाओं का सामना करना पड़ता है। आमतौर पर आपूर्तिकर्ता ग्रामीण उद्यमियों की उपेक्षा करते हैं। ग्रामीण उद्यमियों को भंडारगृह और भंडारण की समस्या का सामना करना पड़ता है। खराब कच्चे माल का उपयोग करने वाले उद्यमियों को ग्रामीण क्षेत्रों में कोल्ड स्टोरेज की सुविधा उपलब्ध नहीं है।

8. तकनीकी कौशल की कमी

ग्रामीण उद्यमियों को तकनीकी ज्ञान की कमी की भारी समस्या का सामना करना पड़ता है। इससे जुड़ी दो समस्याएं हैं। सबसे पहले, ग्रामीण उद्यमी तकनीकी विकास की जानकारी के साथ खुद को अपडेट नहीं रखते हैं। दूसरा, तकनीकी कौशल के बिना कर्मचारी और कर्मचारी उत्पादकता को भी प्रभावित करते हैं।

9. प्रशिक्षण सुविधाओं का अभाव

ग्रामीण क्षेत्रों में प्रशिक्षण और कौशल विकास सुविधाओं की कमी भी एक गंभीर समस्या है। ग्रामीण उद्यमियों को अपनी उत्पादकता को बढ़ाने के लिए अपने श्रमिकों को प्रशिक्षित करने और उनके विकास से सम्बंधित कार्यक्रम आयोजित करने में समस्यायों का सामना करना पड़ता है ।

10. बुनियादी सुविधाओं का निम्न स्तर

आमतौर पर ग्रामीण क्षेत्रों में सड़कों, संचार सुविधाओं और बिजली की आपूर्ति का स्तर मानक से नीचे होता है। ढांचागत सुविधाओं का निम्न स्तर ग्रामीण उद्यमिता के विकास को पीछे छोड़ देता है।

11. उत्पादों की खराब गुणवत्ता

ग्रामीण क्षेत्रों के उद्यमियों को अपने उत्पादों और सेवाओं में उच्च स्तर के मानक बनाए रखना बेहद कठिन लगता है। इंटरनेट पहुंच की कमी के कारण व निर्धारित मानकों के बारे में उचित जानकारी का अभाव होने के कारण गुणवत्ता में कमी आती है । उनके पास मानक उपकरण और मशीनों की भी कमी होती है।

12. सकारात्मक और प्रेरक वातावरण की कमी

अधिकांश मामलों में, ग्रामीण उद्यमी स्वयं पैदा नहीं होते हैं बल्कि उन्हें ऐसे माहौल में लाया जाता है जो उद्यमशीलता को बढ़ावा देता है। युवाओं को उद्यमशीलता के लिए प्रोत्साहित करने के लिए सामाजिक वातावरण, पारिवारिक रीति–रिवाज, परंपराएँ अनुकूल नहीं हैं। ग्रामीण क्षेत्रों में उद्यमशीलता के अवसरों के बारे में जागरूकता और ज्ञान की कमी है।

13. जोखिम का तत्व शामिल

ग्रामीण उद्यमी अपने समकक्षों के विपरीत भारी जोखिम उठाने के लिए अच्छी तरह तैयार नही होते है । वित्तीय संसाधनों, क्रेडिट सुविधाओं और बाहरी सहायता की कमी के कारण ग्रामीण उद्यमियों में जोखिम सहन करने की क्षमता कम होती है ।

ग्रामीण क्षेत्रों में उद्यमियों की तमाम कमियों के बावजूद, ग्रामीण क्षेत्रों की ताकत का आकलन करना और ग्रामीण क्षेत्रों में अवसर पैदा करना आवश्यक है।

भारत में ग्रामीण उद्यमिता विकास पहल – सरकारी प्रयास, नीतियां, योजनाएँ और संभावनाएँ

सरकारी प्रयास

खादी और ग्रामोद्योग आयोग (केवीआईसी) द्वारा कार्यान्वित ग्रामीण रोजगार सृजन कार्यक्रम (केवीआईसी) केवीआईसी की नकारात्मक सूची में निर्दिष्ट लोगों को छोड़कर सभी व्यवहार्य ग्राम उद्योग परियोजनाओं को शामिल करता है। बैंकों द्वारा वित्तपोषण के लिए सात प्रमुखों के तहत 119 ग्रामीण उद्योगों को निर्दिष्ट किया गया है।ये प्रमुख खनिज आधारित उद्योग, वन–आधारित उद्योग, कृषि–आधारित और खाद्य उद्योग, बहुलक और रसायन–आधारित उद्योग, इंजीनियरिंग और गैर–पारंपरिक ऊर्जा, कपड़ा उद्योग (खादी को छोड़कर) और सेवा उद्योग हैं। इसके अलावा प्क्व्ए ज्ल्ल्म्ड और जवाहर रोजगार योजना जैसे ग्रामीण विकास कार्यक्रम लक्ष्य समूहों और ग्रामीण अवसंरचना सुविधाओं पर ध्यान केंद्रित कर रहे हैं।जमीनी स्तर पर अंतर–क्षेत्रीय समन्वय और योजनाबद्ध संबंध मजबूत होने के संकेत हैं। स्वैच्छिक प्रयासों को भी उचित मान्यता मिल रही है और नीति समर्थन के माध्यम से एक प्रोत्साहन प्रदान किया जा रहा है। सरकार की कार्य योजना ग्रामीण विकास पर राष्ट्रीय संसाधनों का आधा खर्च करने की इच्छा रखती है।

ग्रामीण औद्योगीकरण कार्यक्रम

ग्रामीण क्षेत्रों और शहरी क्षेत्रों में एक लाख तक की आबादी वाले गैर–कृषि क्षेत्र (एनएफएस) की गतिविधियाँ ग्रामीण औद्योगीकरण कार्यक्रम के

अंतर्गत आती हैं। कार्यक्रम के तहत, लघु, सूक्ष्म, लघु और मध्यम में विनिर्माण और सेवा उद्यम स्थापित करने के लिए उद्यमियों को वित्तीय सहायता और प्रोत्साहन दिया जाता है।

नेशनल बैंक फॉर एग्रीकल्चर एंड रूरल डेवलपमेंट (छ।ठ।त्व) कृषि–उद्योगों, सेरीकल्चर और ग्रामीण गैर–कृषि क्षेत्र के उत्पादों के विपणन के लिए पुनर्वित्त प्रदान करता है। 50,000 आबादी तक के स्थानों में अन्य उद्योगों के लिए, नाबार्ड द्वारा पुनर्वित्त स्वीकृत किया जाता है। कुछ अखिल भारतीय बोर्डों (जैसे केंद्रीय रेशम बोर्ड कॉयर बोर्ड, केंद्रीय ऊन बोर्ड) और निकायों जैसे – केवीआईसी, अखिल भारतीय हथकरघा बोर्ड, और अखिल भारतीय हस्तशिल्प बोर्ड द्वारा कवर किए गए पारंपरिक उद्योगों के माध्यम से विकेंद्रीकृत औद्योगिक विकास। । एक लाख आबादी तक के ग्रामीण और अध र्ा–शहरी क्षेत्रों में स्थित बिजली करघों सहित कई अन्य कृषि, खाद्य प्रसंस्करण और खनिज आधारित उद्योग भी इस कार्यक्रम में शामिल हैं। ग्रामीण औद्योगिकीकरण कार्यक्रम में उद्योगों के समूहों की पहचान करके एक एकीकृत दृष्टिकोण अपनाया जा रहा है। उपायों के पैकेज में निम्नलिखित शामिल हो सकते हैं – क्रेडिट, प्रौद्योगिकी उन्नयन आधुनिकीकरण, प्रौद्योगिकी हस्तांतरण, निर्यात सहित विपणन जहां व्यावहारिक, बुनियादी ढांचा विकास, सामान्य सेवाएं, कच्चे माल की आपूर्ति, आदि। ग्रामीण औद्योगीकरण (एनपीआरआई) के लिए राष्ट्रीय कार्यक्रम को क्लस्टर दृष्टिकोण का उपयोग करते हुए 1999–2000 से 2004–2005 तक पांच वर्षों के लिए लागू किया गया था। इस कार्यक्रम को लागू करने में शामिल संस्थान ज्ञटप्ब और अन्य विकेन्द्रीकृत संगठन हैं, जैसे लघु उद्योग सेवा संस्थान ैप्टप्द्ध, छ।ठ।त्व और ैप्क्ठप्।

नीतियां और योजनाएँ

भारत सरकार ग्रामीण उद्यमिता को प्रत्यक्ष या अप्रत्यक्ष रूप से बढ़ाने के लिए कई योजनाएँ चला रही है। ये योजनाएं प्रत्यक्ष या अप्रत्यक्ष रूप से ग्रामीण उद्यमिता को बढ़ावा देने में मदद करती हैं।

1. स्वरोजगार के लिए ग्रामीण युवाओं का प्रशिक्षण (ज्त्ल्म्ड) एक ऐसी योजना थी जिसका उद्देश्य ग्रामीण गरीबों को 18–35 वर्ष की आयु में बुनियादी तकनीकी और उद्यमशीलता कौशल प्रदान करना था ताकि वे आय सृजन गतिविधियों को अपना सकें। इस योजना को अप्रैल, 1999 से प्क्च्एक्ब्। आदि के साथ स्वर्णजयंती ग्राम स्वरोजगार योजना (एसजीएसवाई) में मिला दिया गया।

2. एसजीएसवाई का उद्देश्य सामाजिक सहायता, उनके प्रशिक्षण और क्षमता निर्माण और आय सृजन परिसंपत्तियों के प्रावधान के माध्यम से ग्रामीण गरीबों को स्वयं सहायता समूहों (एसएचजी) में संगठित करना है। एसजीएसवाई जोर देकर कहता है कि विभिन्न गतिविधियों के वित्तपोषण के बजायय प्रत्येक ब्लॉक को कुछ चुनिंदा गतिविधियों (प्रमुख गतिविधियों) पर ध्यान केंद्रित करना चाहिए और इन गतिविधियों के सभी पहलुओं में भाग लेना चाहिए, ताकि स्वरोजगारियां अपने निवेश से स्थायी आय प्राप्त कर सकें।

3. ग्रामीण क्षेत्रों के सतत विकास के लिए स्वैच्छिक संगठनों और सरकार के बीच उभरती हुई साझेदारी को उत्प्रेरित और समन्वित करने के लिए नोडल एजेंसी के रूप में पीपल्स एक्शन एंड रूरल टेक्नोलॉजी (ब।च।त्ज) की उन्नति परिषद का गठन 1986 में किया गया था।

भारत में ग्रामीण उद्यमिता की संभावनाएँ

1. स्थापना की कम लागत

शहरी समकक्षों के मुकाबले ग्रामीण उद्यमिता का एक लाभ यह है कि ग्रामीण उद्यम की स्थापना में कम लागत आती है। ग्रामीण उद्यमी इसका लाभ उठा सकते हैं और अपना उद्यम शुरू कर सकते हैं।

2. श्रम की बेहतर उपलब्धता

अधिकांश ग्रामीण आबादी प्रत्यक्ष या अप्रत्यक्ष रूप से कृषि से जुड़ी हुई है। श्रम शक्ति में अर्ध–कुशल और अकुशल दोनों तरह के मजदूर शामिल हैं। ग्रामीण उद्यमी द्वारा प्रच्छन्न रोजगार की समस्या का समाधान किया जा सकता हैं। अतिरिक्त श्रमिक क्षमता को ग्रामीण उद्यमों की और स्थानांतरित किया जा सकता है। ग्रामीण उद्यमशीलता के लिए सस्ती दर पर श्रम बल प्रचुर मात्रा में उपलब्ध है। यहां तक कि शहरी क्षेत्रों में काम करने वाले ग्रामीण क्षेत्रों के मजदूर भी ग्रामीण उद्यमिता में शामिल होने पर पुनर्विचार कर सकते हैं।

3. स्थानीय संसाधनों की उपलबध्ता

उपलब्ध स्थानीय कच्चे माल पर आधारित ग्रामीण उद्यमशीलता एक मजबूत स्थिति में है। स्थानीय कृषि आधारित या खनिज आधारित कच्चा माल आसानी से उपलब्ध हो जाता है और इसमें भारी परिवहन और भंडारण लागत भी नहीं आती है।

4. उत्पादन की लागत

उत्पादन के लिए आवश्यक साधन; जैसे– माल, श्रम आदि सस्ती दर पर उपलब्ध हो जाते हैं, जिस कारण ग्रामीण उद्यम में शामिल उत्पादन की लागत तुलनात्मक रूप से कम हो जाती है। पूंजी और स्थानीय संसाधनों का पूर्ण और कुशलतापूर्वक प्रयोग किया जाए तो ग्रामीण उद्योग देश के आर्थिक विकास में महत्त्वपूर्ण भूमिका निभा सकते हैं।

5. उपलब्ध संसाधनों का सर्वश्रेष्ठ उपयोग

ग्रामीण क्षेत्रों में उपलब्ध संसाधनों के इष्टतम उपयोग की जिम्मेदारी ग्रामीण उद्यमिता उठा सकती है।

6. सरकारी सहायता और नीतियां

केंद्र सरकार और राज्य सरकारों ने भारत में ग्रामीण उद्यमिता के विकास को हमेशा समर्थन और बढ़ावा दिया है। सरकारों ने नीतियां बनाई हैं और ग्रामीण उद्यमिता को बढ़ावा देने के लिए सब्सिडियां प्रदान की हैं। राज्य ग्रामीण उद्यमिता के महत्व और क्षमता से अवगत है। राज्य निश्चित रूप से ग्रामीण उद्यमिता को बढ़ावा देगा। यह ग्रामीण उद्यमिता के उम्मीदवारों के लिए एक बहुत ही सकारात्मक संभावना है।

निष्कर्ष

ग्रामीण उद्यमिता भारत के आर्थिक विकास में विशेष रूप से ग्रामीण अर्थव्यवस्था में एक महत्वपूर्ण भूमिका निभाती है। यह ग्रामीण क्षेत्रों में कम पूंजी के साथ रोजगार के अवसर पैदा करने, लोगों की वास्तविक आय बढ़ाने, प्रच्छन्न बेरोजगारी को कम करने, गरीबी को कम करने, प्रवासन, आर्थिक विषमता को कम करके कृषि के विकास में योगदान देने में मदद करता है। जैसे–जैसे जनसंख्या बढ़ेगी, वैसे–वैसे भूमि पर दबाव बढ़ता जाएगा और कृषि बढ़ती हुई श्रम शक्ति को पूर्ण रोजगार नहीं दे पाएगी। ग्रामीण उद्यमिता विकासशील देश को विकसित राष्ट्र में बदलने का तरीका है। इसलिए लाभकारी रोजगार पैदा करने तथा ग्रामीण और शहरी क्षेत्रों के बीच बढ़ती असमानताओं को कम करने के संदर्भ में ग्रामीण उद्यमिता को बढ़ावा देना अत्यंत महत्वपूर्ण है। इस प्रकार ग्रामीण उद्यमिता ग्रामीण और पिछड़े क्षेत्रों से जुड़ी गरीबी, पलायन, आर्थिक विषमता, बेरोजगारी और अल्परोजगार की समस्याओं का रामबाण इलाज हो सकता है। वैश्वीकरण के युग में, ग्रामीण संदर्भ में उद्यमिता विकास एक चुनौती है। ग्रामीण क्षेत्रों के उत्थान के लिए सरकार को ग्रामीण उद्यमिता विकास योजनाओं और कार्यक्रमों का मूल्यांकन करना चाहिए। ग्रामीण विकास कार्यक्रमों में बुनियादी ढांचे के विकास, शिक्षा, स्वास्थ्य सेवाओं, कृषि में निवेश और ग्रामीण गैर–कृषि गतिविधियों को बढ़ावा देना चाहिए जिसमें महिलाएं और ग्रामीण आबादी खुद को शामिल कर सकें। ग्रामीण क्षेत्रों में व्यवहार्य विकास लाने के लिए स्थानीय संसाधनों के साथ स्थानीय जनशक्ति का विवेकपूर्ण मिश्रण आवश्यक है।

संदर्भ–

https://censusindia.gov.in/census.website/

https://msme.gov.in/

https://ngosindia.com/capart-council-for-advancement-of-peoples-action-and-rural-technology/

https://www.india.gov.in/topics/industries/micro-small-medium-enterprises

https://www.kvic.gov.in/

https://www.nabard.org/

https://www.sidbi.in/en